



저작자표시-비영리-변경금지 2.0 대한민국

이용자는 아래의 조건을 따르는 경우에 한하여 자유롭게

- 이 저작물을 복제, 배포, 전송, 전시, 공연 및 방송할 수 있습니다.

다음과 같은 조건을 따라야 합니다:



저작자표시. 귀하는 원저작자를 표시하여야 합니다.



비영리. 귀하는 이 저작물을 영리 목적으로 이용할 수 없습니다.



변경금지. 귀하는 이 저작물을 개작, 변형 또는 가공할 수 없습니다.

- 귀하는, 이 저작물의 재이용이나 배포의 경우, 이 저작물에 적용된 이용허락조건을 명확하게 나타내어야 합니다.
- 저작권자로부터 별도의 허가를 받으면 이러한 조건들은 적용되지 않습니다.

저작권법에 따른 이용자의 권리는 위의 내용에 의하여 영향을 받지 않습니다.

이것은 [이용허락규약\(Legal Code\)](#)을 이해하기 쉽게 요약한 것입니다.

[Disclaimer](#)

Doctoral Thesis

Design, Synthesis, and Characterization of
Polymer and Small-Molecule Organic
Semiconductors based on Tricyclic Heterocycles
for Opto-Electronic Devices

Kyu Cheol Lee

Department of Energy Engineering
(Energy Engineering)

Graduate School of UNIST

2017

Design, Synthesis, and Characterization of
Polymer and Small-Molecule Organic
Semiconductors based on Tricyclic Heterocycles
for Opto-Electronic Devices

Kyu Cheol Lee

Department of Energy Engineering
(Energy Engineering)

Graduate School of UNIST

Design, Synthesis, and Characterization of
Polymer and Small-Molecule Organic
Semiconductors based on Tricyclic Heterocycles
for Opto-Electronic Devices

A thesis/dissertation
submitted to the Graduate School of UNIST
in partial fulfillment of the
requirements for the degree of
Doctor of Philosophy

Kyu Cheol Lee

12/13/2016 of submission

Approved by

Advisor

Changduk Yang

Design, Synthesis, and Characterization of Polymer and Small-Molecule Organic Semiconductors based on Tricyclic Heterocycles for Opto-Electronic Devices

Kyu Cheol Lee

This certifies that the thesis/dissertation of Kyu Cheol Lee is
approved.

12/13/2016 of submission

Advisor: Changduk Yang

Jin Young Kim: Thesis Committee Member #1

Sung You Hong: Thesis Committee Member #2

Hyesung Park: Thesis Committee Member #3

Sung Heum Park: Thesis Committee Member #4;

Devoted to my loved family, especially my parents

Abstract

As next-generation electronic applications, organic semiconductors based on organic small molecules and polymers with a π -conjugated backbone have shown remarkable results for past decades. In particular, unlike inorganic semiconductors, which have reached the limitation of development, they still have growth potentiality in both industry and academia because of advantages such as low cost, light weight, roll-to-roll (R2R) technology, and so on. Despite tremendous scientific progress, an efficient molecular design and optimization of the fabrication process is needed for further advancement and commercialization of organic electronics. In this work, in order to seek an optimal semiconducting system, organic small molecules/polymers that have various properties were designed and synthesized. The resulting small molecules and polymers were characterized *via* diverse analysis tools, including NMR, GPC, mass spectroscopy, MADI-TOF, UV-Vis spectrum, TGA, cyclic voltammetry, AFM, XRD, GIWAX. Furthermore, all synthesized organic materials were tested with electronic applications like organic photovoltaics (OPVs) and organic transistors.

In the first chapter, the general background of conjugated conducting materials is described to more properly frame the present study. At the same time, essential chemical reactions, mechanisms, and electronic applications are introduced. The second chapter demonstrates synthesis and characterization of benzodipyrrolidone (BDP)-based polymer with electron rich units containing calcogen atoms for OFETs. Thirdly, by tuning the side chain, a powerful and facile control method, polymers based on benzodithiophene (BDT) are designed and synthesized. Subsequently, BDT-based polymer are characterized and applied as active layer of OPVs. Finally, a new class of n-channel semiconducting small molecules based on a BDT core unit, end-capped with the dicyanomethylene and dicyanovinyl groups (DCM-*Q*-BDT and DCV-*B*-BDT) was obtained, and their various properties fully analyzed. Furthermore, these molecules were applied as *n*-type organic transistors and their air stabilities measured

Keywords: organic photovoltaics, organic field-effect transistors, conjugated polymers, small molecules, cross-coupling reaction.

Contents

Abstract	i
Contents	iii
List of Figures	v
List of Tables	ix
List of Schemes	x
Nomenclature	xi
Chapter I Introduction	1
1. General Conjugated Conducting Materials: A Brief Overview	1
1.1 The History of Conducting Materials	2
1.2 The Electromagnetic Theory for Conducting Polymer (CPs)	2
1.3 Conjugated Materials Synthesis: Methods and Reactions	3
1.3.1 Chemical and Electronical polymerization	3
1.3.2 Palladium (Pd) Catalyzed Cross Coupling Reaction	4
1.3.2.1 Understanding Palladium Catalytic Cycle	5
1.3.2.2 Stille Coupling Reaction	6
1.3.2.3 Suzki-Miyaura Cross Coupling Reaction	7
1.3.2.4 Some Examples of Conjugated polymers <i>via</i> Stille and Suzki-Miyaura Reaction	8
1.3.3 Knoevenagel Condensation for Conjugated Small Molecules	9
1.4 Electronic Applications	10
1.4.1 Organic Photovoltaics (OPVs)	11
1.4.1.1 A Brief History of Development of OPVs	11
1.4.1.2 Device Structures and Working Mechanism	12
1.4.1.3 Device Characterization	13
1.4.1.4 Organic Active Materials for OPVs	14
1.4.2 Organic Field-Effect Transistors (OFETs)	17
1.4.2.1 A Brief History of Development of OFETs	17
1.4.2.2 The Device Architectures and Working Principle for OFETs	18
1.4.2.3. <i>p</i> - , <i>n</i> -, and Ambipolar Channel Organic Materials for OFETs	21
1.5 Reference	24
Chapter II Synthesis of Characterization of Benzodipyrrolidone (BDP)-Based Polymers Containing Chalcogen Atoms (Fu, Th, Se) and Their Application to Organic Semiconducting Devices	29

2.1 BDP-Based Polymers-----	29
2.1.1 Introduction -----	29
2.1.2 Synthesis and Characterization-----	31
2.1.3 Photophysical and Electrochemical Properties and Computational Studies-----	33
2.1.4 Thin Film Microstructure Analyses -----	36
2.1.5 OFETs Performance-----	37
2.1.6 Conclusions-----	42
2.1.7 Experimental Section-----	43
2.1.8 Reference-----	46
Chapter III Synthesis and Characterization of Conjugated Benzodithiophene-Based Photovoltaic Polymers with Branched Alkyl Substitutions -----	50
3.1 BDT-Based Polymers-----	50
3.1.1 Introduction-----	50
3.1.2 Design, Synthesis, and Characterization-----	52
3.1.3 Optical and Electrochemical Properties-----	53
3.1.4 Computational Studies-----	55
3.1.5 Solar Cell Performance and Film Morphology-----	56
3.1.6 Conclusions-----	64
3.1.7 Experimental Section-----	64
3.1.8 Reference-----	69
Chapter IV Solution Processable TIPS-Benzodithiophene Based Small Molecules for <i>n</i>-Channel OFETs -----	71
4.1 BDT-Based Small Molecules -----	71
4.1.1 Introduction-----	71
4.1.2 Synthesis and Characterization-----	73
4.1.3 Optical and Electrochemical Properties and DFT Calculation-----	74
4.1.4 Evaluation of OFET Device Properties-----	76
4.1.5 Thin-film Microstructure and Morphology-----	79
4.1.6 Conclusion-----	82
4.1.7 Experimental Section-----	82
4.1.8 Reference-----	86
Chapter V Acknowledgement (English version)-----	89
Acknowledgement (Korean version)-----	90

List of Figures

Figure 1.1. The Nobel Prize in Chemistry 2000 was awarded jointly to Alan J. Heeger, Alan G. (a) MacDiarmid (b) and Hideki Shirakawa (c) "for the discovery and development of conductive polymers".

Figure 1.2. Examples of representative conjugated polymers.

Figure 1.3. Potential applications of conducting polymers

Figure 1.4. A broad conductivity range from inorganic materials to doped conjugated materials.

Figure 1.6. Example of electrochemical polymerization.

Figure 1.5. Basic *n*-type and *p*-type doping processes of polyacetylene.

Figure 1.7. A brief timeline of discovery and development metal-catalyzed name reactions.

Figure 1.8. Examples of conjugated polymers using Stille reaction a) and Suzuki reaction b).

Figure 1.9. A representative OPVs history developed.

Figure 1.10. Best solar cell efficiencies chart from NREL in 2010.

Figure 1.11. Schematics of OPV device structure (conventional, inverted, and tandem from left) a), operating principle b), and bi-layer (left) and bulk heterojunction structures (right) between donor and acceptor c) for OPVs.

Figure 1.12. The global standard spectrum a), and current density–voltage (*J*–*V*) characteristic of a typical solar cell in the dark (dashed line) and under illumination (solid line). Typical solar cell parameters such as short-circuit current density J_{sc} , open-circuit voltage V_{oc} , and the maximum power point P_m are illustrated on the graph b).

Figure 1.13. The chemical structures of *p*-type active materials for OPVs.

Figure 1.14. The chemical structures of *n*-type active materials for OPVs.

Figure 1.15. Device structures of three kinds of field-effect transistor: a) the metal insulator-semiconductor FET (MISFET), b) the metal-semiconductor FET (MESFET), and c) the thin film transistor (TFT).

Figure 1.16. The conventional structures of *n*- a) and *p*- type b) OFETs.

Figure 1.17. The device structures of four possible configuration of OFETs: bottom gate (BG)-bottom contact (BC) a), bottom gate (BG)-top contact (TC) b), top gate (TG)-bottom contact (BC) c), and top gate (TG)-top contact (TC) d).

Figure 1.18. Schematic of *p*- and *n*-channel working principle for OFETs.

Figure 1.19. Examples of representative *p*-type small molecules and polymers for OFETs.

Figure 1.20. Examples of representative *n*-type small molecules and polymers for OFETs.

Figure 1.21. Examples of representative ambipolar small molecules and polymers for OFETs.

Figure 2.1. Structures of diketopyrrolopyrrole (DPP), benzodipyrrolidone (BDP), isoindigo (IIG), and thienoisoindigo (TIIG).

Figure 2.2. TGA plots of BDP-based polymers with a heating rate of 10 °C/min in N₂ atmosphere.

Figure 2.3. UV-Vis absorption spectra of BDP-based polymers in chloroform solution (a) and as thin solid films (b). Cyclic voltammograms of BDP-based polymer thin films (c). Energy level diagrams for BDP-based polymers (d).

Figure 2.4. (a) DFT-optimized geometries and charge-density isosurfaces for the model dimers of BDP-based polymers (B3LYP/6-31G*) and their top views.

Figure 2.5. Out-of-plane X-ray diffraction (XRD) patterns of BDP-based polymer films at ambient temperature (a) and annealed at 200 °C (b)

Figure 2.6. AFM height (top) and phase (bottom) images of (a, d) **PBDP-Fu**, (b, e) **PBDP-Th**, and (c, f) **PBDP-Se** films annealed at 200 °C

Figure 2.7. Transfer and output curve of 200 °C annealed **PBDP-Fu** (red line), **PBDP-Th** (blue line), and **PBDP-Se** (green line) OFETs. (a) *p*-channel and (b) *n*-channel transfer characteristics. (c) *p*-channel and (d) *n*-channel output characteristics.

Figure 2.8. (a) Hole and electron contact resistance per unit channel width versus annealing temperature of **PBDP-Fu**, **PBDP-Th**, and **PBDP-Se** OFETs. (b) Hole and electron contact resistance of **PBDP-Fu**, **PBDP-Th**, and **PBDP-Se** OFETs annealed at 200 °C.

Figure 2.9. (a) Hole and (b) electron mobility (μ) versus 1000/temperature 200 °C annealed **PBDP-Fu**, **PBDP-Th**, and **PBDP-Se** OFETs. Devices were measured at various temperatures from 297.15 K to 78.15 K at 20 K steps.

Figure 2.10. (a) Output characteristics of ambipolar complementary **PBDP-Fu**, **PBDP-Th**, and **PBDP-Se** inverters (W/L = 1000/20 μm for *n*- and *p*-channel transistors), (b) gain and inverting voltage of complementary inverters annealed at 200 °C versus ambipolar polymers.

Figure 3.1. Structures of **PBDTTPD-Cn**.

Figure 3.2. UV-vis absorption spectra of **PBDTTPD-Cn** in chloroform solution (a) and as a thin solid films spin-cast from chloroform (b) Cyclic voltammograms of **PBDTTPD-Cn** thin films (c) Energy level diagrams for **PBDTTPD-Cn** and PC₇₁BM (d).

Figure 3.3. DFT-optimized geometries and charge-density isosurfaces for BDT-TPD-BDT (B3LYP/6-31G*) (a) and their dihedral angles (b).

Figure 3.4. J-V Characteristics (a) and external quantum efficiency (EQE) spectra of **PBDTTPD-C1** (black), **C3** (blue) and **C4** (red) (b).

Figure 3.5. Grazing incident wide angle X-ray scattering (GIWAXS) results for neat **PCDTTPD-Cn** in-plane and out-of-plane line cuts (a) of the corresponding above patterns (b).

Figure 3.6. GIWAXS images for blends of **PBDTTPD-Cn:PC₇₁BM** and with additive (a). In-plane and out-of-plane line cuts of the corresponding above patterns for **PBDTTPD-Cn:PC₇₁BM** (solid line) and with additive (symbol line)films (b).

Figure 3.7. Atomic force microscopy(AFM) images (2x2 μm^2) of polymer:PC₇₁BM on ITO substrate: root-mean-square (RMS) as (a) 3.32 nm (top), 2.13 nm (bottom) of **PBDTTPD-C1** (b) 5.22 nm (top), 4.02 nm of **PBDTTPD-C3** (c) 7.68 nm (top), 2.64 nm (bottom) of **PBDTTPD-C4**, respectively

Figure 3.8. Double-logarithmic plot from dark J-V characteristics of (a) hole-only devices (ITO/PEDOT:PSS/polymer:PC₇₁BM/Au) and (b) electron only devices (FTO/polymer:PC₇₁BM/Al).

Figure 3.9. The performance of OFETs used OTS treatment as a passive layer (a) The output characteristics, (b) the transfer characteristics and plots of the square root the drain current as a function of the gate voltage for **PBDTTPD-C1**(black), **C3**(blue) and **C4**(red). (I_D : Drain current. V_G : Voltage of gate in an OFET. V_{DS} : Voltage between drain and source in an OFET.)

Figure 4.1. Thermogravimetric analysis (TGA) for DCM-Q-BDT and DCV-B-BDT.

Figure 4.2. UV-Vis absorption spectra of DCM-Q-BDT and DCV-B-BDT in chloroform solution (a) and as a thin solid films spin-cast from chloroform (b) Cyclic voltammograms of DCM-Q-BDT and DCV-B-BDT in dichloromethane solution (c) DFT calculation for DCM-Q-BDT and DCV-B-BDT (d).

Figure 4.3. Top-gate/bottom-contact structure of OFETs and transfer and output curves of DCM-Q-BDT (a), (b) and DCV-B-BDT OFETs(c), (d) without post-annealing treatments.

Figure 4.4. Output curves at low V_{DS} of OFETs with extracted contact resistance by YFM with DCM-Q-BDT (a) and DCV-B-BDT (b), Schematic energy diagram between OFETs electrode and organic semiconductors for carrier injection DCM-Q-BDT and DCV-B-BDT(c).

Figure 4.5. Normalized I_{ds} change of DCM-*Q*-BDT and DCV-*B*-BDT OFETs according to the time in the air for ambient (60% humidity and 25 °C) stability.

Figure 4.6. Atomic force microscopy (AFM) images of DCM-*Q*-BDT and DCV-*B*-BDT on glass substrate at room temperature: height (a); phase (b) for DCM-*Q*-BDT and height (c); phase (d) for DCV-*B*-BDT, respectively.

Figure 4.7. XRD results of DCM-*Q*-BDT and DCV-*B*-BDT thin films at room temperature.

Figure 4.8. GIWAXD images of DCM-*Q*-BDT (a) and DCV-*B*-BDT (b) at room temperature.

List of Tables

Table 2.1. Photophysical and electrochemical properties of BDP-based polymers

Table 2.2. Summary of the electrical characteristics of **PBDP-Fu**, **PBDP-Th**, and **PBDP-Se** OFETs annealed at various temperatures.

Table 2.3. Summary of hole and electron contact resistance for **PBDP-Fu**, **PBDP-Th**, and **PBDP-Se** OFETs various annealed temperatures.

Table 2.4. Summary of hole and electron activation energy (E_A) of **PBDP-Fu**, **PBDP-Th**, and **PBDP-Se** OFETs.

Table 2.5. Summary of Gain and inverting voltage (V_{inv}) for **PBDP-Fu**, **PBDP-Th**, and **PBDP-Se** complementary inverters.

Table 3.1. Photophysical and electrochemical properties of **PBDTTPD-Cn**.

Table 3.2. Parameters of performance for **PBDTTPD-Cn** devices with structure of ITO/PEDT:PSS/Polymer:PC₇₁BM/Al measured under AM 1.5G illumination at 100mW/cm².

Table 3.3. Summary of GIWAXS analysis on **PBDTTPD-Cn** as neat and blend films.

Table 3.4. Calculated electron and hole mobility of **PBDTTPD**-based polymers by space charge limited current (SCLC) devices and their thickness layers.

Table 3.5. Summarized the performance values of OFET device with hole mobility, threshold voltage and on-off ratio for **PBDTTPD-C1**, **C3** and **C4**.

Table 4.1. Optical and electrochemical properties of DCM-*Q*-BDT and DCV-*B*-BDT.

Table 4.2. Electrical characteristics of DCM-*Q*-BDT and DCV-*B*-BDT OFETs depending on the post-annealing temperature.

Table 4.3. Crystallographic parameters calculated from GIWAXD profiles of DCM-*Q*-BDT and DCV-*B*-BDT.

List of Schemes

Scheme 1.1. Chemical procedure for benzene polymerization.

Scheme 1.2. General mechanism for Pd-catalyzed cross coupling reaction.

Scheme 1.3. The discovery of stannane cross coupling reactions

Scheme 1.4. The general reaction a) and mechanism cycle b) for Stille cross coupling reaction.

Scheme 1.5. Example of Suzuki-Miyaura reaction.

Scheme 1.6. Typical Suzuki-Miyaura reaction mechanism cycle.

Scheme 1.7. An example of Knoevenagel condensation reaction

Scheme 1.8. The mechanism for Knoevenagel condensation reaction.

Scheme 2.1. Synthetic routes of BDP-based polymers.

Scheme 3.1. Synthetic routes to **PBDTTTPD-Cn**.

Scheme 4.1. Synthetic routes for DCM-*Q*-BDT and DCV-*B*-BDT.

Nomenclature

OPVs	Organic photovoltaics
OFET	Organic field-effect transistors.
XRD	X-ray diffraction analysis
SCLC	Space charge-limited current (SCLC) model
OLEDs	Organic light emitting diodes
DSSCs	Dye-sensitized solar cells
OFETs	organic field effect transistors
AsF₅	Pentafluoride
CPs	Conducting Polymers
PCs	Phthalocyanines
PCEs	power conversion efficiency
PPV	polyphenylenevinylene
J–V	current density–voltage (PCE)
MEH-PPV	Poly[2-methoxy-5-(2'-ethylhexyloxy)-1,4-phenylenevinylene
P3HT	Poly(3-hexylthiophene))
PCPDTBT	Poly[2,6-(4,4-bis-(2-ethylhexyl)-4H-cyclopenta[2,1- <i>b</i> ;3,4- <i>b'</i>]-dithiophene)-alt-4,7-(2,1,3-benzothiadiazole))]
PCDTBT	Poly[<i>N</i> -9'-heptadecanyl-2,7-carbazole- <i>alt</i> -5,5-(4',7'-di-2-thienyl-2',1',3'-benzothiadiazole)]
PTB7-Th	Poly[4,8-bis(5-(2-ethylhexyl)thiophen-2-yl)benzo[1,2- <i>b</i> :4,5- <i>b'</i>]dithiophene- <i>alt</i> -3-fluorothieno[3,4- <i>b</i>]thiophene-2-carboxylate]
NFAs	Non-fullerene acceptors
PDI	Perylene diimide
NDI	Naphthalene diimide
MOSFET	Metal-oxide-semiconductor FET
MISFET	Metal-insulator-semiconductor FET
IGFET	Insulated gate FET
BG-TC	Bottom-gate and top-contact
BG-BC	Bottom-gate and bottom-contact
TG-BC	Top-gate and bottom-contact
TG-TC	Top-gate and top-contact
DPP	diketopyrrolopyrrole
PPV	Poly(p-phenylene vinylene)
J_{sc}	Short-circuit current density
V_{oc}	Open-circuit voltage
FF	Fill factor
P_m	The maximum power point
BDT	4,8-bis(alkyloxy)benzo[1,2- <i>b</i> :4,5- <i>b'</i>]dithiophene
BDP	Benzodipyrrolidone
IIG	Isindigo
TIIG	Thienoisindigo
ICT	Intramolecular charge transfer
HOMO	Highest occupied molecular orbital

LUMO	Lowest unoccupied molecular orbital
XRD	X-ray diffraction
AFM	Atomic force microscopy
RMS	Root mean square
TMS	Tetramethylsilane
BHJ	Bulk-heterojunction
<i>n</i>-Bu₄NPF₆	0.1 M tetra- <i>n</i> -butylammonium hexafluorophosphate
D-A	Donor-acceptor
TT	Thieno[3,4- <i>b</i>]thiophene
DTBT	4,7-dithiophene-2-yl-2,1,3-benzothiadiazole
TPD	<i>N</i> -alkylthieno[3,4- <i>c</i>]pyrrole-4,6-dione (TPD)
DFT	Density functional theory high PCE in BHJ devices. Beside
GIWAX	Grazing-incidence wide-angle X-ray scattering
CV	Cyclic voltammetry
DDQ	2,3-dichloro-5,6-dicyano-1,4-benzoquinone
TGA	Thermogravimetric analysis
T_d	The 5% weight-loss temperatures
OSCs	Organic semiconductors

Chapter I

Introduction

1. General Conjugated Conducting Materials: A Brief Overview.

1.1 The History of Conducting Materials

A polymer so-called 'plastics' has been widely used before 1970s as electrical insulator because of their intrinsic properties that have high resistance and do not comprise valence band in the system like pure metal.^{1,2}

For decades ago, however, long chain polyene have been studied by scientists as possibilities of conductor or semiconductors. In 1958, the presence of Ziegler Natta catalysts were able to overcome a limit to the length of polyene.³ Since then, the synthesis and characterization of conducting polymer was first reported by Pohl, Katon and their co-workers in 1960s, which the discovery took the first step toward conducting polymer research.⁴

At the beginning of 1970s, Shirakawa and their co-workers synthesized polyacetylene through serendipitous addition of 1000 times the typical amount catalyst when they proceed polymerization.⁵ After that, this collaborated with MacDiarmid and Heeger group for studying electrical conduction of polymer. (see **Figure 1.1**) In 1977, they reported that conjugated polymer, polyacetylene, shows high electrical conductivity when exposed strong acceptor such as halogens chlorine, bromine (Br_2), iodine (I_2), and arsenic pentafluoride (AsF_5),^{6,7} whose scientific breakthrough revolutionized macromolecular chemistry field as seen in **Figure 1.2** as well as electronic application such as organic light emitting diodes (OLEDs),^{8,9} organic photovoltaics (OPVs),^{10,11} and organic field effect transistors (OFETs),^{12,13} dye-sensitized solar cells (DSSCs),^{14,15} and chemical sensors.¹⁶ (see **Figure 1.3**)



Figure 1.1. The Nobel Prize in Chemistry 2000 was awarded jointly to Alan J. Heeger, Alan G. (a) MacDiarmid (b) and Hideki Shirakawa (c) "for the discovery and development of conductive polymers".

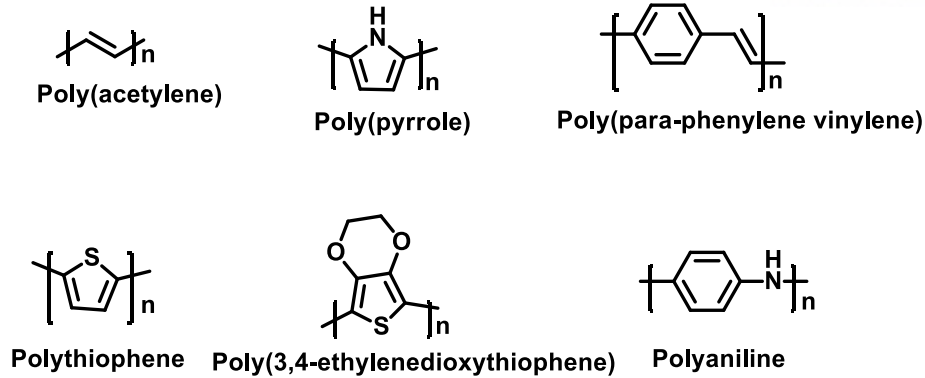


Figure 1.2. Examples of representative conjugated polymers.

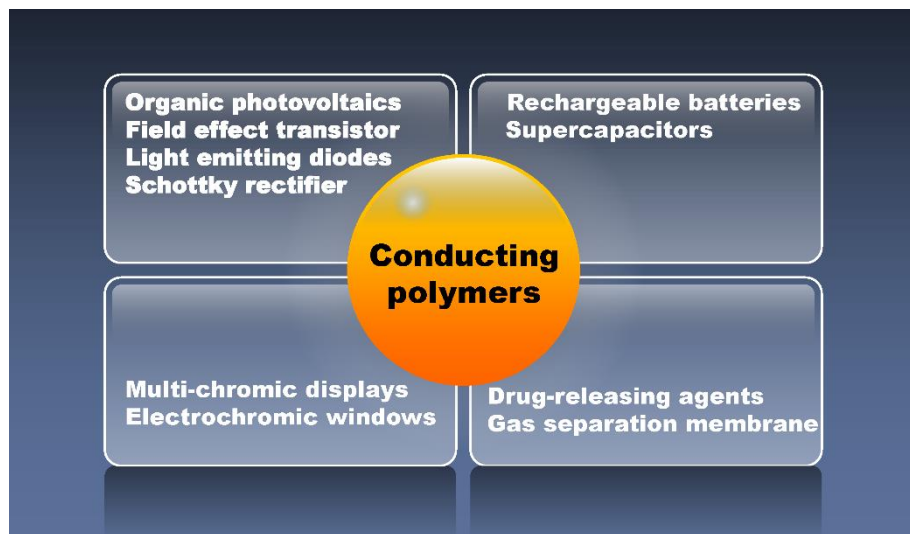


Figure 1.3. Potential applications of conducting polymers.

1.2 The Electromagnetic Theory for Conducting Polymers (CPs)

The conjugated polymers which consists of alternating single and double bond in the polymer chain enable electron to delocalize in the polymer system due to their unique conjugation system. In addition, the delocalized electron may move along conjugated chain, giving rise to the conductivity in CPs.¹⁷ However, such CPs with regard to bond alternation are difficult to transfer electron in the system because of an energy band gap in the energy spectrum.^{18,19}

Figure 1.4 presented conductivity comparison between conducting polymer and other materials inorganic materials. As seen in **Figure 1.4**, doping process could be facilitated by helping π -electron transfer in the conjugated polymer chain because the presence of doping in polymer chain, which loosely bound, is able to jump energy band gap. Consequently, doped conjugated polymers have good conductor for two reasons: i) *n*-type (reduces) or *p*-type (oxidize) can be doped to relatively high charge carrier densities now that every conjugated repeat unit have a potential. ii)

The attraction of electron in conjugated system influences nuclei in the neighboring repeat unit, leading to delocalization along polymer chain and charge carrier mobility. (Figure 1.5 showed basic doping system in polyacetylene)²⁰

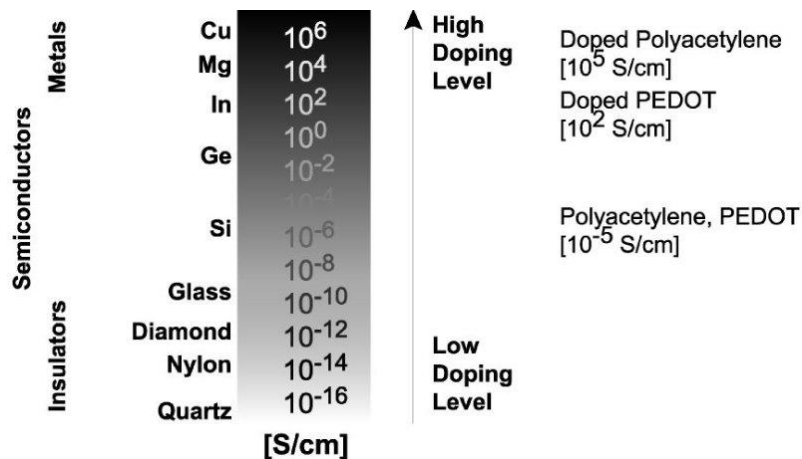
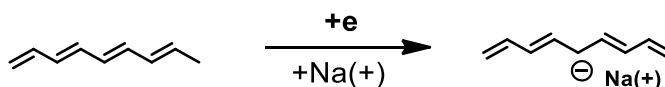


Figure 1.4. A broad conductivity range from inorganic materials to doped conjugated materials.

n-type doping: reduction with cations



p-type doping: oxidation with anions

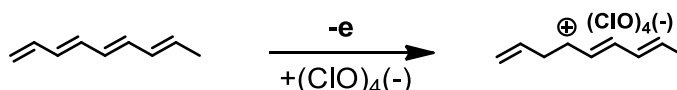
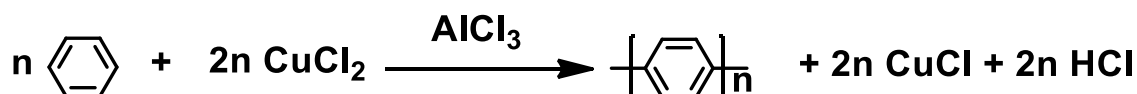


Figure 1.5. Basic *n*-type and *p*-type doping processes of polyacetylene.

1.3. Conjugated Materials Synthesis: Methods and Reactions

1.3.1. Chemical and Electrical Polymerization

In terms of synthetic methods used to build conjugated polymer, this can be classified two strategies. One synthetic method is chemically polymerization through chemical reaction as it used oxidant reagent and catalyst in suitable solvent. Scheme 1.1 is one of the classic chemical procedure for benzene polymerization by Kovacic.²¹



Scheme 1.1. Chemical procedure for benzene polymerization.

The second method is electrochemical polymerization ²², which contains placing both of two electrode (reference and count electrode) into the solution that dissolved chemical monomer and dopant in a solvent as seen in **Figure 1.6**. After that, by applying voltage, the monomer starts to polymer film on the working electrode surface. Both chemical and electrochemical procedures have cons and pros. The major advantage of chemical polymerization ^{22,23} is able to mass produce products at the reasonable cost whereas by product can happen, in accordance with chemical reaction rate or scale. On the other hand, the electrochemical polymerization can directly forms conducting polymer film that highly conductivity as well as suitable for use in electric devices. In this section, general chemical polymerization methods are briefly investigated for effective conjugated polymer process, and their some examples are described.

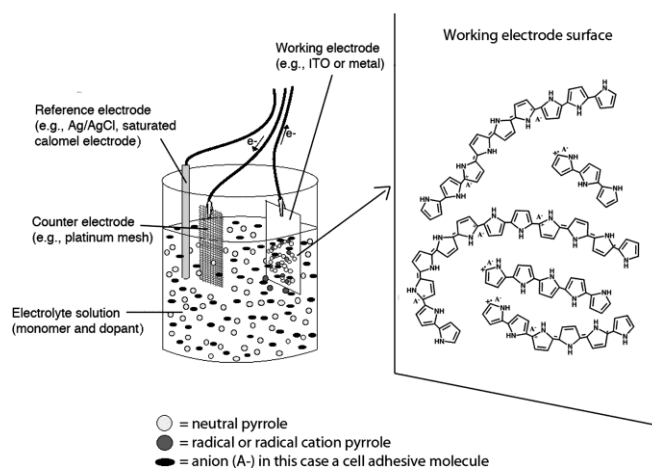


Figure 1.6. Example of electrochemical polymerization. ²⁴

1.3.2. Palladium (Pd) Catalyzed Cross Coupling Reaction

Figure 1.7 outlined timeline of metal-catalyzed cross coupling reactions from the early 19th to 20th. Among such numerous metal-catalyzed cross coupling reactions, the discovery of C-C bond forming processes using palladium catalyst brought a great change for chemical synthesis research area, both in academia and in industry. ²⁵ (In 2010, Heck ²⁶, Negishi ²⁷, and Suzuki²⁸ were received the Nobel Prize in chemistry for “palladium-catalyzed cross-coupling in organic synthesis”) In particular, today, together with the development of polycondensation method as well as new type molecular back bones for electronic applications, palladium cross-coupling reaction such as Suzuki and Stille reaction plays a critical role as commonly used synthetic method.

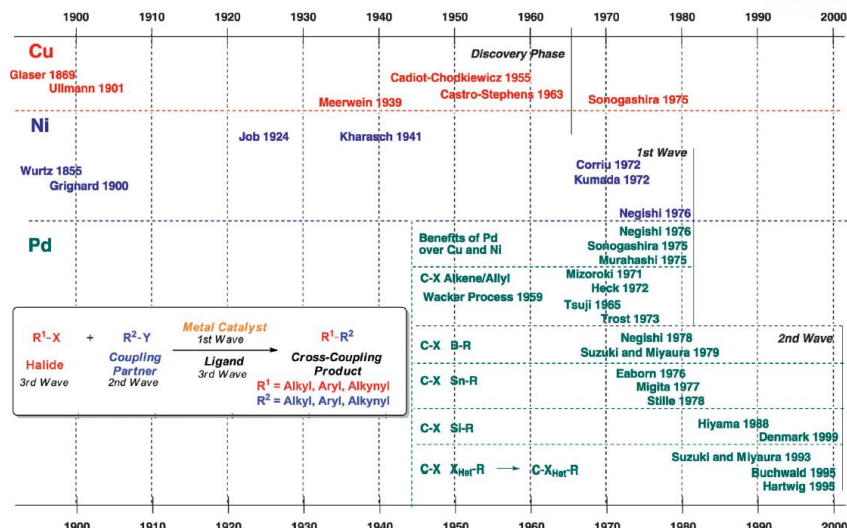
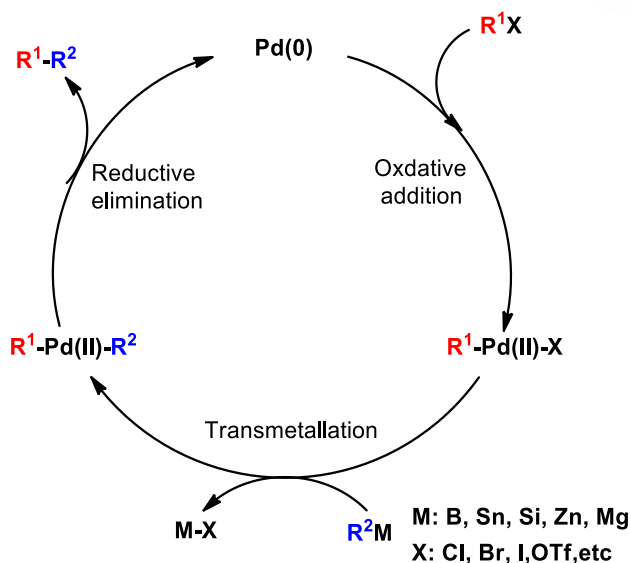


Figure 1.7. A brief history table of discovery and development metal-catalyzed name reactions.²⁵

1.3.2.1. Understanding Palladium Catalytic Cycle

Even if the mechanism for metal-catalyzed coupling reactions is not perfectly presented, generally, to date, well-known mechanisms for these Pd-catalyzed cross coupling reactions are depicted in **Scheme 1.2**. Firstly the catalyst sources such as $\text{Pd}_2(\text{dba})_3$ or $\text{Pd}(\text{OAc})_2$ containing the vital ligand or $\text{Pd}(\text{PPh}_3)_4$ or $\text{Pd}(\text{PtBu}_3)_2$, a preformed catalyst, can be formed by oxidative addition of organic halides or triflate group (ordered reactivity of X usually $\text{I} > \text{OTf} \sim \text{Br} \gg \text{Cl}$, alkenyl- $\text{OTf} \gg$ aryl- OTf). Subsequently through transmetalation step, another counterpart with halides or triflate group can be transferred from metal to other halides or triflate. At this moment this process is irreversible step by thermal dynamic and kinetic theory, but the exactly mechanism is still disclosed. In the final step of catalytic cycle, reductive elimination results in C-C bond formation with the regeneration of Pd (0) species to re-enter into the catalytic cycle.^{29,30}

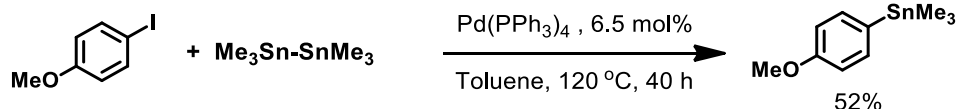


Scheme 1.2. A universal mechanism of Pd-catalyzed cross-coupling reaction.

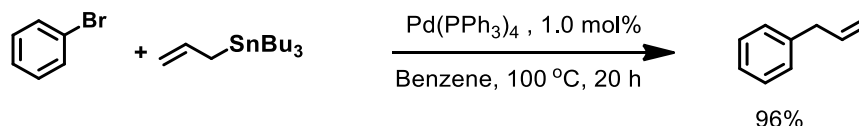
1.3.2.2. Stille Coupling Reaction

In 1973, before the development of Stille coupling reaction, Atwell and Bokermen proved that the reaction of allyl halides with a disilane under palladium catalysis can form the corresponding organosilane derivatives.³¹ Subsequently Matsumoto showed that aryl bromides react with hexamethyldisilane.^{32,33} However, these organometallic reactions, including organosilane groups, were not reported under the reaction conditions, and the discovery of organotin reagents provided us with numerous synthetic methodologies. In 1977, Eaborn first reported the cross-coupling of organodistannane reagents with aryl iodides under palladium catalysis. Shortly thereafter, Migita reported on the Pd-catalyzed cross-couplings of organotin reagents with aryl bromides.³² Based on initial reactions, Stille and Milstein showed the synthesis of ketones by the coupling of aryl chlorides with organostannanes under mild conditions.^{33,34} (see **Scheme 1.3**) In the beginning of the 1980s, Stille further investigated and developed the reaction using organostannanes to apply various organic functional groups and C-C bonds. Such remarkable and broad bonding capabilities changed the way chemists thought about complicated synthetic routes.³¹ In addition, with the rapid growth of donor-acceptor alternating conjugated polymers for electronic applications, this reaction has attracted avid attention as a new step polymerization method because of its high selectivity, leading to low homo polymer and molecular weight. Nonetheless, the disadvantages of toxicity and a harmful effect on the environment of organostannanes would need to be further discussed. Typical reactions for Stille cross-coupling consist of the interaction of organostannanes and halides, shown in **Scheme 1.4a** and the mechanism is the same as the general palladium-catalyzed cycle: oxidation, transmetallation, and reductive elimination, depicted in **Scheme 1.4b**.

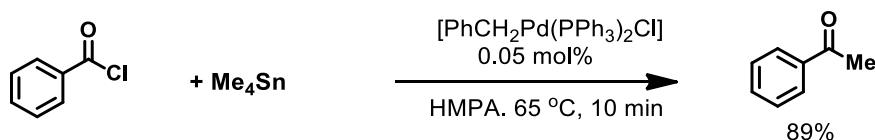
Eaborn 1976



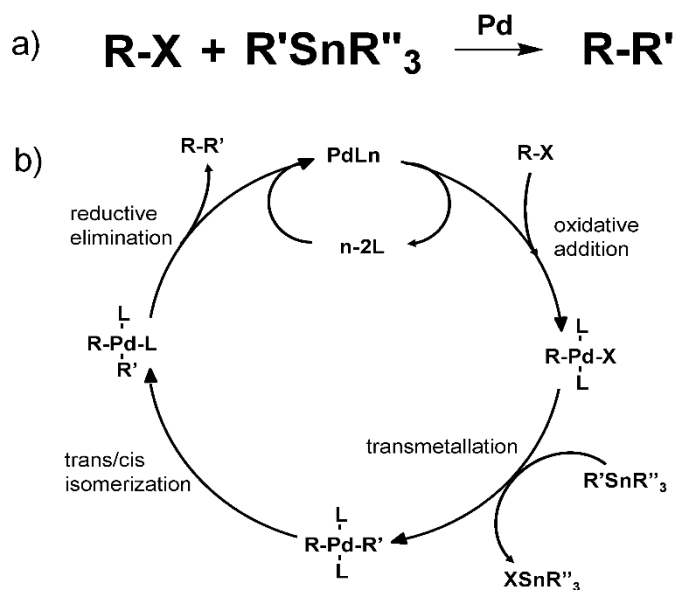
Migita 1977



Stille 1978



Scheme 1.3. The discovery of stannane cross coupling reactions

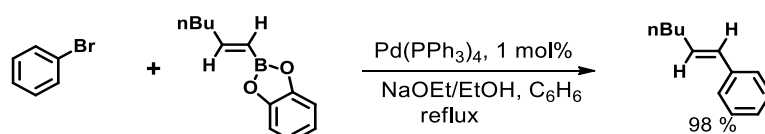


Scheme 1.4. The general reaction a) and mechanism cycle b) for Stille cross coupling reaction.

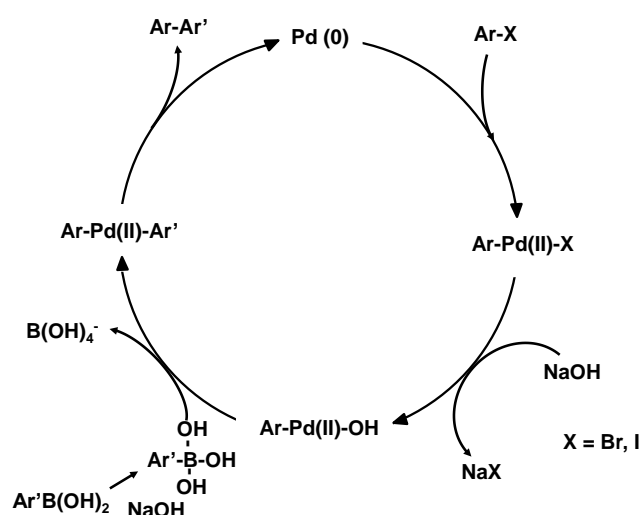
1.3.2.3. Suzuki-Miyaura Cross Coupling Reaction

Although, in 1975³⁵, Heck and their research group had reported that boronic acid as cross coupling partner under palladium catalyst can be shown, it might be, in reality, Suzuki-Miyaura reaction, developed in 1979 by Suzuki and Miyaura, which name reaction could be moved into catalyst field.³⁶ (Scheme 1.5) Such a useful and powerful chemical reaction that formed C-C bond has many advantages comparing with other Pd-catalyst cross coupling.³⁷ Firstly organoboron designed to withstand air and moisture can facilitate reaction handling. In addition, this chemical

reaction is able to afford high products yield under mild and convenient reaction conditions. Finally the less-toxic byproducts, relatively, are very easy to remove or recover. For these reasons, Suzuki-Miyaura reaction has attracted attention for industrial field need to be scaled up. As shown in **Scheme 1.6**, Suzuki-Miyaura mechanism cycle does not differ greatly in appearance from original Pd-catalyzed or Stille cross coupling. Compared to other things, the tiny difference is that for enhancing polarization of organic ligand and facilitating transmetalation the organoboronic acid should be needed with base.



Scheme 1.5. Example of Suzuki-Miyaura reaction.²⁵



Scheme 1.6. Typical Suzuki-Miyaura reaction mechanism cycle.

1.3.2.4. Some Examples of Conjugated polymers *via* Stille and Suzuki-Miyaura Reaction

Since the development of alternating donor acceptor conjugated polymer in organic electronics, Stille and Suzuki cross coupling are one of the most common way for polymerization. The Stille polycondensation is mainly consists of ditincompounds as donor unit and dihalide compounds as acceptor unit. According to the reaction mechanism, organohalides or triflates carrying electron-withdrawing groups can facilitate the first oxidative addition step. For the second transmetalation step, the process may also be facilitated by organotin compounds with electron-rich properties. Therefore, the best combination for high molecular weight polymers is to construct electron-rich organotin compounds and an electron-deficient halide or triflate, as shown in **Figure 1.8a**.³⁸ The

Suzuki polycondensation, on the other hand, involves coupling reaction of diboronocompounds and dihalide compounds, but the reaction mechanism is similar to Stille polycondensation. (Figure 1.8b).³⁹

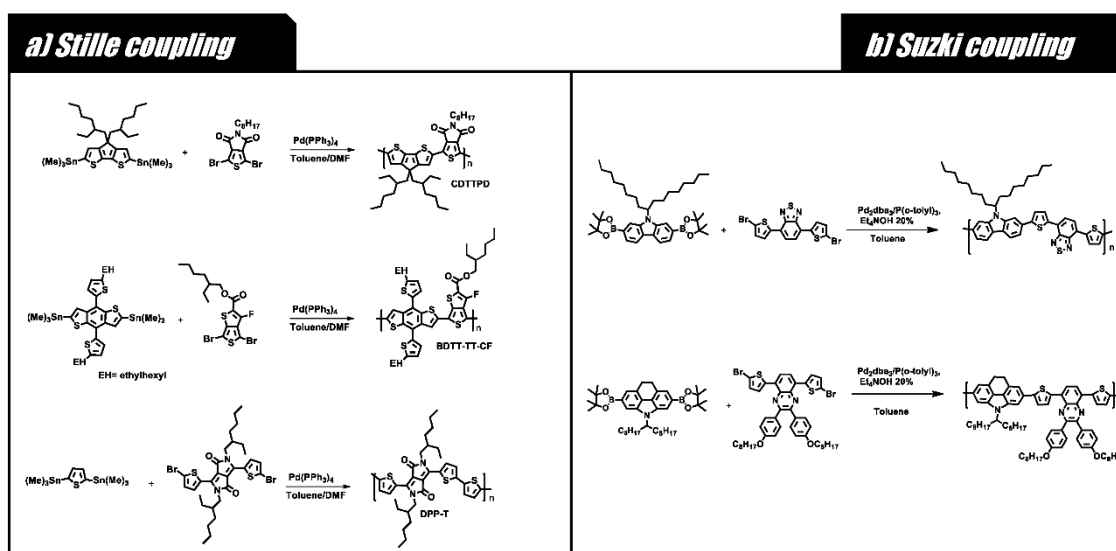
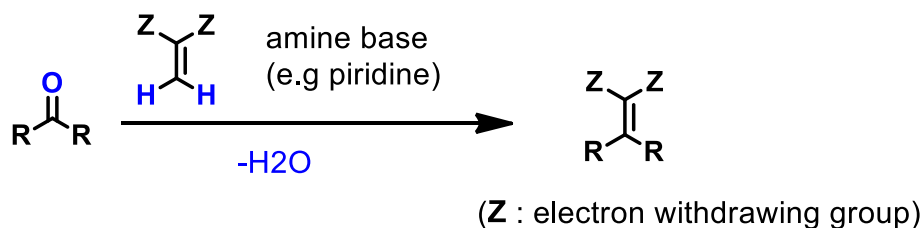


Figure 1.8. Examples of conjugated polymers using Stille reaction a) and Suzuki reaction b).⁴⁰⁻⁴²

1.3.3 Knoevenagel Condensation for Conjugated Small Molecules

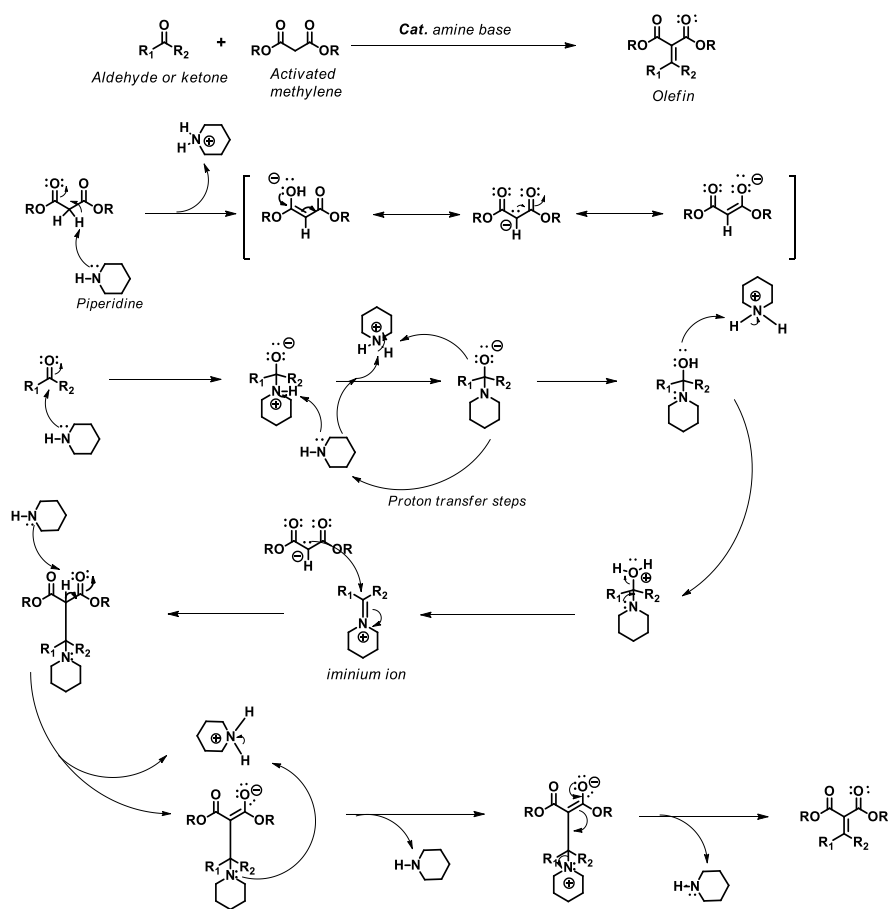
Knoevenagel condensations which one of classic and useful C-C formation named reaction in organic chemistry were discovered by the Germany chemist Emil Knoevenagel in 1894. These condensations are formed by ketone and active methylene compounds with ammonia or amine analogues as catalyst in organic solvents, as depicted in Scheme 1.7. These reactions are basically considered to be modification of aldol reaction. Compared to aldol reaction with carbonyl group, Knoevenagel condensation has higher acidity of active methylene hydrogen.⁴³

Subsequently, the Doebner modification in 1900 that utilized pyridine as solvent and piperidine as catalyst was introduced to Knoevenagel condensation. In addition to the Doebner modification, these condensations affected the Hantzsch pyridine synthesis,^{44,45} the Gewald reaction^{46,47} and the Feist–Benary furan synthesis,⁴⁸ leading to the discovery of CS gas.⁴⁹



Scheme 1.7. An example of Knoevenagel condensation reaction.

The general mechanism for Knoevenagel condensation reaction is illustrated in **Scheme 1.8**. The reaction starts with deprotonation of the activated methylene by base such as piperidine and formed a resonance stabilized enolate. Afterwards, the intermediate form gets deprotonated by the base to give another enolate whilst the amine or piperidine of the intermediate gets protonated. Subsequently, a rearrangement of the amine base, regenerating the catalyst, and afforded the final olefin product.⁵⁰



Scheme 1.8. The mechanism for Knoevenagel condensation reaction.

1.4. Electronic Applications

Since inorganic or metal is always concerned with the depletion of natural resources as well as the environment harm by their toxicity, potential electronics for organic material, including conjugated polymer and small molecules can be a good alternative. In this chapter, here, organic electronic applications using conjugated materials are introduced, and the principles of operation of devices are discussed.

1.4.1. Organic Photovoltaics (OPVs)

1.4.1.1. A Brief History of Development of OPVs

As depicted in **Figure 1.9**, in 1839,⁵¹ photovoltaic effect, which was discovered by Becquerel, leads to the first report on photoconductivity in 1873 and 1876, respectively. (Smith and Adams) Since then, anthracene was the first organic compound in which photoconductivity was founded by Pochettino in 1906 and Volmer in 1913.⁵² After a long time, in the late 1950s and early 1960s, the observation that organic materials, such as methylene blue, had conducting properties and photovoltaic (PV) effect gave related research group good motivation and the major reasons for discovering many organic dyes such as carotenes, chlorophylls⁵³ and other porphyrins,⁵⁴ as well as the structural related phthalocyanines (PC).⁵⁵ Despite the improvement of OPVs, they still had many technical limitations for reaching the market place compared to inorganic photovoltaics. Inorganic solar cell base on silicon (Si) was firstly developed at Bell laboratories in 1954 and had a power conversion efficiency (PCE) of around 6 %.⁵⁶ Whereafter, through the betterment of Si purity, state-of-the-arts it achieved the PCE of close to 40 %. Together with the development of inorganic solar cell, OPVs also make great strides in efficiency and technical limitations for communication over last two decades. Currently, the efficiency of OPVs has achieved up to 10~12 %, meaning that it is able to apply to industry. (see **Figure 1.10**) Both of inorganic/organic solar cells which may seem similar, but they have different working principle and applied area has been continuously studied as next energy generation to replace a fossil fuel. ⁵²

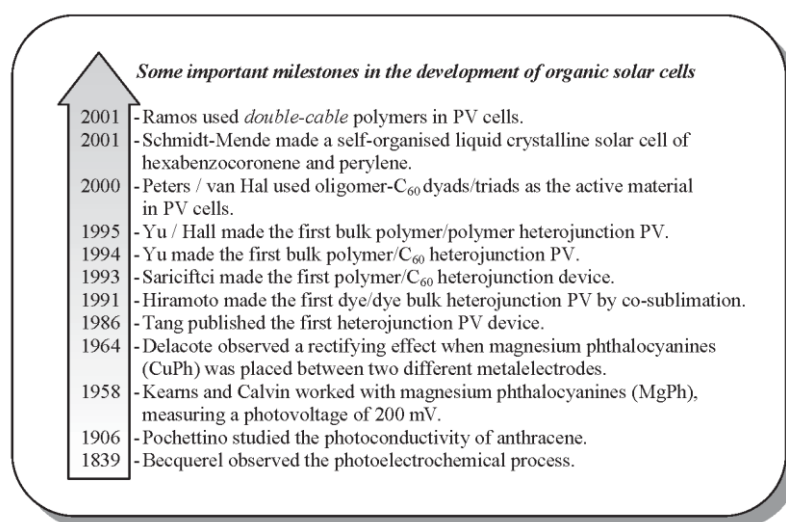


Figure 1.9. A representative OPVs history developed.⁵²

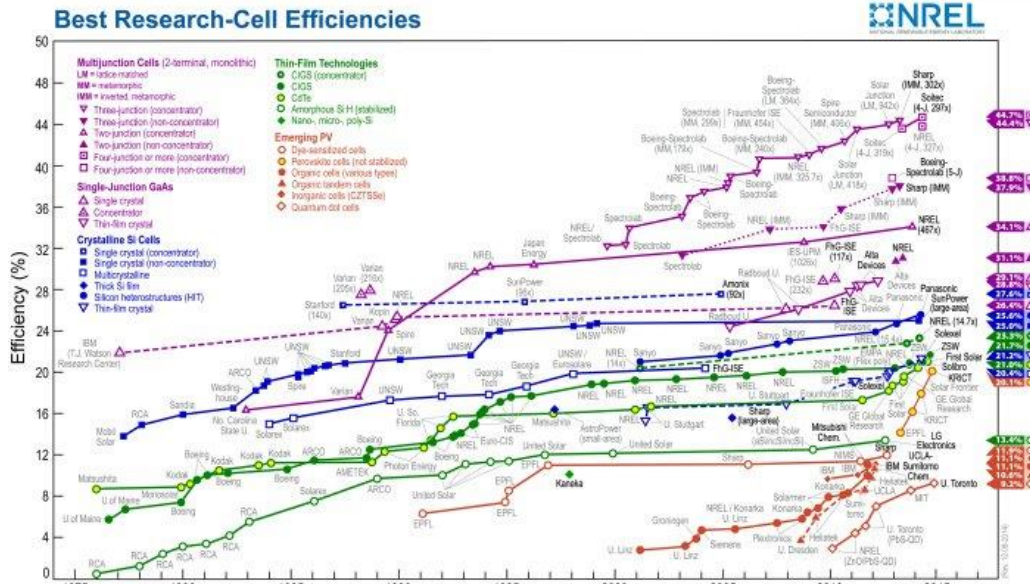


Figure 1.10. Best solar cell efficiencies chart from NREL in 2010.⁵⁷

1.4.1.2. Device Structures and Working Mechanism

Depending on a number of layer and priority coated, OPV devices have different architectures, as shown in **Figure 1.10**. Normal (or conventional) device structure,⁵⁷ where active materials are sandwiched between two different metal electrodes with different work function. Indium-tin-oxide (ITO), one of the conductive and transparent material, on flexible plastic or glass, is often used as anode. Conjugated polymers or small molecules as active material are mainly used and can be divided into *n*-type and *p*-type from molecular energy level. The other metal electrodes as cathode (e.g. Al, LiF/Al, Ca/Al) are vacuum deposited onto active layer.⁵⁸ In addition to standard device architecture, hole transport buffer layers such as PEDOT:PSS, polyelectrolytes⁵⁹ between active layer and anode are introduced to prevent from anode and facilitate electron transfer. Inverted device structure, which geometry consisted of switched electrode and different buffer layer, often, used for increasing device stability from air, resulting in large area printing process, as depicted in **Figure 1.11a**. Recently, unlike two single cell, multiple active layers with different absorption spectra and band gaps, so-called tandem cell, sometimes are applied to achieve high power conversion efficiencies. Moreover, OPV unique system such as bulk heterojunction composed of the mixture of electron donor and acceptor have developed to enhance solar cell efficiency, as shown in **Figure 1.11c**.³⁸

The photocurrent generation of OPV system in bulk heterojunction is multiple steps, as demonstrated in **Figure 1.11b**. In short, there are following four steps: (1) light absorption and exciton generation (2) exciton dissociation into free carriers (holes and electrons) (3) the free carriers are transported to their respective electrodes via the drift/diffusion phenomenon under the

influence of the built-in potential and (4) collection of the free carriers at the electrodes and the current flows through the external load.

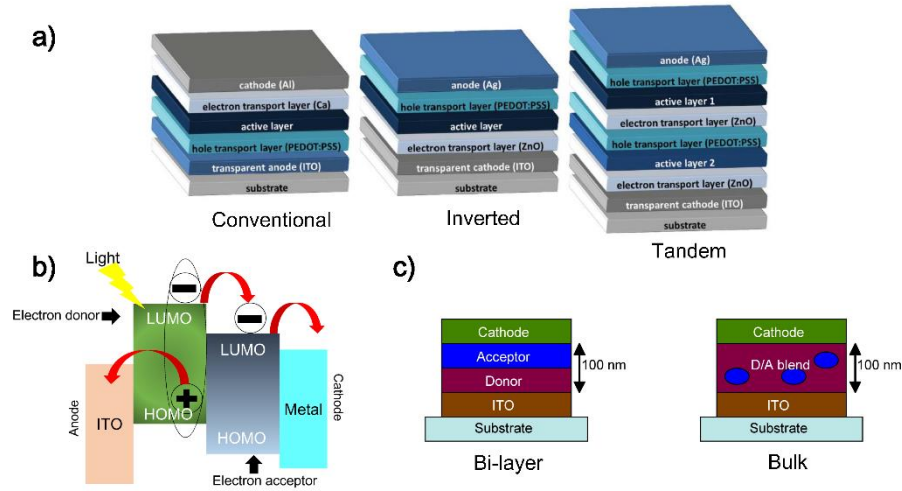


Figure 1.11. Schematics of OPV device structure (conventional, inverted, and tandem from left) a), operating principle b), and bi-layer (left) and bulk heterojunction structures (right) between donor and acceptor c) for OPVs.

1.4.1.3. Device Characterization

To characterize OPV performance, power conversion efficiency (PCE) is important parameter, which is defined as the percentage of maximum output of electrical power to the incident light power. A brief overview of general solar cell equation can be estimated by (eq.1) and **Figure 1.12** shows a schematic of a current density–voltage (J – V) characteristic for a typical hybrid solar cell in the dark and under illumination.

$$PCE = \frac{P_m}{P_{in}} = \frac{J_{sc} \times V_{oc} \times FF}{P_{in}} \quad [\text{eq. 1}]$$

Where, P_m is maximum power point, P_{in} is the incident light intensity, J_{sc} is the short-circuit current density, and V_{oc} is the open-circuit voltage, and FF is the fill factor, which is described as the ratio of P_m to the product of J_{sc} and V_{oc} . (eq.2)

$$FF = \frac{P_m}{J_{sc} \times V_{oc}} \quad [\text{eq. 2}]$$

International accepted solar intensity conditions, which are referred are to a cell temperature of 25 °C under air mass 1.5 global (AM1.5G) illumination spectrum at an intensity of 1000 W m⁻², is very crucial rule to reduce errors with various results from many related research group. Here, the AM1.5G condition corresponds to the spectrum and irradiance of sunlight incident upon an inclined plane at 37° tilt towards the equator with an elevation of 41.81° above the horizon as shown in **Figure 1.12a**. External quantum efficiency (EQE) is another important parameter for

solar cell characterization. It is calculated by the number of electrons extracted in an external circuit divided by the number of incident photons at a certain wavelength under short-circuit condition.

$$\text{EQE}(\lambda) = \frac{\text{number of electrons}}{\text{number of photons}} = \frac{J_{sc}(\lambda)/e}{P_{in}(\lambda)/(hc/\lambda)} = \frac{J_{sc}(\lambda)/hc}{P_{in}(\lambda)e\lambda} \quad [\text{eq. 3}]$$

where λ is the wavelength, e is the elementary charge, h is the Planck constant, and c is the speed of light in vacuum.

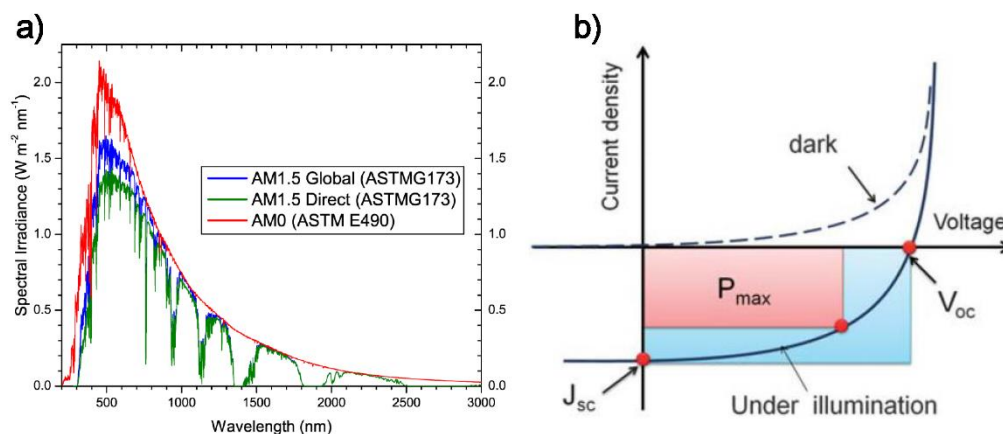


Figure 1.12. The global standard spectrum* a), and current density–voltage (J – V) characteristic of a typical solar cell in the dark (dashed line) and under illumination (solid line). Typical solar cell parameters such as short-circuit current density J_{sc} , open-circuit voltage V_{oc} , and the maximum power point P_m are illustrated on the graph b).⁶⁰ (*<http://www.pveducation.org/pvc/drom/appendices/standard-solar-spectra>)

1.4.1.4. Organic Active Materials for OPVs

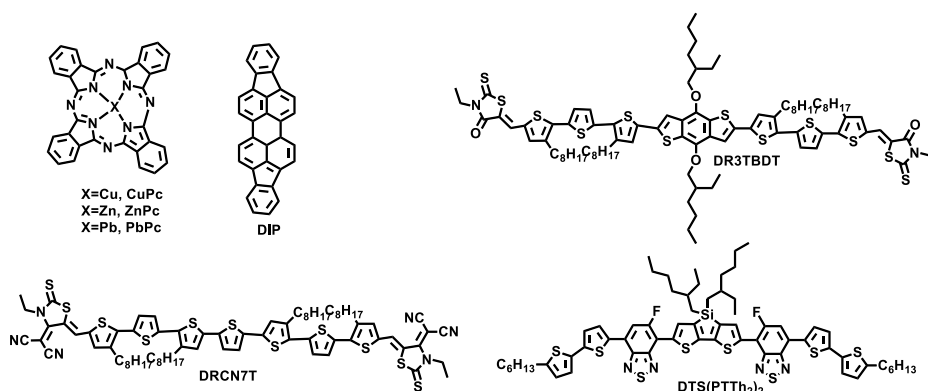
To generate charge in OPV system, active materials which consist of HOMO and LUMO energy level are undoubtedly essential with new device architecture. Accordingly, the design of both the donor and acceptor active materials has been remarkably developed. In case of p-type active materials (see **Figure 1.13**), vapor-deposited two common small molecules started from the development of copper and zinc phthalocyanines and polyphenylenevinylene (PPV) derivatives as polymer used in OPV cells. Subsequently, poly[2-methoxy-5-(2'-ethylhexyloxy)-1,4-phenylenevinylene] (MEH-PPV) achieved PCE of 2.07 % in the BHJ OPV device.^{61,62} Since then, Tajima et al showed improved PCE of ~3% *via* modified MEH-PPV (poly[2-methoxy-1-5-(3,7-dimethyloxy)-1,4-phenylenevinylene, so-called MDMO-PPV]⁶³ Among these conjugated polymers, poly(3-hexylthiophene) (P3HT) is the most commonly used polymer as donor material. The PCE of this material (around 4-5%) maintained top ranking in OPV filed for a few years and have been studied until now.⁶⁴ After developing homo-polymers for OPVs, many research group became interested in molecular energy level control of active materials to seek optimal OPV condition and they finally found that the design of an alternating donor and acceptor structure is

one of the most useful method for reducing bandgap polymers and improving the solar spectrum coverage, leading to new hybridized HOMO/LUMO orbitals and a narrower optical gap than either the donor or acceptor unit.⁶⁵ Furthermore, low band gap materials using the different ability of donor and acceptor were developed. For example, poly[2,6-(4,4-bis-(2-ethylhexyl)-4H-cyclopenta[2,1-*b*:3,4-*b'*]-dithiophene)-alt-4,7-(2,1,3-benzothiadiazole)] (PCPDTBT),⁶⁶

incorporating of a dialkyl-cyclopentabithiophene as donor unit and a benzothiadiazole as acceptor unit is representative low optical bandgap polymer with optical bandgap of about 1.4 eV and a long-wavelength absorption edge of up to 900 nm, which not only shows efficiency of up to ~5 %, but can apply tandem solar cell structure.⁶⁷

Additionally, the discovery of diverse electron weak donor units such as fluorene, carbazole, contributes to deep HOMO level control, resulting in synthesis of poly[*N*-9'-heptadecanyl-2,7-carbazole-*alt*-5,5-(4',7'-di-2-thienyl-2',1',3'-benzothiadiazole)] (PCDTBT).¹⁰ Benzo[1,2-*b*:4,5-*b'*]dithiophene (BDT), currently, has attracted attention as promising donor unit and studied by many scientists.⁶⁸ To date, poly[4,8-bis(5-(2-ethylhexyl)thiophen-2-yl)benzo[1,2-*b*:4,5-*b'*]dithiophene-*alt*-3-fluorothieno[3,4-*b*]thiophene-2-carboxylate] (PTB7-Th) as polymer solar cell has recorded best PCE that exceed 10%.^{69,70} Since the discovery solution-processed *p*-type small molecules (or oligomer) for OPVs, These active materials, also, have been significant exploited for the last 4-5 years in company with diverse *p*-type polymers. Recently, Bazan and their co-worker firstly reported high PCE of exceed 6% *via* blending system of small molecule, DTS(FBTTTh₂)₂, as donor unit and PC₇₁BM as acceptor.⁷¹ Y. Chen et al. presented acceptor-donor-acceptor type small molecules, the so-called DR3TBDT and DRCN7T, with extremely high PCEs of 8-9 % in BHJ system.^{71,72} At present, such small molecules, containing BDT or SiDT core unit are most popular among *p*-type small molecules and based on them, the research still actively being studied.

p-type smallmolecules



p-type polymers

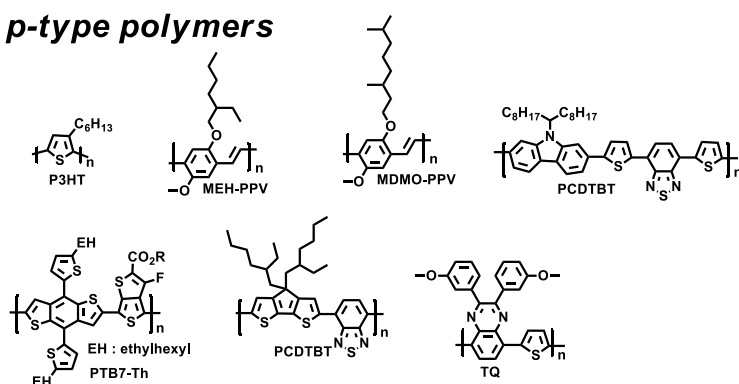


Figure 1.13. The chemical structures of *p*-type active materials for OPVs.

In case of *n*-type materials for OPVs (see **Figure 1.14**), since PCBM firstly have been developed by Wudl *et al.* fullerene derivatives such as PC₆₁BM and PC₇₁BM showed powerful and successful solar performance for a long time under bulk heterojunction system.^{73,74} Nonetheless, the modified fullerenes have some disadvantages, such as limited absorption, spectral breadth as well as band gap control. Subsequently, small molecules and polymers based on a rylene dye have been widely applied to non-fullerene acceptors (NFAs)⁷⁵ thanks to their similar electron affinities with PCBM, outstanding photo-stability, and easy alternation of their band gap tuning. For example, polymer acceptors incorporating rylene diimides such as perylene diimide (PDI),⁷⁶ naphthalene diimide (NDI) and their analogs were designed. Zhan *et al.* announced the first soluble polymer based on rylene with high mobility ($1.3 \times 10^{-2} \text{ cm}^2\text{V}^{-1}\text{s}^{-1}$) and PCE of 1.3 % in BHJ OPVs.⁷⁷ Marks *et al.* developed polymer acceptors based on NDI derived from PDI and showed a PCE of around 2.7%.⁷⁸ However, in terms of efficiency, these molecules still have showed the lack of performance to replace modified fullerene series. Very recently, calamitic shaped molecules, which consist of electron donor and strong electron acceptor, have showed an exceptional growth as a promising class of NFAs.⁷⁹ Sarah Holliday *et al.* reported new non-

fullerene acceptor with fluorine as electron donor unit, benzothiadiazole as electron deficient unit, and rhodanine as flank group, which gave PCE up to 4.11% under inverted OPV system employing P3HT as donor.⁸⁰ Xiaowei Zhan and their co-workers firstly exhibited a novel small molecule based indacenodithiophene and 1,1-dicyanomethylene-3-indanone and PCE of 3.93% with PBDTTT-C-T.⁸¹ Since then, such small molecule was modified and showed excellent PCE of up to 6.31%, blending with PTB7 as donor unit in fullerene-free solar cell system.⁸² Yongfang Li *et al.* developed PCE of up to 9.53% using a medium band gap polymers composed of bithienylbenzodithiophene-alt-fluorobenzotriazole copolymers, which result is among best solar cell efficiency reported for non-fullerene system.⁸³

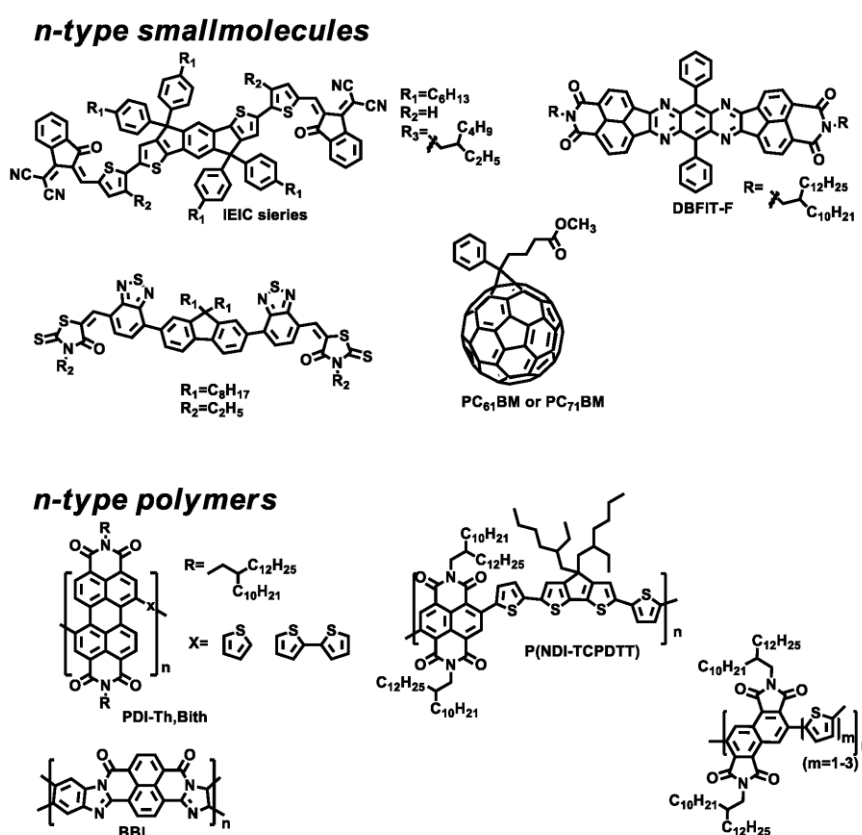


Figure 1.14. The chemical structures of *n*-type active materials for OPVs.

1.4.2. Organic Field-Effect Transistors (OFETs)

1.4.2.1. A Brief History of Development of OFETs

The development of field-effect transistors (FETs) was firstly suggested by Lilienfeld in 1930.⁸⁴ Subsequently, the first silicon-based metal-oxide-semiconductor FET (MOSFET) was fabricated by Kahng and Atalla in 1960s.⁸⁵ Nowadays, the MOSFET based on inorganic materials is the most prominent constituent of modern industry. The MOSFET can be divided into MISFET

(metal-insulator-semiconductor FET), which will be mainly used here, and IGFET (insulated gate FET), according to device structure as shown in **Figure 1.15**. The MOSFETs are mainly fabricated with single-crystalline silicon, due to the excellent quality of the silicon–silicon oxide interface. Unlike FETs based on inorganic materials, although the initial studies on organic field-effect transistors (OFETs) described new fundamental issues of semiconducting and their great potential for next generation device in 1970s,^{76,80,86} synthesis of organic materials for semiconducting was not major in this field before 1980s. Koezuka *et al.* reported, in 1987, chemical structure based on electrochemically polymerized polythiophene and their electronic device application.^{87,88} Afterwards, various organic materials, which are based on π -conjugated small molecules and polymer, have been developed because of their advantages, such as inexpensive, large area, and flexible fabrication. Additionally, organic materials can easily and freely molecular design to optimize charge transport, band gap and energy level control, compared with inorganic materials. At present, in terms of the efficiency for OFETs, some organic materials based FETs already achieved high mobilities of over $10 \text{ cm}^2\text{V}^{-1}\text{s}^{-1}$, exceeding amorphous silicon based FETs.^{89,90} However, the research for improving performance and stabilities is still needed to compete with crystallized silicon based FETs and to apply industry.

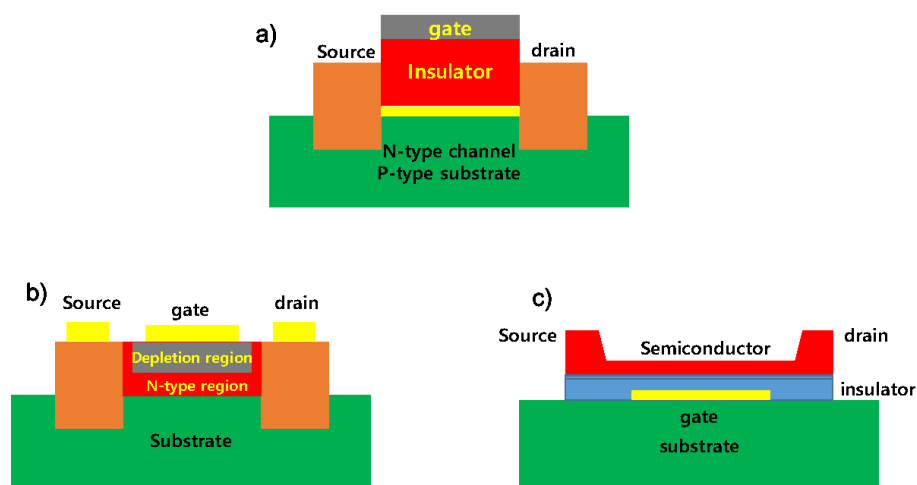


Figure 1.15. Device structures of three kinds of field-effect transistor: a) the metal insulator-semiconductor FET (MISFET), b) the metal-semiconductor FET (MESFET), and c) the thin film transistor (TFT)

1.4.2.2. The Device Architectures and Working Principle for OFETs

Figure 1.16 illustrated schematic structure for typical OFETs. As shown in **Figure 1.16**, OFETs are, basically, comprised of three terminals such as source, drain, and gate electrode as well as semiconducting layer and insulator between semiconducting and gate electrode. Different

deposition orders of the device layer lead to different device structure of OFETs and there are possible four device types according to the position of contact and gate electrode in OFET device: bottom-gate and top-contact (BG-TC), bottom-gate and bottom-contact (BG-BC), top-gate and bottom-contact (TG-BC), and top-gate and top-contact (TG-TC). (**Figure 1.16**) Although the performance of OFETs is mainly determined, depending on semiconducting layer, different device architectures can influence the carrier injection and contact resistance. BG-TC and BG-BC, for example, are often utilized for *p*-type semiconductor. On the other hands, TG-BC are used for ambipolar or *n*-type OFETs to protect oxygen and moisture. The device performance of BG-TC system, in addition, has reported higher mobilities than those of BG-BC system because of reducing contact resistance between electrode and organic layer whereas BG-BC system can be utilized commercially due to protection of organic layer.^{91,92}

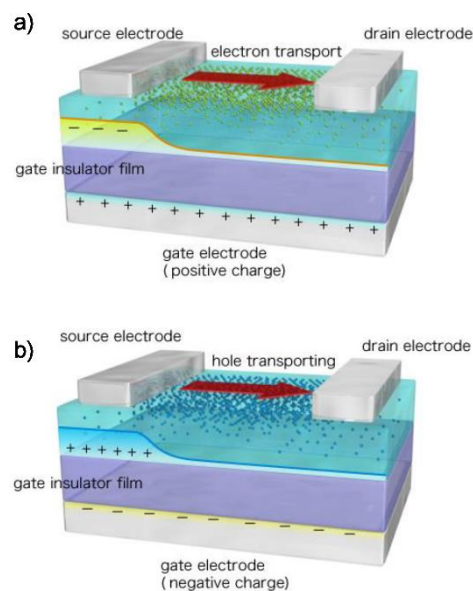


Figure 1.16. The conventional structures of *n*- a) and *p*- type b) OFETs.

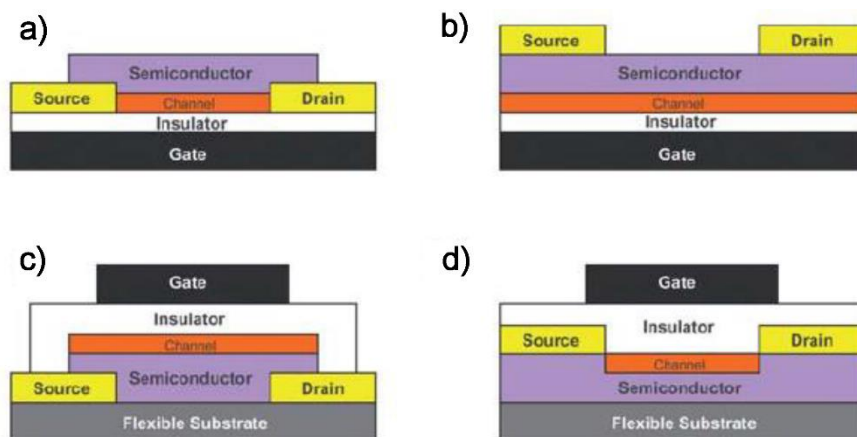


Figure 1.17. The device structures of four possible configuration of OFETs: bottom gate (BG)-bottom contact (BC) a), bottom gate (BG)-top contact (TC) b), top gate (TG)-bottom contact (BC) c), and top gate (TG)-top contact (TC) d).

The operation principle of OFETs is described, as depicted in **Figure 1.17**. The nominal current value between source (S) and drain (D) electrode is measured when none of voltage is applied to the gate. At this time, device condition indicates OFF state. While a voltage is applied to the gate, electrons or holes can be induced at the semiconductor-dielectric interface and thus the current between S and D increases (device ‘ON’ state). The basic relationships describing OFETs drain current can be calculated using the following equation:

$$(I_{SD})_{lin} = (W/L)\mu C_i(V_{SG} - V_{Th} - V_{SD}/2)V_{SD} \quad (\text{eq. 1})$$

$$(I_{SD})_{sat} = (W/2L)\mu C_i(V_{SG} - V_{Th})^2 \quad (\text{eq. 2})$$

Here, where μ is the field-effect carrier mobility of the semiconductor, W the channel width, L the channel length, C_i the capacitance per unit area of the insulator layer, V_{Th} the threshold voltage, V_{SD} the source-drain voltage, and V_{SG} the source-gate voltage. According to the extent of V_{SD} and V_{SG} , a linear current regime (eq. 1) is initially observed at low drain voltages ($V_{SD} < V_{SG}$), followed by a saturation regime (eq. 2) when the drain voltage exceeds the gate voltage. It is worth noting that in contrast to inorganic based transistor, OFETs operate in the accumulation state, where an increase in magnitude of V_{SG} are proportional to channel conductivity. When working OFETs, on the application of negative V_{SG} and V_{SD} , the organic materials have p -channel since the intensity of holes is increased. On the other hands, when the positive current between S and D, on the application of positive V_{SG} and V_{SD} , the semiconducting layer is n -channel because of the majority of electron, as shown in **Figure 1.18**. In some cases, OFETs operate for both of V_{SG} and V_{SD} polarities and their property is called ambipolar. More importantly, the crucial difference between organic and inorganic transistors is that organic transistors are based on the gate voltage sign at which they are active whereas the carrier type of latter in inorganic-based transistors are largely determined by doped chemical source. Therefore, organic semiconductors as p - or n - channel has no absolute and are determined by valance between metal work function and organic materials in OFETs. In next section, here, various organic materials which have p -, n -, and ambipolar type are described.

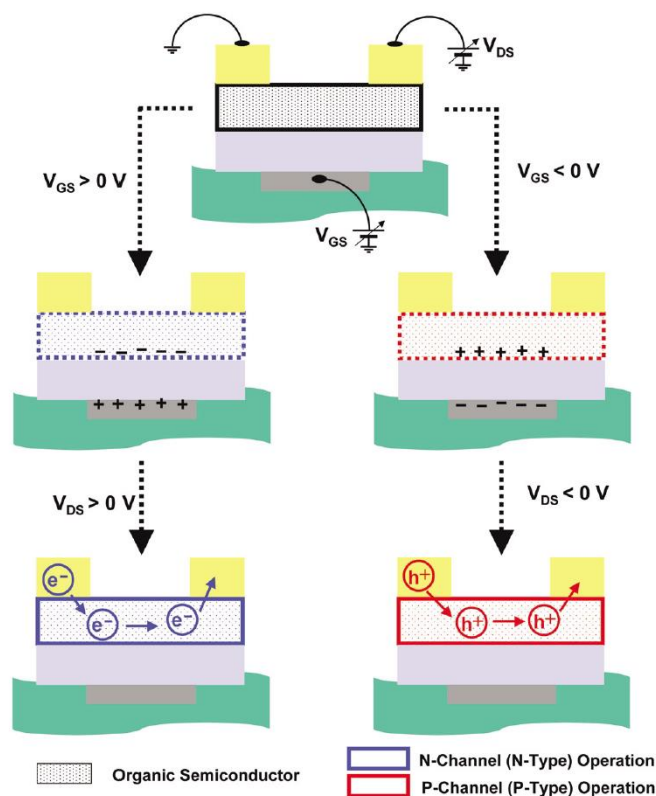


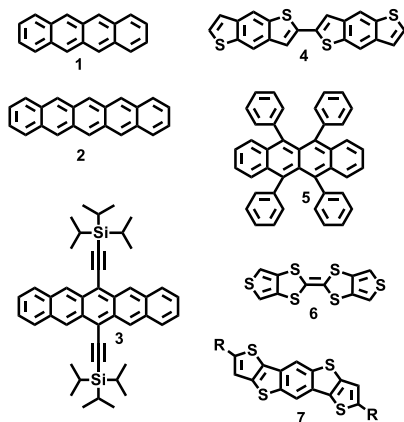
Figure 1.18. Schematic of *p*- and *n*-channel working principle for OFETs.⁹³

1.4.2.3. *p*-, *n*-, and Ambipolar Channel Organic Materials for OFETs

For the past few decades, organic semiconducting materials which have *p*-type, *n*-type, and ambipolar characteristic based on small molecules and polymers have been developed. Currently, among semiconducting candidates, the most useful organic materials possess the common feature of planar or planar-like π -conjugated system. **Figure 1.19** shows examples of *p*-type small molecule and polymer. Although the initial study on *p*-type molecules started from linearly fused acenes such as anthracene and tetracene (1), pentacene (2) has become one of the widely used in OFETs with high hole mobilities (μ_h) of $5 \text{ cm}^2\text{V}^{-1}\text{s}^{-1}$ as a thin film and $40 \text{ cm}^2\text{V}^{-1}\text{s}^{-1}$ as a single crystal.⁹⁴ Rubrene (5)-based transistor has also exhibited high carrier mobility of $24.5 \text{ cm}^2\text{V}^{-1}\text{s}^{-1}$.⁹⁵ In solution process, TIPS-pentacene (3) has received attention due to superior air stability and excellent performance on drop casting ($1.8 \text{ cm}^2\text{V}^{-1}\text{s}^{-1}$).⁹⁶ Beside small molecules, polymers have shown low carrier mobilities, relatively, despite the use of coating process and high physical stability. Very recently, however, copolymers with fused backbones (cyclopentadithiophene, indacenodithiophene, fluorene etc.), and organic dyes (diketopyrrolopyrrole, isoindigo etc.) have exhibited impressive results with superior performances.^{95,97-102} In particular, Bazan *et al.* and Heeger *et al.* reported an extremely high carrier mobility of up to $50 \text{ cm}^2\text{V}^{-1}\text{s}^{-1}$ using PCDTBT (12) with polymer alignment, which so far shows best performance among polymer-based

transistor, exceeding amorphous silicon, on convenient solution-processed transistors.¹⁰³

p-type small molecules



p-type polymers

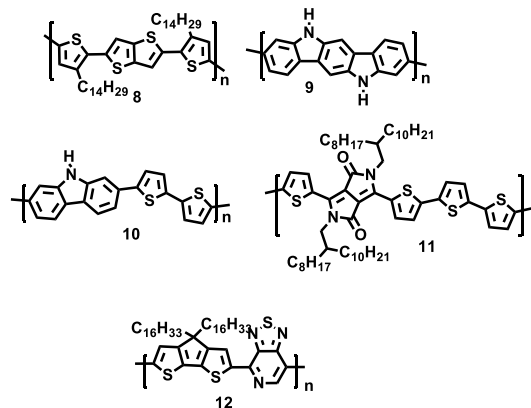


Figure 1.19. Examples of representative *p*-type small molecules and polymers for OFETs.

Compared to *p*-type organic materials with the high promising performance for OFETs, much less attention have been devoted to *n*-type organic semiconducting materials because of relatively low mobility in spite of their crucial role for boosting industrialization. (see **Figure 1.20**) Therefore, focusing on the development of *n*-type materials is very important and reasonable issue, and thus, currently, various related results are presented from many scientist. Among many *n*-type small molecules, quinoid-type terthiophene (1) and fused anthracene-based material with electron withdrawing group (2) have exhibited *n*-type characteristics and good electron mobilities (μ_e) on BG-TC system. In addition, combination with NDI-based molecules and electron rich groups have been utilized as strong *n*-type semiconductors as small molecules or polymer. Although poor absorption range, the fullerene, C₆₀, is also the most powerful acceptor due to its strong electron affinity and thus fullerene derivatives has been used as efficient acceptor in organic transistors. Recently, C₆₀-based transistors have achieved extremely high electron mobility ($6 \text{ cm}^2\text{V}^{-1}\text{s}^{-1}$).¹⁰⁴ As effective *n*-type polymer-based transistors, so far NDI-based polymer has been spotlighted as solution processability and striking performance ($2\text{-}3 \text{ cm}^2\text{V}^{-1}\text{s}^{-1}$)¹⁰⁵ However, 2-pyridnyl substituted DPP-based polymers, incorporating bithiophene unit as donor have reported by Y.Li *et al.* in 2014, which showed remarkable electron mobilities of up to $6.3 \text{ cm}^2\text{V}^{-1}\text{s}^{-1}$ by (11).¹⁰⁶ Furthermore, modified poly(*p*-phenylene vinylene) (PPV) based polymer that have high Electron mobility over $1 \text{ cm}^2 \text{V}^{-1}\text{s}^{-1}$ under ambient conditions is represented by J. Pei *et al.*, which could be applied to broad electronic applications.¹⁰⁷

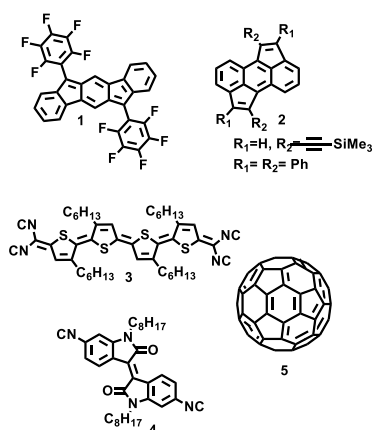
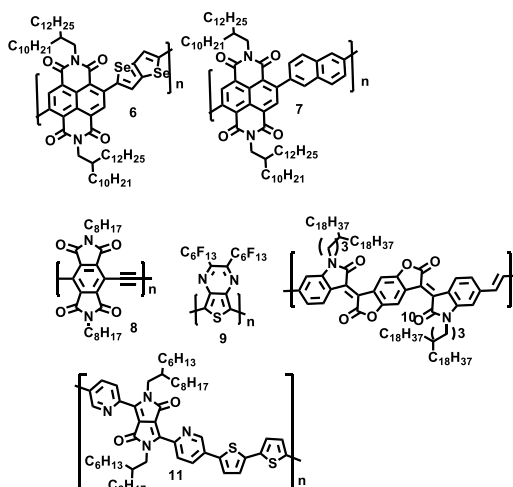
n*-type small molecules**n*-type polymers**

Figure 1.20. Examples of representative *n*-type small molecules and polymers for OFETs.

In ambipolar organic semiconductors, almost small molecules or polymers for OFETs basically have exhibited ambipolar characteristics to varying degrees. Among them, DPP-based organic semiconductors are most useful, effective, well-balanced candidates. Thus, DPP-based copolymer have been utilized as promising ambipolar semiconductors. As another approach, with DPP moiety, ambipolar materials could be modified by controlling each molecular polarity using various existing *n*- or *p*- channel organic materials. **Figure 1.21** illustrated representative ambipolar small molecules or polymers.^{108,108,109}

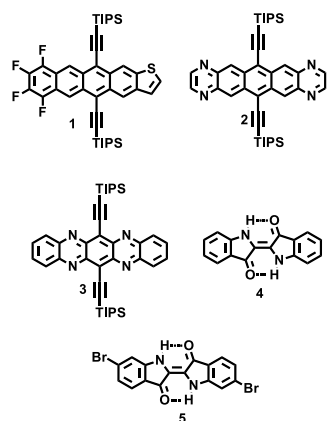
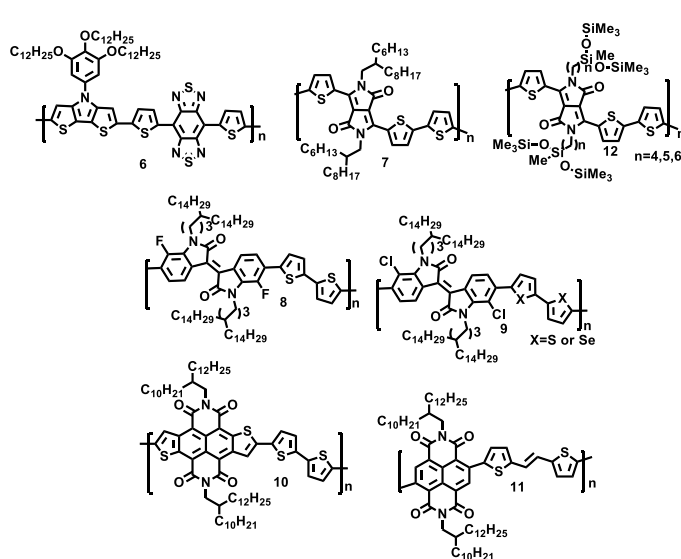
Ambipolar small molecules**Ambipolar polymers**

Figure 1.21. Examples of representative ambipolar small molecules and polymers for OFETs.

Reference

- (1) Harun, M. H.; Saion, E.; Kassim, A.; Yahya, N.; Mahmud, E. *UCSI Academic Journal: Journal for the Advancement of Science & Arts* **2007**, *2*, 63.
- (2) Pollak, P. I.; Salem, L.; JSTOR: 1968.
- (3) Natta, G.; Mazzanti, G.; Corradini, P. *Sci. Fis., Mat. Nat., Rend* **1958**, *25*.
- (4) Stenger-Smith, J. D. *Prog. in Polym. Sci.* **1998**, *23*, 57.
- (5) Wan, M. *Conducting polymers with micro or nanometer structure*; Springer, **2008**.
- (6) Shirakawa, H.; Louis, E. J.; MacDiarmid, A. G.; Chiang, C. K.; Heeger, A. J. *J. Chem. Soc., Chem. Commun.* **1977**, 578.
- (7) Mikulski, C.; Russo, P.; Saran, M.; MacDiarmid, A.; Garito, A.; Heeger, A. *J. Am. Chem. Soc.* **1975**, *97*, 6358.
- (8) Burroughes, J.; Bradley, D.; Brown, A.; Marks, R.; Mackay, K.; Friend, R.; Burns, P.; Holmes, A. *Nature* **1990**, *347*, 539.
- (9) Friend, R.; Gymer, R.; Holmes, A.; Burroughes, J.; Marks, R.; Taliani, C.; Bradley, D.; Dos Santos, D.; Bredas, J.; Lögdlund, M. *Nature* **1999**, *397*, 121.
- (10) Park, S. H.; Roy, A.; Beaupre, S.; Cho, S.; Coates, N.; Moon, J. S.; Moses, D.; Leclerc, M.; Lee, K.; Heeger, A. J. *Nat. photonics* **2009**, *3*, 297.
- (11) Yu, G.; Gao, J.; Hummelen, J. C.; Wudl, F.; Heeger, A. J. *Science* **1995**, *270*, 1789.
- (12) Facchetti, A.; Deng, Y.; Wang, A.; Koide, Y.; Sirringhaus, H.; Marks, T. J.; Friend, R. H. *Angew. Chem. Int. Ed.* **2000**, *39*, 4547.
- (13) Wen, Y.; Liu, Y. *Adv. Mater.* **2010**, *22*, 1331.
- (14) Grätzel, M. *Nature* **2001**, *414*, 338.
- (15) O'Regan, B.; Schwartz, D. T.; Zakeeruddin, S. M.; Grätzel, M. *Adv. Mater.* **2000**, *12*, 1263.
- (16) Thomas, S. W.; Joly, G. D.; Swager, T. M. *Chemical Reviews* **2007**, *107*, 1339.
- (17) Heeger, A. J. *Angew. Chem. Int. Ed.* **2001**, *40*, 2591.
- (18) Chiang, C. K.; Fincher Jr, C.; Park, Y. W.; Heeger, A. J.; Shirakawa, H.; Louis, E. J.; Gau, S. C.; MacDiarmid, A. G. *Phys. Rev. Lett.* **1977**, *39*, 1098.
- (19) Kaur, G.; Adhikari, R.; Cass, P.; Bown, M.; Gunatillake, P. *RSC Adv.* **2015**, *5*, 37553.
- (20) Chiang, C.; Gau, S.; Fincher Jr, C.; Park, Y.; MacDiarmid, A.; Heeger, A. *Appl. Phys. Lett.* **1978**, *33*, 18.
- (21) Kovacic, P.; Wu, C. *J. of Polym. Sci.* **1960**, *47*, 45.

- (22) Inzelt, G. In *Conducting Polymers*; Springer: **2012**, 149.
- (23) Wei, Y.; Hariharan, R.; Patel, S. A. *Macromolecules* **1990**, *23*, 758.
- (24) Rao, S. S.; Winter, J. *Front. in Neuroeng.* **2009**, *2*, 6.
- (25) Johansson Seechurn, C. C.; Kitching, M. O.; Colacot, T. J.; Snieckus, V. *Angew. Chem. Int. Ed.* **2012**, *51*, 5062.
- (26) Astruc, D. *Anal. Bioanal. Chem.* **2011**, *399*, 1811.
- (27) Negishi, E.-i. *Angew. Chem* **2011**, *123*, 6870.
- (28) Suzuki, A. *Angew. Chem. Int. Ed.* **2011**, *50*, 6722.
- (29) Yin, L.; Liebscher, J. *Chem. Rev.* **2007**, *107*, 133.
- (30) Bäckvall, J. *The Royal Swedish Academy of Sciences* **2010**.
- (31) Stille, J. K. *Angew. Chem. Int. Ed.* **1986**, *25*, 508.
- (32) Kosugi, M.; Sasazawa, K.; Shimizu, Y.; Migita, T. *Chem. Lett.* **1977**, *6*, 301.
- (33) Milstein, D.; Stille, J. *J. Am. Chem. Soc.* **1978**, *100*, 3636.
- (34) Matsumoto, H.; Nagashima, S.; Yoshihiro, K.; Nagai, Y. *J. Organomet. Chem.* **1975**, *85*, C1.
- (35) Dieck, H. A.; Heck, R. F. *J. Org. Chem.* **1975**, *40*, 1083.
- (36) Miyaura, N.; Suzuki, A. *J. Che. Soc., Chem. Commun.* **1979**, 866.
- (37) Suzuki, A. *J. Organomet. Chem.* **1999**, *576*, 147.
- (38) Li, C.; Bo, Z. New Chemistry for Organic Photovoltaic Materials, in *Polymer Photo voltaics: Materials, Physics, and Device Engineering*, **2015**, 1-31.
- (39) Carsten, B.; He, F.; Son, H. J.; Xu, T.; Yu, L. *Chem. Rev.* **2011**, *111*, 1493.
- (40) Cheng, X.; Wan, Q.; Wu, Y.; Guo, B.; Guo, X.; Li, Y.; Zhang, M.; Cui, C.; Li, Y. *Solar Energy Mater. and Sol. Cells* **2016**, *149*, 162.
- (41) Guo, X.; Zhou, N.; Lou, S. J.; Hennek, J. W.; Ponce Ortiz, R.; Butler, M. R.; Boudreault, P.-L. T.; Strzalka, J.; Morin, P.-O.; Leclerc, M. *J. Am. Chem. Soc.* **2012**, *134*, 18427.
- (42) Kim, J.; Yun, M. H.; Kim, G.-H.; Lee, J.; Lee, S. M.; Ko, S.-J.; Kim, Y.; Dutta, G. K.; Moon, M.; Park, S. Y. *ACS appl. Mater. interfaces* **2014**, *6*, 7523.
- (43) Menegatti, R. *Green Chemistry-Aspects for the Knoevenagel Reaction*; INTECH Open Access Publisher, **2012**.
- (44) Laue, T.; Plagens, A.; Laue, T.; Plagens, A. *Namen-und Schlagwort-Reaktionen der Organischen Chemie* **1998**, 168.
- (45) Plagens, D.-C. A. In *Namen-und Schlagwort-Reaktionen der Organischen Chemie*; Springer: **1994**, 166.
- (46) Gewald, K. *Angew. Chem.* **1961**, *73*, 114.

- (47) Gewald, K. *Chem. Ber.* **1965**, *98*, 3571.
- (48) Calter, M. A.; Phillips, R. M.; Flaschenriem, C. *J. Am. Chem. Soc.* **2005**, *127*, 14566.
- (49) Knoevenagel, E. *Berichte der deutschen chemischen Gesellschaft* **1898**, *31*, 2596.
- (50) Smith, M. B.; March, J. *March's advanced organic chemistry: reactions, mechanisms, and structure*; John Wiley & Sons, **2007**.
- (51) Lorenzo, E. *Solar electricity: engineering of photovoltaic systems*; Earthscan/James & James, **1994**.
- (52) Spanggaard, H.; Krebs, F. C. *Sol. Energy Mater. Cells* **2004**, *83*, 125.
- (53) Castelfranco, P. A.; Jones, O. T. *Plant Physiol.* **1975**, *55*, 485.
- (54) Ivanov, A. S.; Boldyrev, A. I. *Org. Biomol. Chem.* **2014**, *12*, 6145.
- (55) McKeown, N. B. *Phthalocyanine materials: synthesis, structure and function*; Cambridge University Press, **1998**.
- (56) Goetzberger, A.; Hebling, C. *Sol. Energy Mater. Cells* **2000**, *62*, 1.
- (57) Darling, S. B.; You, F. *Rsc Adv.* **2013**, *3*, 17633.
- (58) Yip, H.-L.; Jen, A. K.-Y. *Energy Environ. Sci.* **2012**, *5*, 5994.
- (59) Huang, L.; Cheng, X.; Yang, J.; Zhang, L.; Zhou, W.; Xiao, S.; Tan, L.; Chen, L.; Chen, Y. *ACS appl. Mater. interfaces* **2016**, *8*, 27018.
- (60) Zhou, Y.; Eck, M.; Krüger, M. *Energy Environ. Sci.* **2010**, *3*, 1851.
- (61) Chang, E. C.; Chao, C. I.; Lee, R. H. *J. Appl. Polym. Sci.* **2006**, *101*, 1919.
- (62) Zhang, F.; Johansson, M.; Andersson, M. R.; Hummelen, J. C.; Inganäs, O. *Adv. Mater.* **2002**, *14*, 662.
- (63) Tajima, K.; Suzuki, Y.; Hashimoto, K. *J. Phys. Chem. C* **2008**, *112*, 8507.
- (64) Nguyen, L. H.; Hoppe, H.; Erb, T.; Guenes, S.; Gobsch, G.; Sariciftci, N. S. *Adv. Funct. Mater.* **2007**, *17*, 1071.
- (65) Cao, W.; Xue, J. *Energy Environ. Sci.* **2014**, *7*, 2123.
- (66) Nisato, G.; Lupo, D.; Ganz, S. *Organic and Printed Electronics: Fundamentals and Applications*; CRC Press, **2016**.
- (67) Mühlbacher, D.; Scharber, M.; Morana, M.; Zhu, Z.; Waller, D.; Gaudiana, R.; Braubec, C. *Adv. Mater.* **2006**, *18*, 2884.
- (68) Logothetidis, S. *Handbook of Flexible Organic Electronics: Materials, Manufacturing and Applications*; Elsevier, **2014**.
- (69) He, Z.; Xiao, B.; Liu, F.; Wu, H.; Yang, Y.; Xiao, S.; Wang, C.; Russell, T. P.; Cao, Y. *Nat. Photonics* **2015**, *9*, 174.
- (70) Lu, L.; Yu, L. *Adv. Mater.* **2014**, *26*, 4413.

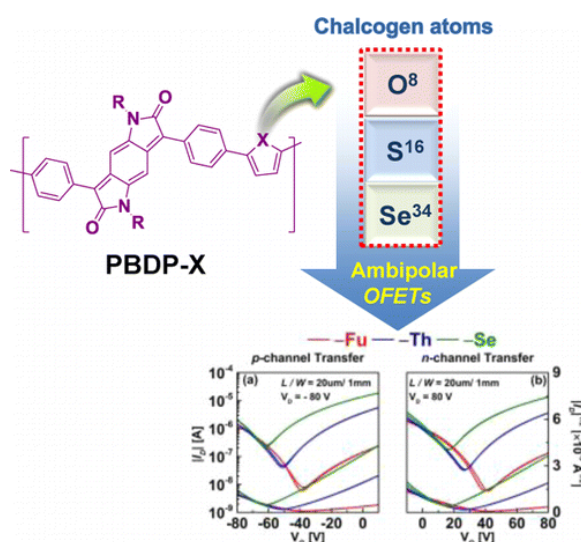
- (71) Sun, Y.; Welch, G. C.; Leong, W. L.; Takacs, C. J.; Bazan, G. C.; Heeger, A. J. *Nat. Mater.* **2012**, *11*, 44.
- (72) Zhang, Q.; Kan, B.; Liu, F.; Long, G.; Wan, X.; Chen, X.; Zuo, Y.; Ni, W.; Zhan g, H.; Li, M. *Nat. Photonics* **2015**, *9*, 35.
- (73) Anderson, H. L.; Boudon, C.; Diederich, F.; Gisselbrecht, J. P.; Gross, M.; Seiler, P. *Angew. Chem.* **1994**, *106*, 1691.
- (74) Hummelen, J. C.; Knight, B. W.; LePeq, F.; Wudl, F.; Yao, J.; Wilkins, C. L. *The J. Org. Chem.* **1995**, *60*, 532.
- (75) Holcombe, T. W.; Woo, C. H.; Kavulak, D. F.; Thompson, B. C.; Fréchet, J. M. *J. Am. Chem. Soc.* **2009**, *131*, 14160.
- (76) Li, C.; Wonneberger, H. *Adv. Mater.* **2012**, *24*, 613.
- (77) Zhan, X.; Tan, Z. a.; Domercq, B.; An, Z.; Zhang, X.; Barlow, S.; Li, Y.; Zhu, D.; Kippelen, B.; Marder, S. R. *J. Am. Chem. Soc.* **2007**, *129*, 7246.
- (78) Zhou, N.; Lin, H.; Lou, S. J.; Yu, X.; Guo, P.; Manley, E. F.; Loser, S.; Hartnett, P.; Huang, H.; Wasielewski, M. R. *Adv. Energy Mater.* **2014**, *4*.
- (79) Nielsen, C. B.; Holliday, S.; Chen, H.-Y.; Cryer, S. J.; McCulloch, I. *Acc. Chem. Res.* **2015**, *48*, 2803.
- (80) Holliday, S.; Ashraf, R. S.; Nielsen, C. B.; Kirkus, M.; Röhr, J. A.; Tan, C.-H.; Collado-Fregoso, E.; Knall, A.-C.; Durrant, J. R.; Nelson, J. *J. Am. Chem. Soc.* **2015**, *137*, 898.
- (81) Bai, H.; Wang, Y.; Cheng, P.; Wang, J.; Wu, Y.; Hou, J.; Zhan, X. *J. Mater. Chem. A* **2015**, *3*, 1910.
- (82) Lin, Y.; Zhang, Z.-G.; Bai, H.; Wang, J.; Yao, Y.; Li, Y.; Zhu, D.; Zhan, X. *Energy Environ. Sci.* **2015**, *8*, 610.
- (83) Bin, H.; Zhang, Z.-G.; Gao, L.; Chen, S.; Zhong, L.; Xue, L.; Yang, C.; Li, Y. *J. Am. Chem. Soc.* **2016**, *138*, 4657.
- (84) Horowitz, G. *Adv. Mater.* **1998**, *10*, 365.
- (85) Kahng, D.; Atalla, M. *Carnegie Institute of Technology, Pittsburgh, PA* **1960**.
- (86) Barbe, D.; Westgate, C. *J. Phys. Chem. Solids* **1970**, *31*, 2679.
- (87) Tsumura, A.; Koezuka, H.; Ando, T. *Synth. Met.* **1988**, *25*, 11.
- (88) Koezuka, H.; Tsumura, A.; Ando, T. *Synth. Met.* **1987**, *18*, 699.
- (89) Han, A.; Dutta, G. K.; Lee, J.; Lee, H. R.; Lee, S. M.; Ahn, H.; Shin, T. J.; Oh, J. H.; Yang, C. *Adv. Funct. Mater.* **2015**, *25*, 247.
- (90) Kim, G.; Kang, S.-J.; Dutta, G. K.; Han, Y.-K.; Shin, T. J.; Noh, Y.-Y.; Yang, C. *J. Am. Chem. Soc.* **2014**, *136*, 9477.

- (91) Xu, Y.; Liu, C.; Khim, D.; Noh, Y.-Y. *Phys. Chem. Chem. Phys.* **2015**, *17*, 26553.
- (92) Kim, C. H.; Bonnassieux, Y.; Horowitz, G. *IEEE Transactions on Electron Devices* **2013**, *60*, 280.
- (93) Facchetti, A. *Mater. Today* **2007**, *10*, 28.
- (94) Klauk, H.; Zschieschang, U.; Weitz, R. T.; Meng, H.; Sun, F.; Nunes, G.; Keys, D. E.; Fincher, C. R.; Xiang, Z. *Adv. Mater.* **2007**, *19*, 3882.
- (95) Dong, H.; Wang, C.; Hu, W. *Chem. Commun.* **2010**, *46*, 5211.
- (96) Kaur, I.; Jia, W.; Kopreski, R. P.; Selvarasah, S.; Dokmeci, M. R.; Pramanik, C.; McGruer, N. E.; Miller, G. P. *J. Am. Chem. Soc.* **2008**, *130*, 16274
- (97) Tsao, H. N.; Cho, D. M.; Park, I.; Hansen, M. R.; Mavrinskiy, A.; Yoon, D. Y.; Graf, R.; Pisula, W.; Spiess, H. W.; Müllen, K. *J. Am. Chem. Soc.* **2011**, *133*, 2605.
- (98) McCulloch, I.; Heeney, M.; Bailey, C.; Genevicius, K.; MacDonald, I.; Shkunov, M.; Sparrowe, D.; Tierney, S.; Wagner, R.; Zhang, W. *Nat. Mater.* **2006**, *5*, 328.
- (99) Tsao, H. N.; Cho, D.; Andreasen, J. W.; Rouhanipour, A.; Breiby, D. W.; Pisula, W.; Müllen, K. *Adv. Mater.* **2009**, *21*, 209.
- (100) Zhang, W.; Smith, J.; Watkins, S. E.; Gysel, R.; McGehee, M.; Salleo, A.; Kirkpatrick, J.; Ashraf, S.; Anthopoulos, T.; Heeney, M. *J. Am. Chem. Soc.* **2010**, *132*, 11437.
- (101) Zhang, M.; Tsao, H. N.; Pisula, W.; Yang, C.; Mishra, A. K.; Müllen, K. *J. Am. Chem. Soc.* **2007**, *129*, 3472.
- (102) Donald, A. M.; Windle, A. H.; Hanna, S. *Liquid crystalline polymers*; Cambridge University Press, **2006**.
- (103) Luo, C.; Kyaw, A. K. K.; Perez, L. A.; Patel, S.; Wang, M.; Grimm, B.; Bazan, G. C.; Kramer, E. J.; Heeger, A. J. *Nano lett.* **2014**, *14*, 2764.
- (104) Brabec, C. J.; Heeney, M.; McCulloch, I.; Nelson, J. *Chem. Soc. Rev.* **2011**, *40*, 1185.
- (105) Caironi, M.; Bird, M.; Fazzi, D.; Chen, Z.; Di Pietro, R.; Newman, C.; Facchetti, A.; Sirringhaus, H. *Adv. Funct. Mater.* **2011**, *21*, 3371.
- (106) Sun, B.; Hong, W.; Yan, Z.; Aziz, H.; Li, Y. *Adv. Mater.* **2014**, *26*, 2636.
- (107) Lei, T.; Dou, J.-H.; Cao, X.-Y.; Wang, J.-Y.; Pei, J. *J. Am. Chem. Soc.* **2013**, *135*, 12168.
- (108) Gruber, M.; Jung, S.-H.; Schott, S.; Venkateshvaran, D.; Kronemeijer, A. J.; Andreasen, J. W.; McNeill, C. R.; Wong, W. W.; Shahid, M.; Heeney, M. *Chem. Sci.* **2015**, *6*, 6949.
- (109) Lee, J.; Han, A.-R.; Kim, J.; Kim, Y.; Oh, J. H.; Yang, C. *J. Am. Chem. Soc.* **2012**, *134*, 20713.

Chapter II

Synthesis of Characterization of Benzodipyrrolidone (BDP)-Based Polymers Containing Chalcogen Atoms (Fu, Th, Se) and Their Application to Organic Semiconducting Devices

In chapter II, we presented synthesis and characterization of benzodipyrrolidone (so-called BDP)-based polymers with different oxygen atoms (or chalcogen atoms), as well as their electronic application to OFETs. This chapter is reproduced in part with permission of “benzodipyrrolidone (BDP)-based polymer semiconductors containing a series of chalcogen atoms: comprehensive investigation of the effect of heteroaromatic blocks on intrinsic semiconducting properties” from K. C. Lee *et. al.* *ACS Appl. Mater. Interfaces* **2014**, 6, 4872–4882.



2.1 BDP-Based Polymers

2.1.1 Introduction

π -Conjugated polymer semiconductors are expected to be one of the promising key elements¹⁻³ for innovative display technologies⁴⁻⁸ because, in spite of their current poor stability, they have many advantages over silicon-based semiconductor materials, including flexibility, light-weight, ultralow-cost, and processability. Special attention has been paid to the design of conjugated donor (D)-acceptor (A) polymers, since this approach can enhance the intermolecular and intramolecular interactions which directly govern the molecular ordering and π - π stacking of the polymer chains in the solid state, thus boosting the effective charge transport efficiency.⁹ In addition, D-A polymers enable the realization of large area integrated circuits (ICs) based on complementary inverters and light emitting transistors (LETs) by a simple blanket coating without

the sophisticated patterning processes of the organic semiconducting layer since the polymers can have both electron and hole transport in one polymer chain.¹⁰⁻¹¹ To achieve high performance ambipolar ICs and LETs, high and well-balanced electron and hole mobility is required.¹² In recent years, bislactam-based chromophores such as diketopyrrolopyrrole (DPP),¹³⁻¹⁸ benzodipyrrolidone (BDP),¹⁹⁻²² isoindigo (IIG),²³⁻²⁸ and thienoisindigo (TIIG)²⁹⁻³³ (Figure 2.1.), so-called ‘high-performance pigments’, have been the most frequently used electron-accepting building blocks for constructing D-A type polymers with high charge carrier mobility.

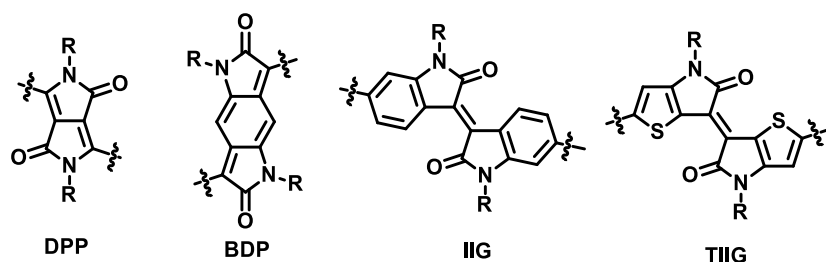


Figure 2.1. Structures of diketopyrrolopyrrole (DPP), benzodipyrrolidone (BDP), isoindigo (IIG), and thienoisindigo (TIIG).

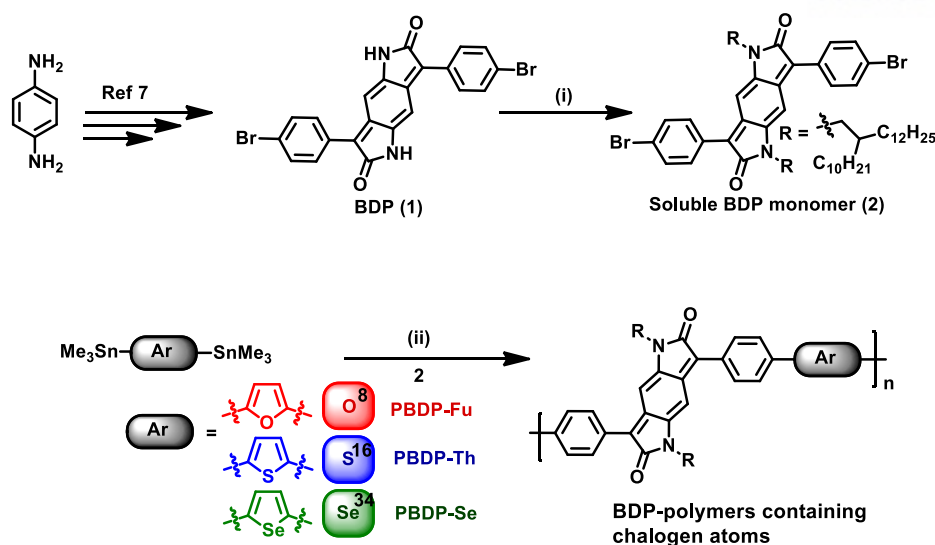
In line with the consideration of an effective D-A strategy, various thiophene-based moieties as the natural choice for electron-donating units within the main backbone have been ubiquitously incorporated into bislactam-containing D-A polymers for applications in organic field-effect transistors (OFETs).³⁴ In order to maximize the charge transport caused by effective overlap integrals of wave functions between neighboring molecules, our group and several other groups recently developed selenophene-comprising D-A polymers based on a bislactam core having higher charge-transport performances.³⁵⁻³⁹ At the same time, a growing interest in oligofurans as an alternative to other heteroaromatics used has developed since it is believed they can be obtained from biomass and are considered ‘green’ electronic materials;⁴⁰⁻⁴¹ they also have similar energy levels and a comparable degree of aromaticity relative to thiophene counterparts.⁴²⁻⁴³ Despite the fact that furans are smaller overlap integrals and have lower polarizabilities than thiophenes,⁴⁴⁻⁴⁶ recent progress in the development of bislactam-based D-A polymers containing furan for OFETs has yielded materials with high charge carrier mobilities comparable with those obtained for their thiophene analogues.⁴⁷⁻⁴⁹ However, systematic investigations of heteroaromatics-comprising D-A polymers with different aromaticities have not yet been subjected to the same bislactam framework and their own unique advantages as aforementioned have been enjoyed within the different acceptor building blocks. For example, the analogues of DPP-benzothiadiazole polymer (PDPP-BT), in which the neighboring thiophene units on DPP core are replaced with either thiophene (Th) or selenophene (Se), were developed by Heeney and Sirringhaus et al. Besides,

Sonar, Li, and Dodabalapur et al. reported the synthesis of BT-based polymer comprised of furan (Fu)-substituted DPP combined with BT and its use in OFETs,⁵⁰ A series of publications based on the molecules of varying chalcogen atoms in different research groups followed,⁵¹⁻⁵⁶ shedding light on their interesting properties.

From our attempt to uncover the actual ‘chalcogen atom’ impact on intrinsic polymer properties, we selected the recently conceived benzodipyrrolidone (BDP) accepting moiety that is described as an elongated DPP structure. Herein, we report the synthesis of a series of BDP-based D-A polymers, **PBDP-Fu**, **PBDP-Th**, and **PBDP-Se**, by polymerizing donor moieties, Fu, Th, and Se, with the soluble BDP acceptor unit. Other comparative studies of these polymers also represent a step toward a structure-property relationship regarding the chalcogen atoms as the counterpart co-monomers for OFETs based on bislactam structures. We believe that these cogent studies, relating to energy levels, morphology, molecular packing, and carrier transport as a function of heteroaromatic building blocks, are extremely significant for guiding the rational design and synthesis of novel, high-performance semiconductors.

2.1.2 Synthesis and Characterization

The synthetic routes to the monomers and polymers (**PBDP-Fu**, **PBDP-Th**, and **PBDP-Se**) are outlined in **Scheme 2.1**. Briefly, the key BDP (**1**) core was synthesized in three steps starting from *p*-phenylenediamine and the final oxidation step ensured conjugation of the quinodimethane structure (isolated yield of 60% over the three steps) according to the procedures established by Wudl *et al.*¹⁹ A soluble BDP monomer was conveniently obtained by the subsequent alkylation of **2** with 2-decyltetradecyl bromide in anhydrous DMF in the presence of potassium carbonate, which was almost the same condition as that for other alkylated bislactam-based compounds (55% yield). All chalcogen-based counterpart distannylated co-monomers (Fu, Th, and Se) were prepared using a lithiation and subsequent quenching with trimethyltin chloride.



^aReagents and conditions: (i) K_2CO_3 , DMF, 2-decyltetradecyl bromide 130 °C, 55%; (ii) $Pd(PPh_3)_4$, toluene, 110 °C, for **PBDP-Fu** (75%), **PBDP-Th** (70%), and **PBDP-Se** (81%).

Scheme 2.1. Synthetic routes of BDP-based polymers.

With all monomers in hand, the polymerizations were performed under a palladium (Pd)-catalyzed Stille-type coupling reaction, with 1:1 monomer ratio, to give the target polymers (see details in Experimental section). This was followed by successive Soxhlet extraction with methanol, acetone, and hexane to remove catalyst residues and low molecular weight oligomers. The remaining material was dissolved in chloroform and precipitated into methanol, resulting in the pure target polymers, **PBDP-Fu**, **PBDP-Th**, and **PBDP-Se**. All of the polymers are highly soluble in organic solvents such as chloroform, THF, and chlorobenzene at room temperature. The number-average molecular weights (M_n) and the polydispersity index (PDI) of the polymers were determined by gel permeation chromatography (GPC) with THF as an eluent against polystyrene standards (**Table 2.1**). All polymerizations produced polymers with moderate to high molecular weights (37-74 kDa); the rather high molecular weight for **PBDP-Se** could be due to the aggregation that induced overestimation of molecular weight in THF. The thermal stability of all the polymers was also investigated by thermogravimetric analysis (TGA). **PBDP-Fu**, **PBDP-Th**, and **PBDP-Se** show a 5% weight loss at 458 °C, 401 °C, and 475 °C, respectively, which indicates their excellent thermal stability (see **Table 2.1** and **Figure 2.2**).

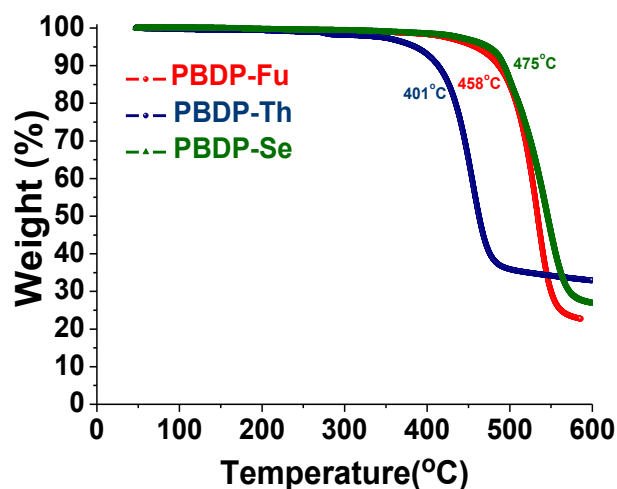


Figure 2.2. TGA plots of BDP-based polymers with a heating rate of 10 °C/min in N₂ atmosphere.

Table 2.1. Photophysical and electrochemical properties of BDP-based polymers

Polymer	M_n (kDa)	PDI	T_d (°C) ^a	$\lambda_{\max}^{\text{sol}}$ (nm) ^b	$\lambda_{\max}^{\text{film}}$ (nm)	E_g^{opt} (eV) ^c	E_{LUMO} (eV) ^d	E_{HOMO} (eV) ^d	E_g^{CV} (eV) ^e
PBBDP-Fu	47.0	1.64	458	594	635	1.67	-3.60	-5.37	1.77
PBBDP-Th	37.0	1.13	401	611	630	1.67	-3.58	-5.34	1.76
PBBDP-Se	74.0	1.74	475	611	652	1.64	-3.59	-5.32	1.73

^aThe temperature of 5% weight-loss under nitrogen; ^bChloroform solution; ^cDetermined from the onset of the electronic absorption spectra; ^dCyclic voltammetry determined with Fc/Fc⁺ ($E_{\text{HOMO}} = -4.80$ eV) as the internal reference; ^e $E_g^{\text{CV}} = E_{\text{LUMO}} - E_{\text{HOMO}}$

2.1.3 Photophysical and Electrochemical Properties and Computational Studies

The optical properties of the polymers were analyzed and are shown in **Figure 2.3**, with the detailed values listed in **Table 2.1**. All three polymers possess similar optical features with wide absorptions from 320 nm to 850 nm. Shorter and longer wavelength peaks are attributed to the π - π^* transition band and intramolecular charge transfer (ICT) between donors and the acceptor BDP moiety, respectively. The absorption spectra of all the copolymer films show an obvious red-shift relative to their solutions, which is a general feature of D-A conjugated polymers because of their more ordered molecular organization in the solid films. It is worth noting that **PBBDP-Se** exhibits an enhanced absorption intensity of the ICT band relative to that of the π - π^* transition band, when compared to the strength ratios of the two peaks for **PBBDP-Fu** and **PBBDP-Th**.

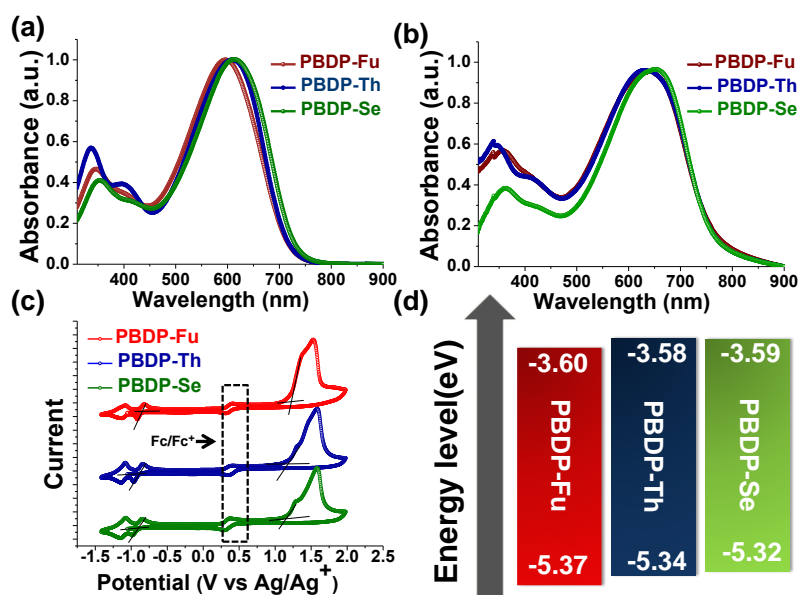


Figure 2.3. UV-Vis absorption spectra of BDP-based polymers in chloroform solution (a) and as thin solid films (b). Cyclic voltammograms of BDP-based polymer thin films (c). Energy level diagrams for BDP-based polymers (d).

Structurally, the three polymers differ from each other based on the identity of the donor conjugated with, and adjacent to, each BDP unit. Thereby, for **PBBDP-Se**, the slight red-shift in the absorption maximum as well as the more pronounced ICT band imply the relatively stronger electron-donating ability of the Se than that of the other two moieties (Fu and Th). The optical bandgaps (E_g^{opt}), calculated from absorption cut off values, are determined as 1.67 eV, 1.67 eV, and 1.64 eV for **PBBDP-Fu**, **PBBDP-Th**, and **PBBDP-Se** thin films, respectively. It is relatively clear that organic semiconducting materials should have a delocalized electron-density-state and appropriate levels of the highest occupied molecular orbital (HOMO) and the lowest unoccupied molecular orbital (LUMO) to facilitate the efficient injection of the hole and electron from the electrode. Therefore, the electrochemical redox properties of the polymers were investigated as thin films using cyclic voltammetry (CV). The CV curves were recorded with reference to an Ag/Ag⁺ electrode and calibrated by the ferrocene/ferrocenium (Fc/Fc⁺) redox couple (absolute energy level of -4.80 eV to a vacuum) as an internal standard. These three polymers have two reversible redox processes at negative potential and quasi-reversible oxidation processes at a positive scan. Notably, these two characteristic BDP reduction waves not only indicate initial radical anion and subsequent dianion formation, but the reversibility in the reduction processes is also interpreted as a good sign of the stability of the BDP-polymer anions. The oxidation and reduction onset potentials are translated to HOMO and LUMO energy levels, which are

summarized in **Table 2.1** and schematically depicted in **Figure 2.3**. Changing the donor parts (Fu, Th, and Se) of the BDP-based polymers barely affects the LUMO levels of the polymers (the three polymers with values between -3.58 and -3.60 eV), because their LUMOs are predominately localized on the strong accepting BDP core. On the other hand, the HOMOs relatively vary from -5.32 eV to -5.37 eV as a function of the electron donating ability of the donor monomer and polymer backbone conformation. This implies that the electron donating abilities of the donor chromophores increase in the order of Fu < Th < Se. The reasonably deep HOMO energy levels (below -5 eV) indicate good stability towards unintentional doping by atmospheric oxidants,⁵⁷ which is very important for manufacturing stable organic electronic devices. The electrochemical bandgaps defined as $E_g^{CV} = E_{LUMO} - E_{HOMO}$ for each polymer follow the same trends as the optical gaps, but are consistently somewhat larger. To gain insight into the structural and electronic features of the polymers, distributions of HOMO and LUMO of **PBDP-Fu**, **PBDP-Th**, and **PBDP-Se** were calculated using the DFT method at the B3LYP/6-31G* level and are shown in **Figure 2.4**. Interestingly, the HOMO is mostly distributed along the polymer backbone, whereas the LUMO is localized on the BDP moiety. This is consistent with the HOMO-LUMO distribution observed in several D-A polymers.^{29, 35, 58-60} In addition, from the optimized structures of the polymers in the horizontal view, small dihedral angles of 1.6 ~ 14.7 ° between the BDP and chalcogen-based co-units are observed, leading to the existence of good co planarity in the main backbones.

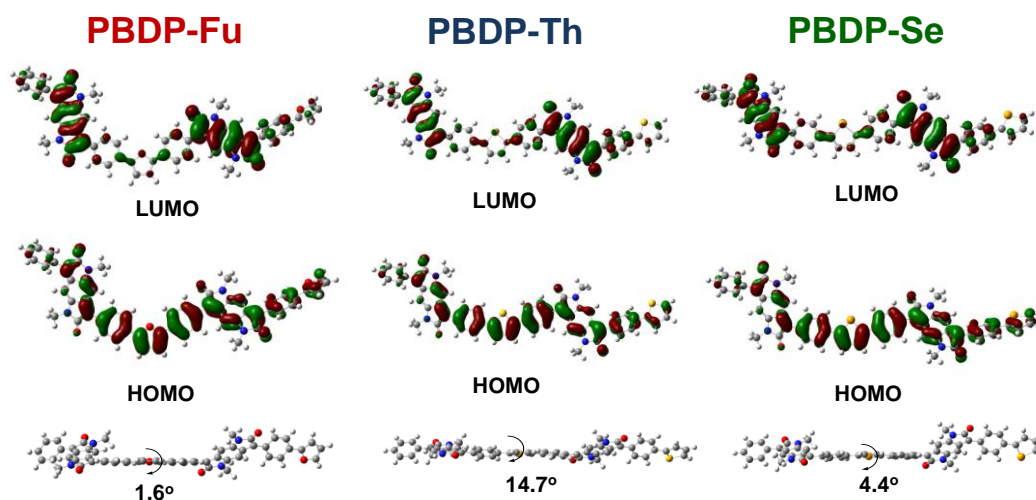


Figure 2.4. (a) DFT-optimized geometries and charge-density isosurfaces for the model dimers of BDP-based polymers (B3LYP/6-31G*) and their top views.

2.1.4. Thin Film Microstructure Analyses

Conventional X-ray diffraction (XRD) and tapping-mode atomic force microscopy (AFM) analyses were carried out to investigate the thin film microstructures and morphologies on the substrate, which are the key factors that govern OFET device performance. **Figure 2.5** exhibits XRD patterns of the annealed thin films of the BDP-based polymers, which enables us to specifically study the polymer chain alignment.

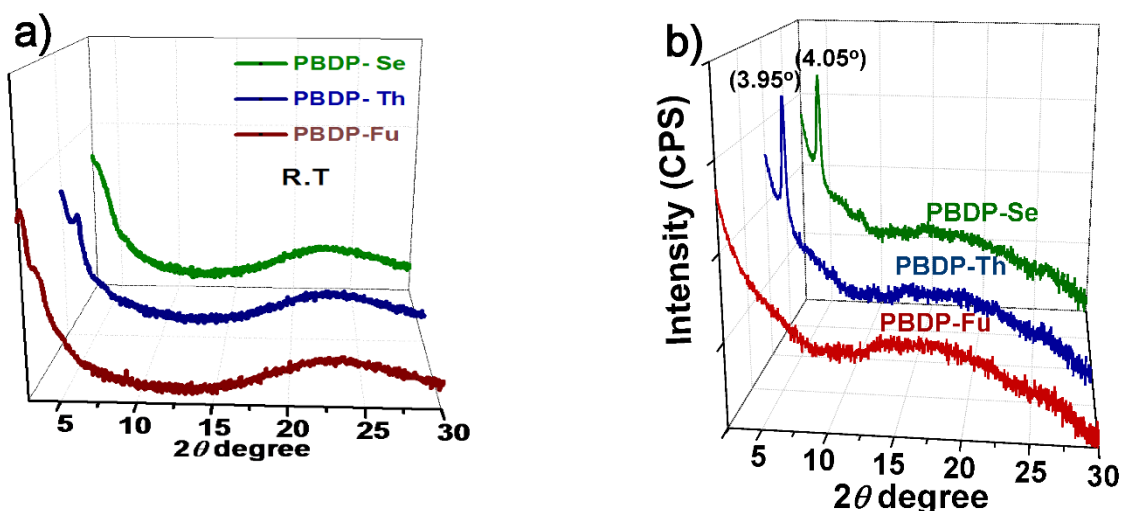


Figure 2.5. Out-of-plane X-ray diffraction (XRD) patterns of BDP-based polymer films at ambient temperature (a) and annealed at 200 °C (b)

As shown in **Figure 2.5**, both **PBDP-Th** and **PBDP-Se** films show noticeable primary diffraction peaks with similar intensities at 2θ of 3.95° and 4.05° , corresponding to $d(001)$ -spacing values of 22.36 and 21.82 Å respectively, while no clear $d(001)$ -diffraction peaks appeared in the films of **PBDP-Fu**. In addition, no observable π -stacking diffractions of polymer $d(010)$ appeared in any of the cases. Judging from these XRD results, the films of **PBDP-Th** and **PBDP-Se** polymers preferentially adopt an edge-on orientation respective to the substrate, whereas **PBDP-Fu** are rather amorphous and exhibit no apparent surface structures, which is likely attributed to the less ordered intermolecular packing. In addition, as illustrated in **Figure 2.6**, compared to the **PBDP-Fu** film, both the **PBDP-Th** and **PBDP-Se** films have relatively denser grains. This visible change in the film crystallinity and morphology between **PBDP-Fu** and **PBDP-Th/PBDP-Se** likely stems from the stronger intermolecular interaction of **PBDP-Th/PBDP-Se** relative to **PBDP-Fu** films. This can be attributed to the larger overlap integrals and higher polarizabilities of sulfur and selenium (in Th and Se, respectively) compared to the lighter oxygen atom (in Fu).⁴⁴ ⁴⁶ Therefore, we would expect a facile charge transport in the **PBDP-Th** and **PBDP-Se** polymers, when compared to **PBDP-Fu** (*vide infra*).

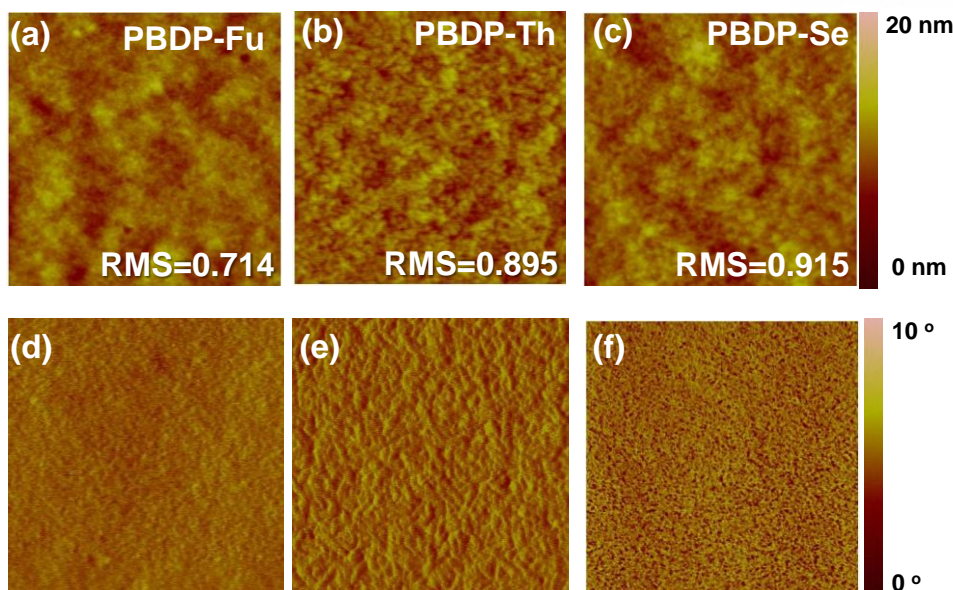


Figure 2.6. AFM height (top) and phase (bottom) images of (a, d) **PBDP-Fu**, (b, e) **PBDP-Th**, and (c, f) **PBDP-Se** films annealed at 200 °C

2.1.5 OFETs Performance

Top gate, bottom contact OFETs with **PBDP-Th**, **PBDP-Se**, and **PBDP-Fu** were fabricated on a glass substrate with a poly(methyl methacrylate) (PMMA) gate dielectric layer. The conjugated polymer films are annealed at various temperatures from 100 to 250 °C for 30 min to improve device characteristics. **Figure 2.7** shows the typical transfer and output curves of the OFETs that were annealed at 200 °C; details of device properties including hole (μ_h) and electron mobility (μ_e), and threshold voltage (V_{TH}) are summarized in **Table 2.2**. All devices showed typical ambipolar OFETs characteristics with well-balanced μ_h and μ_e . The charge carrier mobilities of all devices are improved up to an order of magnitude by increasing the annealing temperature from 100 to 200 °C. This is mainly due to the improved crystallinity of polymer films by thermal annealing, which is observed in the XRD results (**Figure 2.5**). A comparison between polymers revealed that **PBDP-Th** and **PBDP-Se** OFETs showed better μ_h and μ_e than **PBDP-Fu** OFETs due to a shorter intermolecular distance via a larger intermolecular interaction.⁶¹ In addition, this result is consistent with our expectation based on XRD and AFM results. 200 °C annealed **PBDP-Se** OFETs showed the best and most well-balanced μ_h and μ_e of $1.7 \times 10^{-2} \text{ cm}^2/\text{V}\cdot\text{s}$ and $1.9 \text{ cm} \times 10^{-2} \text{ cm}^2/\text{V}\cdot\text{s}$, respectively. Even though the balance of μ_h and μ_e is one of the key factors to realize high performance complementary inverter based ICs and LETs, almost all ‘push-pull’ ambipolar conjugated polymers exhibited less balanced μ_h and μ_e since, not only do various parameters such as the crystallinity and orientation of the molecule, contact resistance, and quality of semiconductor-dielectric interface determine field-effect mobility in OFETs, but we cannot

control the electron accepting and donating properties precisely via the design of the molecule. Therefore, the well balanced mobility in the BDP based copolymers here provides very useful information on how to design the D-A polymer to obtain well-balanced μ_h and μ_e .

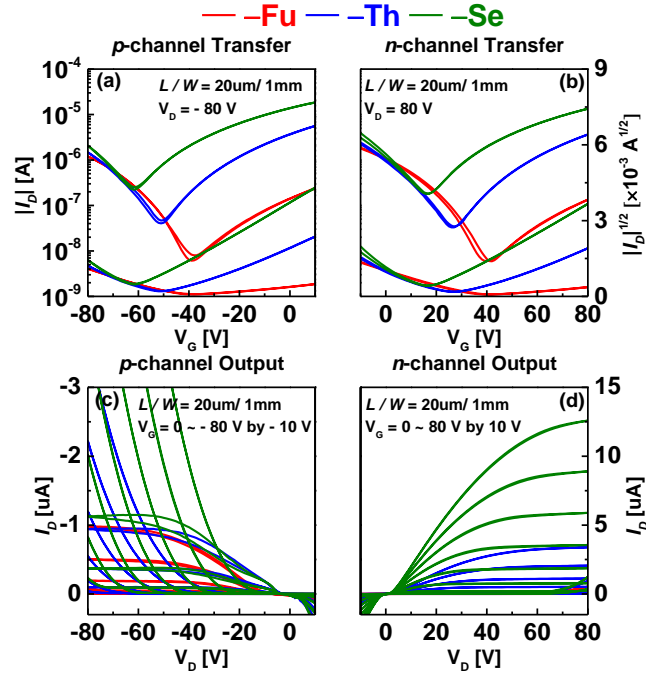


Figure 2.7. Transfer and output curve of 200 °C annealed **PBDP-Fu** (red line), **PBDP-Th** (blue line), and **PBDP-Se** (green line) OFETs. (a) *p*-channel and (b) *n*-channel transfer characteristics. (c) *p*-channel and (d) *n*-channel output characteristics.

Table 2.2. Summary of the electrical characteristics of **PBDP-Fu**, **PBDP-Th**, and **PBDP-Se** OFETs annealed at various temperatures.^a

T _A	PBDP-Fu (aver.)				PBDP-Th (aver.)				PBDP-Se (aver.)				
		μ_{sat} cm ² /V·s	V _{TH} [V]	S.S [V/dec.]	I_{on}/I_{off}	μ_{sat} cm ² /V·s	V _{TH} [V]	S.S [V/dec.]	I_{on}/I_{off}	μ_{sat} cm ² /V·s	V _{TH} [V]	S.S [V/dec.]	I_{on}/I_{off}
100 °C	Hole	5.0 × 10 ⁻⁴	-28.6	-18.2	3 × 10 ²	4.5 × 10 ⁻³	-47.4	-12.4	2 × 10 ²	7.2 × 10 ⁻³	-52.0	-17.9	1 × 10 ¹
	Electron	7.9 × 10 ⁻⁵	17.5	33.1	1 × 10 ¹	2.5 × 10 ⁻³	35.7	19.9	1 × 10 ²	7.3 × 10 ⁻³	11.0	16.0	2 × 10 ²
150 °C	Hole	3.3 × 10 ⁻³	-41.5	-12.0	8 × 10 ³	6.8 × 10 ⁻³	-54.5	-11.8	2 × 10 ²	9.3 × 10 ⁻³	-53.3	-20.2	1 × 10 ¹
	Electron	1.7 × 10 ⁻⁴	34.5	25.0	9 × 10 ²	6.7 × 10 ⁻³	35.5	13.9	7 × 10 ³	1.1 × 10 ⁻²	16.8	17.7	2 × 10 ²
200 °C	Hole	4.8 × 10 ⁻³	-45.6	-10.4	6 × 10 ³	1.2 × 10 ⁻²	-53.4	-14.5	3 × 10 ²	1.7 × 10 ⁻²	-53.4	-18.5	1 × 10 ¹
	Electron	4.3 × 10 ⁻⁴	40.2	18.7	5 × 10 ²	1.1 × 10 ⁻²	34.2	17.2	5 × 10 ³	1.9 × 10 ⁻²	19.1	19.8	2 × 10 ²
250 °C	Hole	3.7 × 10 ⁻³	-47.6	-12.3	2 × 10 ²	6.0 × 10 ⁻³	-54.2	-15.2	8 × 10 ²	9.1 × 10 ⁻³	-53.0	-18.1	1 × 10 ¹
	Electron	5.8 × 10 ⁻⁴	27.5	20.7	4 × 10 ²	3.0 × 10 ⁻²	30.4	10.6	4 × 10 ³	2.2 × 10 ⁻²	19.9	14.1	9 × 10 ³

^aAll values are averaged from 6~9 devices.

To more clearly explain the sources of mobility difference in BDP polymers, contact resistance (R_c) and activation energy (E_A) for the electron and hole were measured using the Y-function method and low temperature I-V measurement, respectively. Details of the Y-function method

have been described in our previous report and elsewhere.⁶²⁻⁶³ As shown in **Figure 2.8(a)** and **Table 2.3**, a lower R_c was extracted from **PBDP-Th** and **PBDP-Se** OFETs than from the **PBDP-Fu** devices and R_c of the electron and hole decreased by thermal annealing. This result indicates that a lower R_c in annealed devices is one of the reasons for the improvement of μ_h and μ_e by thermal annealing. The R_c for hole injection is almost similar for all polymers, whereas electron R_c shows a large difference as shown in **Figure 2.8(b)**. This is an unexpected result since the three polymers have almost the same barrier height for electron and hole injection since all polymers have very similar LUMO and HOMO energetic levels. The larger electron R_c in **PBDP-Fu** OFETs is presumably due to the unfavorable molecular conformation, in particular the BDP unit, for efficient electron injection at the electrode-semiconductor interface.⁶⁴ E_A for electron and hole transport is extracted using Arrhenius plotting of μ_h and μ_e measured at a low temperature and results are shown in **Figure 2.9** and **Table 2.4**. The E_A follows similar trends to R_c . **PBDP-Se** and **PBDP-Th** OFETs showed lower electron and hole E_A than **PBDP-Fu**. Along with the R_c result, this is very consistent with the mobility trend of these devices and implies that the highest μ_h and μ_e in the **PBDP-Se** OFETs is mainly due to the lowest R_c and E_A , which is the result from the high crystallinity in XRD results in **PBDP-Se** and **PBDP-Th** films.

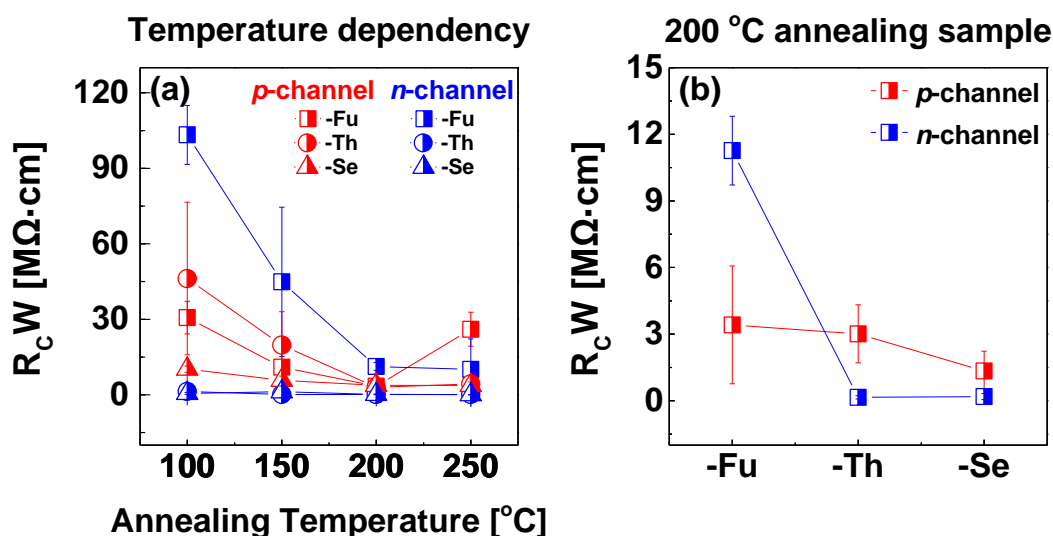


Figure 2.8. (a) Hole and electron contact resistance per unit channel width versus annealing temperature of **PBDP-Fu**, **PBDP-Th**, and **PBDP-Se** OFETs. (b) Hole and electron contact resistance of **PBDP-Fu**, **PBDP-Th**, and **PBDP-Se** OFETs annealed at 200 °C.

Table 2.3. Summary of hole and electron contact resistance for **PBDP-Fu**, **PBDP-Th**, and **PBDP-Se** OFETs various annealed temperatures.^a

T _A		PBDP-Fu	PBDP-Th	PBDP-Se
		R _C W [MΩ·cm]	R _C W [MΩ·cm]	R _C W [MΩ·cm]
100 °C	Hole	30.69 ± 6.48	46.20 ± 30.34	10.20 ± 1.26
	Electron	103.31 ± 11.71	1.37 ± 1.64	0.58 ± 0.39
150 °C	Hole	10.99 ± 7.64	19.76 ± 13.24	5.80 ± 1.65
	Electron	44.87 ± 29.7	0.16 ± 0.09	1.20 ± 2.29
200 °C	Hole	3.41 ± 2.65	3.01 ± 1.31	2.82 ± 3.99
	Electron	11.26 ± 1.54	0.15 ± 0.07	0.13 ± 0.07
250 °C	Hole	26.06 ± 6.75	4.32 ± 1.62	3.74 ± 1.38
	Electron	10.13 ± 12.1	0.14 ± 0.21	0.05 ± 0.02

^a All values are averaged from 6~9 devices.

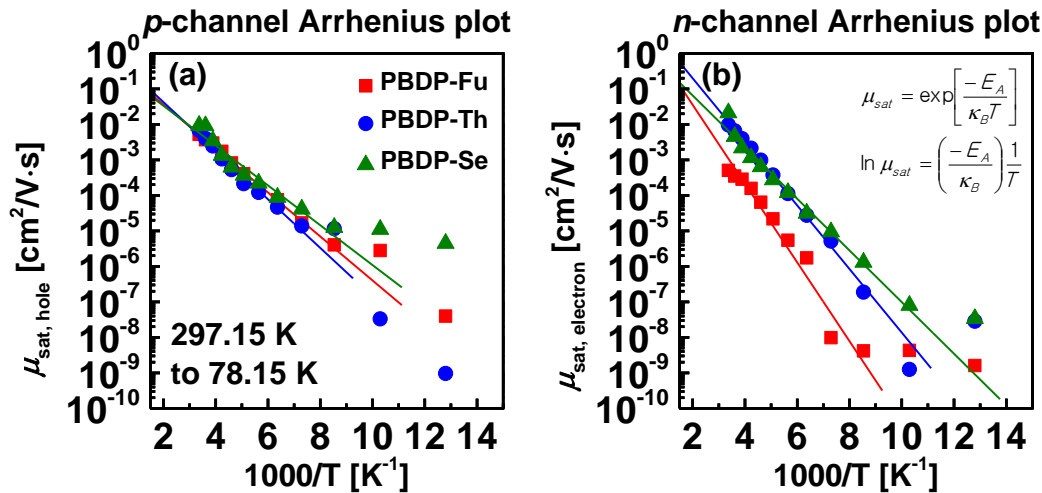


Figure 2.9. (a) Hole and (b) electron mobility (μ) versus $1000/\text{temperature}$ 200 °C annealed **PBDP-Fu**, **PBDP-Th**, and **PBDP-Se** OFETs. Devices were measured at various temperatures from 297.15 K to 78.15 K at 20 K steps.

Finally, we demonstrated ambipolar complementary inverters using three conjugated polymers as a single active layer. Ambipolar conjugated polymers can transport both the electron and hole in one polymer chain so that the p- and n-channel semiconducting active regions in a complementary inverter can be formed by simple blanket coating such as spin coating and bar-coating without any patterning processes.⁶⁵ To achieve excellent inverter performance such as high voltage gain and a right inverting voltage at $V_{DD}/2$, high and well-balanced μ_h and μ_e ($V_{TH,h}$ and $V_{TH,e}$) are required. **Figures 2.10(a)** and **(b)** show the voltage transfer characteristics (VTCs) and the corresponding voltage gains of 200 °C annealed **PBDP-Fu**, **PBDP-Th**, and **PBDP-Se** ambipolar

inverters at $V_{DD} = 80V$. The V_{inv} of the complementary inverter is reached when both the p - and n -channel OFETs operate in the saturation region and can be expressed by Equation (1):

$$V_{inv} = \frac{V_{DD} + V_{Th}^p + V_{Th}^n \sqrt{\frac{\beta_n}{\beta_p}}}{1 + \sqrt{\frac{\beta_n}{\beta_p}}} \quad (1)$$

where $\beta = (W/L)\mu_{FET}C_i$ is a design factor for adjusting the p - and n -channel currents of the transistors and the superscripts p and n denote the semiconductor type.⁶⁶ The V_{inv} of the **PBDP-Fu** device was the most theoretically ideal position at $\frac{1}{2}V_{DD}$, even though a large hysteresis was observed between the forward ($V_{inv} = 57.4$ V) and reverse ($V_{inv} = 31.1$ V) sweep due to the poorer device performances (**Table 2.5**) with the largest R_c (**Table 2.5**). On the other hand, **PBDP-Th** and **PBDP-Se** inverters showed a sharper inverting transition and a smaller hysteresis, but V_{inv} was shifted more to the left direction from $\frac{1}{2}V_{DD}$ by ~ 10 and 20 V, respectively. The right position of V_{inv} in the **PBDP-Fu** device was attributed to the more well-balanced $V_{TH,h} = -45.6$ V and $V_{TH,e} = 40.1$ V of the **PBDP-Fu** OFETs than those of the **PBDP-Th** ($V_{TH,h} = -53.4$ V, $V_{TH,e} = 34.2$ V) and **PBDP-Se** ($V_{TH,h} = -53.0$ V, $V_{TH,e} = 19.1$ V) inverters, since the position of V_{inv} mainly depends on the difference between the absolute value of $V_{TH,h}$ and $V_{TH,e}$. However, the **PBDP-Fu** devices showed the largest hysteresis in VTC because the device showed the largest R_c for electron and hole injection and lowest μ_h and μ_e . Even though the **PBDP-Se** devices showed the most shifted V_{inv} , the largest average inverter gain (~ 20) was achieved in the **PBDP-Se** device compared with that of **PBDP-Th** (~ 15) and **PBDP-Fu** (~ 5). This is due to the highest and most well-balanced μ_h and μ_e in the **PBDP-Se** OFETs. From this study, we can control the inverter characteristics such as the VTCs and gains systematically by changing the molecular structure.

Table 2.4. Summary of hole and electron activation energy (E_A) of **PBDP-Fu**, **PBDP-Th**, and **PBDP-Se** OFETs.

	hole		electron	
	$-E_A$ [meV]	$\mu_{sat,hole}$ [cm ² /V·s]	$-E_A$ [meV]	$\mu_{sat,electron}$ [cm ² /V·s]
	1st region	At 297.15K	1st region	At 297.15K
PBDP-Fu	-123	0.0052	-220.16	0.0006
PBDP-Th	-136	0.0068	-177.67	0.0097
PBDP-Se	-111	0.0093	-144.36	0.0212

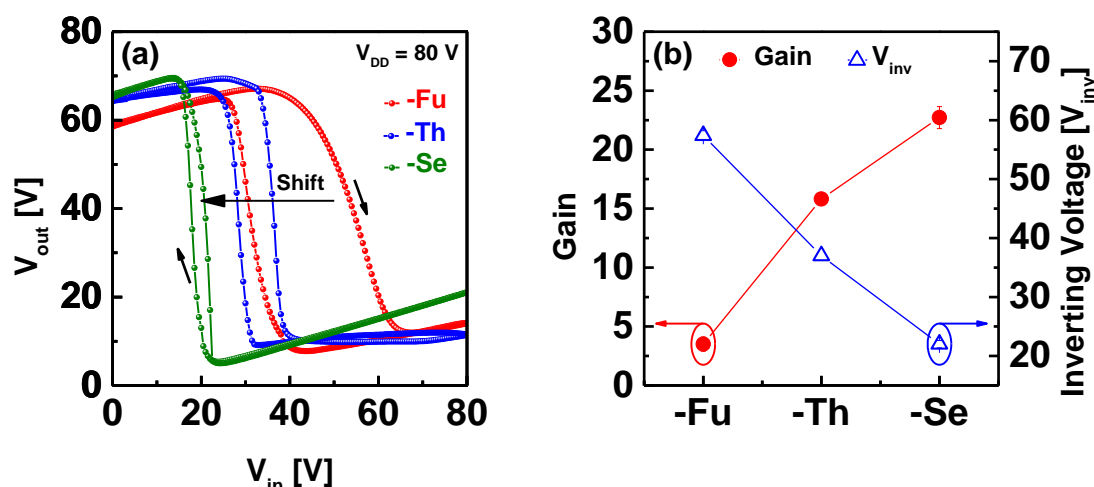


Figure 2.10. (a) Output characteristics of ambipolar complementary **PBBDP-Fu**, **PBBDP-Th**, and **PBBDP-Se** inverters ($W/L = 1000/20 \mu\text{m}$ for n - and p -channel transistors), (b) gain and inverting voltage of complementary inverters annealed at $200 \text{ }^\circ\text{C}$ versus ambipolar polymers.

Table 2.5. Summary of Gain and inverting voltage (V_{inv}) for **PBBDP-Fu**, **PBBDP-Th**, and **PBBDP-Se** complementary inverters.

	PBBDP-Fu			PBBDP-Th			PBBDP-Se		
	Gain	V_{inv}	$\Delta V_{\text{TH,m}}$	Gain	V_{inv}	$\Delta V_{\text{TH,m}}$	Gain	V_{inv}	$\Delta V_{\text{TH,m}}$
Forward	-3.50	57.40	-2.72	-15.81	37.00	-9.59	-22.72	22.00	-17.18
Reverse	-8.61	31.10		-14.33	28.00		-18.73	17.20	

2.1.6 Conclusions

We designed and synthesized a family of three donor (D)-acceptor (A) polymer semiconductors (**PBBDP-Fu**, **PBBDP-Th**, and **PBBDP-Se**) which polymerize donors of varying heteroaromatic blocks (furan (Fu), thiophene (Th), or selenophene (Se)) with the recently conceived benzodipyrrolidone (BDP) acceptor, and that take on microstructural ordering with an edge-on configuration, whereas **PBBDP-Fu** films take on an amorphous/low crystallinity alignment. Thereby, our confidence in both **PBBDP-Th** and **PBBDP-Se** as relatively higher performance polymers is justified by the aiming to systemically investigate the actual impact of the chalcogen atoms on intrinsic semiconducting properties. Given the similarity of the LUMO levels ($-3.58 \sim -3.60 \text{ eV}$) due to the electron-accepting BDP moiety, the HOMO levels are shown to relatively depend on the donating companion units. XRD and AFM measurements reveal that both **PBBDP-Th** and **PBBDP-Se** polymer films with relatively heavier chalcogen atoms take on microstructural ordering with an edge-on configuration, whereas **PBBDP-Fu** films take on a rather amorphous/low crystallinity alignment. Not only does **PBBDP-Se** have both hole and electron mobilities exceeding

$1.8 \times 10^{-2} \text{ cm}^2/\text{V}\cdot\text{s}$, but **PBDP-Th** also shows an almost equivalence between *p*-type operation and *n*-type operation, ($\mu_h = 1.2 \times 10^{-2} \text{ cm}^2/\text{V}\cdot\text{s}$) and ($\mu_e = 1.1 \times 10^{-2} \text{ cm}^2/\text{V}\cdot\text{s}$), respectively. Our studies provide generalizable insights into structure-property relationships on the existence of different heteroaromatic blocks in bislactam-based D-A polymers, which should facilitate the further design of high performance polymer semiconductors for OFETs.

2.1.7 Experimental Section

General information: All reagents were purchased from Aldrich Co., Alfa Aesar., TCI Co and were used without purification. All solvents were used as fresh by distillation. Anhydrous THF was obtained by distillation from sodium/benzophenone prior to use. The intermediates based on benzodipyrrolidone (**1** and **2**)¹⁹⁻²⁰ as well as counterpart co-monomers (2,5-bis(trimethylstannyl)furan, 2,5-bis(trimethylstannyl)thiophene, and 2,5-bis(trimethylstannyl)selenophene)⁶⁷ were prepared according to the methods outlined in the literature. ¹H NMR and ¹³C NMR spectra were recorded on an Agilent 400 MHz spectrophotometer using CDCl₃ as the solvent and tetramethylsilane (TMS) as the internal standard, and UV-VIS-NIR spectra were taken on a UV-1800 (SHIMADZU) spectrometer. The number-average (M_n) and weight average (M_w) molecular weights, and the polydispersity index (PDI) of the polymer products were determined by gel permeation chromatography (GPC) with Perkin-Elmer Series 200 using a series of mono disperse polystyrene standards in THF (HPLC grade) at 313 K. Cyclic voltammetry (CV) measurements were performed on AMETEK VersaSTAT 3 with a three-electrode cell in a nitrogen bubbled 0.1 M tetra-*n*-butylammonium hexafluorophosphate (*n*-Bu₄NPF₆) solution in acetonitrile at a scan rate of 50 mV/s at room temperature. The CV was used as the Ag/Ag⁺ (0.1M of AgNO₃ in acetonitrile) reference electrode, platinum counter electrode, and polymer coated platinum working electrode, respectively. The Ag/Ag⁺ reference electrode was calibrated using a ferrocene/ferrocenium redox couple as an internal standard, of which the oxidation potential is set at -4.8 eV with respect to a zero vacuum level.

General procedure for Stille polymerization and polymer purification: Compound (**2**) (0.13 mol) and distannyl compounds (0.13 mmol) were placed in a Schlenk tube under an argon atmosphere with 5 mL of anhydrous toluene. The mixture was degassed for 20 min followed by the addition of Pd(PPh₃)₄ (9.9 mol, 5mol%). The mixture was heated at 110 °C for 24 h. After cooling to room temperature, the mixture was poured into methanol and the resulting precipitate was filtered. The polymer was purified by Soxhlet extraction using methanol, acetone, and hexane, and finally extracted with chloroform. The chloroform solution was then concentrated by evaporation and re-precipitated in methanol. The resulting dark blue colored solids were collected and dried

overnight under vacuum. The polymers were characterized by ^1H NMR, GPC, and elemental analysis.

PBDP-Fu: Isolated yield = 75%. $M_n = 47.0$ kDa, $M_w = 82.0$ kDa, and PDI = 1.74 (against PS standard), ^1H NMR (CDCl_3 , 400 MHz): δ ppm 7.78-7.92 (br 8H), 6.85 (s, 2H), 6.43 (s, 2H), 3.56 (s, 4H), 1.82 (br, 4H), 1.38 (br 8H), 1.20-1.43 (br, 70H), 0.84-0.92 (br, 12H). Anal. calcd. for $\text{C}_{74}\text{H}_{110}\text{N}_2\text{O}_3$: C, 82.63; H, 10.31; N, 2.60; O, 4.46; found: C, 82.53; H, 10.47; N, 2.38.

PBDP-Th: Isolated yield = 70%. $M_n = 37.0$ kDa, $M_w = 61.0$ kDa, PDI = 1.64 (against PS standard), ^1H NMR (CDCl_3 , 400 MHz) δ ppm 7.75-7.78 (br, 4H), 7.30-7.73 (br, 4H), 6.20-6.42 (br, 4H), 3.54 (br, 4H), 1.80 (br, 2H), 1.65 (br, 10H), 1.22-1.40 (br, 70H), 0.83-0.91 (br, 12H) Anal. calcd. for $\text{C}_{74}\text{H}_{110}\text{N}_2\text{O}_2\text{S}$ C, 81.41; H, 10.16; N, 2.57; O, 2.93; S, 2.94; found: C, 81.54; H, 10.19; N, 2.78; S, 3.10.

PBDP-Se: Isolated yield = 81%. $M_n = 74.0$ kDa, $M_w = 84.0$ kDa, PDI = 1.13 (against PS standard), ^1H NMR (CDCl_3 , 400 MHz): δ ppm 7.59-7.78 (br, 8H), 7.39-7.57 (br, 2H), 6.42 (s, 2H), 3.47-3.54 (br, 4H), 1.80 (br, 2H), 1.65 (br, 10H), 1.22-1.40 (br, 70H), 0.83-0.91 (br, 12H) Anal. calcd. for $\text{C}_{74}\text{H}_{110}\text{N}_2\text{O}_2\text{Se}$: C, 78.06; H, 9.74; N, 2.46; O, 2.81; Se, 6.93; found : C, 78.23; H, 9.78; N, 2.36.

OFETs and complementary inverters fabrication: Cr/Au (2 nm/13 nm) source/drain patterns were performed on Corning Eagle XG glass substrates using a conventional lift-off photolithography process with positive-tone photoresist and thermal evaporation. Before use, the substrates were cleaned sequentially in a sonication bath acetone, isopropanol, and deionized water for 10 min each. Ambipolar **PBDP-X** copolymer was synthesized and used without any further purification. This semiconductor was dissolved in anhydrous chlorobenzene (Sigma Aldrich) to obtain 8 mg/ml solution and was spin coated at 1400 rpm for 90 s and then thermally annealed at temperatures ranging from 100 °C to 250 °C for 30 min in an N_2 purged glove box. 80 mg/ml of PMMA (Sigma Aldrich, ~ 120 k M_w) in nBA concentrate solution was used as the gate-dielectric and was spin-coated at 2000 rpm for 60 s and then baked at 80°C for 1 hr (thickness ~ 500 nm, Capacitance : 6.20 nF/cm 2) in an N_2 purged glove box. The transistors were completed by depositing the top gate electrodes (Al) via thermal evaporation using a metal shadow mask. For the complementary inverters, circuit electrodes were patterned using photo-lithography, as above. In addition, the semiconductor and gate dielectric layers were deposited by a simple spin coating process. Complementary inverters were completed by deposition of the top gate electrodes on the active regions of the *n*- and *p*-channel transistors.

Characterization: The electrical characteristics of the OFETs were extracted from the drain current via gate voltage bias or drain voltage bias (channel width (W)/Length (L): 1000/20 μm). The channel width and length of *n*- and *p*-channel transistors in the complementary inverters are

1000 and 20 μm , respectively. Activation energy was extracted from the mobility via a vacuum state probe chamber while decreasing the temperature from 297.15 K to 78.15 K in 20 K steps using liquid nitrogen. All measurements were taken using a Keithley 4200-SCS semiconductor parameter analyzer connected to an N_2 -purged glove box probe station.

References

- (1) Baeg, K. -J.; Caironi, M.; Noh, Y. -Y. *Adv. Mater.* **2013**, *25*, 4210.
- (2) Schenning, A. P.; Meijer, E. *Chem. Commun.* **2005**, *26*, 3245.
- (3) Barbara, P. F.; Gesquiere, A. J.; Park, S.-J.; Lee, Y. J. *Acc. Chem. Res.* **2005**, *38*, 602.
- (4) Tao, N. *Nat. Nanotechnol.* **2006**, *1*, 173.
- (5) Taniguchi, M.; Nojima, Y.; Yokota, K.; Terao, J.; Sato, K.; Kambe, N.; Kawai, T. *J. Am. Chem. Soc.* **2006**, *128*, 15062.
- (6) Lafferentz, L.; Ample, F.; Yu, H.; Hecht, S.; Joachim, C.; Grill, L. *Science* **2009**, *323*, 1193.
- (7) Chen, X.; Braunschweig, A. B.; Wiester, M. J.; Yeganeh, S.; Ratner, M. A.; Mirkin, C. A. *Angew. Chem., Int. Ed.* **2009**, *48*, 5178.
- (8) Joachim, C.; Gimzewski, J.; Aviram, *Nature* **2000**, *408*, 541.
- (9) Li, J.; Zhao, Y.; Tan, H. S.; Guo, Y.; Di, C.-A.; Yu, G.; Liu, Y.; Lin, M.; Lim, S. H.; Zhou, Y. *Sci. Rep.* **2012**, *2*, 754.
- (10) Baeg, K. -J.; Khim, D.; Jung, S. W.; Kang, M.; You, I. K.; Kim, D. Y.; Facchetti, A.; Noh, Y. -Y. *Adv. Mater.* **2012**, *24*, 5433.
- (11) Zaumseil, J.; Friend, R. H.; Sirringhaus, H. *Nat. Mater.* **2005**, *5*, 69-74.
- (12) Baeg, K.-J.; Kim, J.; Khim, D.; Caironi, M.; Kim, D.-Y.; You, I.-K.; Quinn, J. R.; Facchetti, A.; Noh, Y.-Y. *ACS Appl. Mater. Interfaces* **2011**, *3*, 3205.
- (13) Qu, S.; Tian, H. *Chem. Commun.* **2012**, *48*, 3039.
- (14) Lee, J.; Han, A.; Hong, J.; Seo, J. H.; Oh, J. H.; Yang, C. *Adv. Funct. Mater.* **2012**, *22*, 4128.
- (15) Lee, J.; Cho, S.; Seo, J. H.; Anant, P.; Jacob, J.; Yang, C. *J. Mater. Chem.* **2012**, *22*, 1504.
- (16) Lee, J.; Cho, S.; Yang, C. *J. Mater. Chem.* **2011**, *21*, 8528.
- (17) Lee, J.; Yun, M. H.; Kim, J.; Kim, J. Y.; Yang, C. *Macromol. Rapid Commun.* **2012**, *33*, 140.
- (18) Cho, S.; Lee, J.; Tong, M.; Seo, J. H.; Yang, C. *Adv. Funct. Mater.* **2011**, *21*, 1910.
- (19) Cui, W.; Yuen, J.; Wudl, F. *Macromolecules* **2011**, *44*, 7869.
- (20) Hong, W.; Guo, C.; Li, Y.; Zheng, Y.; Huang, C.; Lu, S.; Facchetti, A. *J. Mater. Chem.* **2012**, *22*, 22282.
- (21) Yue, W.; Huang, X.; Yuan, J.; Ma, W.; Krebs, F. C.; Yu, D. *J. Mater. Chem. A* **2013**, *1*, 10116.

- (22) Deng, P.; Liu, L.; Ren, S.; Li, H.; Zhang, Q. *Chem. Commun.* **2012**, *48*, 6960.
- (23) Stalder, R.; Mei, J.; Reynolds, J. R. *Macromolecules* **2010**, *43*, 8348.
- (24) Zhang, G.; Fu, Y.; Xie, Z.; Zhang, Q. *Macromolecules* **2011**, *44*, 1414.
- (25) Stalder, R.; Mei, J.; Subbiah, J.; Grand, C.; Estrada, L. A.; So, F.; Reynolds, J. R. *Macromolecules* **2011**, *44*, 6303.
- (26) Lei, T.; Dou, J.-H.; Ma, Z.-J.; Yao, C.-H.; Liu, C.-J.; Wang, J.-Y.; Pei, J. *J. Am. Chem. Soc.* **2012**, *134*, 20025.
- (27) Stalder, R.; Grand, C.; Subbiah, J.; So, F.; Reynolds, J. R. *Polym. Chem.* **2012**, *3*, 89.
- (28) Wang, E.; Ma, Z.; Zhang, Z.; Vandewal, K.; Henriksson, P.; Inganäs, O.; Zhang, F.; Andersson, M. R. *J. Am. Chem. Soc.* **2011**, *133*, 14244.
- (29) Dutta, G. K.; Han, A.; Lee, J.; Kim, Y.; Oh, J. H.; Yang, C. *Adv. Funct. Mater.* **2013**, *23*, 5317.
- (30) Koizumi, Y.; Ide, M.; Saeki, A.; Vijayakumar, C.; Balan, B.; Kawamoto, M.; Seki, S. *Polym. Chem.* **2013**, *4*, 484.
- (31) Van Pruissen, G. W.; Gholamrezaie, F.; Wienk, M. M.; Janssen, R. A. *J. Mater. Chem.* **2012**, *22*, 20387.
- (32) Ashraf, R. S.; Kronemeijer, A. J.; James, D. I.; Sirringhaus, H.; McCulloch, I. *Chem. Commun.* **2012**, *48*, 3939.
- (33) Mei, J.; Graham, K. R.; Stalder, R.; Reynolds, J. R. *Org. Lett.* **2010**, *12*, 660.
- (34) Mei, J.; Kim, D. H.; Ayzner, A. L.; Toney, M. F.; Bao, Z. *J. Am. Chem. Soc.* **2011**, *133*, 20130.
- (35) Lee, J.; Han, A.-R.; Yu, H.; Shin, T. J.; Yang, C.; Oh, J. H. *J. Am. Chem. Soc.* **2013**, *135*, 9540.
- (36) Lee, J.; Han, A.-R.; Kim, J.; Kim, Y.; Oh, J. H.; Yang, C. *J. Am. Chem. Soc.* **2012**, *134*, 20713.
- (37) Shahid, M.; McCarthy-Ward, T.; Labram, J.; Rossbauer, S.; Domingo, E. B.; Watkins, S. E.; Stingelin, N.; Anthopoulos, T. D.; Heeney, M. *Chem. Sci.* **2012**, *3*, 181.
- (38) Kronemeijer, A. J.; Gili, E.; Shahid, M.; Rivnay, J.; Salleo, A.; Heeney, M.; Sirringhaus, H. *Adv. Mater.* **2012**, *24*, 1558.
- (39) Ha, J. S.; Kim, K. H.; Choi, D. H. *J. Am. Chem. Soc.* **2011**, *133*, 10364.

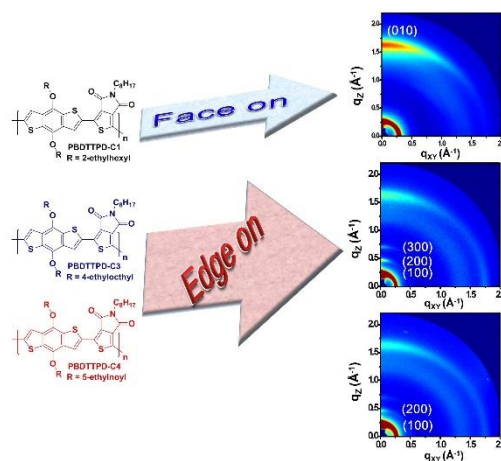
- (40) Gidron, O.; Dadvand, A.; Sheynin, Y.; Bendikov, M.; Perepichka, D. F. *Chem. Commun.* **2011**, 47, 1976.
- (41) Woo, C. H.; Beaujuge, P. M.; Holcombe, T. W.; Lee, O. P.; Fréchet, J. M. *J. Am. Chem. Soc.* **2010**, 132, 15547.
- (42) Bunz, U. H. *Angew. Chem., Int. Ed.* **2010**, 49, 5037.
- (43) Chen, Z.; Wannere, C. S.; Corminboeuf, C.; Puchta, R.; Schleyer, P. v. R. *Chem. Rev.* **2005**, 105, 3842.
- (44) Takimiya, K.; Kunugi, Y.; Konda, Y.; Niihara, N.; Otsubo, T. *J. Am. Chem. Soc.* **2004**, 126, 5084.
- (45) Hutchison, G. R.; Ratner, M. A.; Marks, T. J. *J. Am. Chem. Soc.* **2005**, 127, 16866.
- (46) Sharma, S.; Bendikov, M. *Chem. Eur. J.* **2013**, 19, 13127.
- (47) Bijleveld, J. C.; Karsten, B. P.; Mathijssen, S. G.; Wienk, M. M.; de Leeuw, D. M.; Janssen, R. *J. Mater. Chem.* **2011**, 21, 1600.
- (48) Yuan, J.; Huang, X.; Zhang, F.; Lu, J.; Zhai, Z.; Di, C.; Jiang, Z.; Ma, W. *J. Mater. Chem.* **2012**, 22, 22734.
- (49) Yuan, J.; Zang, Y.; Dong, H.; Liu, G.; Di, C.; Li, Y.; Ma, W. *Polym. Chem.* **2013**, 4, 4199.
- (50) Sonar, P.; Foong, T. R. B.; Singh, S. P.; Li, Y.; Dodabalapur, A. *Chem. Commun.* **2012**, 48, 8383.
- (51) Li, Y.; Sonar, P.; Murphy, L.; Hong, W. *Energy Environ. Sci.* **2013**, 6, 1684.
- (52) Li, Y.; Sonar, P.; Singh, S. P.; Zeng, W.; Soh, M. S. *J. Mater. Chem.* **2011**, 21, 10829.
- (53) Li, Y.; Sonar, P.; Singh, S. P.; Soh, M. S.; van Meurs, M.; Tan, J. *J. Am. Chem. Soc.* **2011**, 133, 2198.
- (54) Dou, L.; Chang, W. H.; Gao, J.; Chen, C. C.; You, J.; Yang, Y. *Adv. Mater.* **2013**, 25, 825.
- (55) Pati, P. B.; Senanayak, S. P.; Narayan, K.; Zade, S. S. *ACS Appl. Mater. Interfaces* **2013**, 5, 12460.
- (56) Nakano, M.; Mori, H.; Shinamura, S.; Takimiya, K. *Chem. Mater.* **2011**, 24, 190.
- (57) Rumer, J. W.; Levick, M.; Dai, S.-Y.; Rossbauer, S.; Huang, Z.; Biniek, L.; Anthopoulos, T. D.; Durrant, J.; Procter, D. J.; McCulloch, I. *Chem. Commun.* **2013**, 49, 4465.
- (58) Kim, Y.; Hong, J.; Oh, J. H.; Yang, C. *Chem. Mater.* **2013**, 25, 3251.
- (59) Kim, Y.; Yeom, H. R.; Kim, J. Y.; Yang, C. *Energy Environ. Sci.* **2013**, 6, 1909.

- (60) Kim, B.; Yeom, H. R.; Yun, M. H.; Kim, J. Y.; Yang, C. *Macromolecules* **2012**, *45*, 8658.
- (61) Kang, I.; An, T. K.; Hong, J.; Yun, H. J.; Kim, R.; Chung, D. S.; Park, C. E.; Kim, Y. H.; Kwon, S. K. *Adv. Mater.* **2013**, *25*, 524.
- (62) Baeg, K.-J.; Bae, G.-T.; Noh, Y.-Y. *ACS Appl. Mater. Interfaces* **2013**, *5*, 5804.
- (63) Xu, Y.; Minari, T.; Tsukagoshi, K.; Chroboczek, J.; Ghibaudo, G. *J. Appl. Phys.* **2010**, *107*, 114507.
- (64) Fabiano, S.; Yoshida, H.; Chen, Z.; Facchetti, A.; Loi, M. A. *ACS Appl. Mater. Interfaces* **2013**, *5*, 4417.
- (65) Khim, D.; Han, H.; Baeg, K. J.; Kim, J.; Kwak, S. W.; Kim, D. Y.; Noh, Y. -Y. *Adv. Mater.* **2013**, *25*, 4302.
- (66) Rabaey, J.; Chandrakasan, A.; Nikolic, B. *Digital Integrated Circuits* (Printice-Hall Electronics and VLSI series). Englewood Cliffs, NJ: Prentice-Hall: **2003**.
- (67) Lei, T.; Cao, Y.; Zhou, X.; Peng, Y.; Bian, J.; Pei, J. *Chem. Mater.* **2012**, *24*, 1762.
- * Chapter II is reproduced in part with permission of “ACS Appl. Mater. Interfaces **2014**, *6*, 4872–4882”. Copyright 2014 American Chemical Society.

Chapter III

Synthesis and Characterization of Conjugated Benzodithiophene-Based Photovoltaic Polymers with Branched Alkyl Substitutions

In chapter III, we described synthesis and characterization of benzodithiophene (BDT) based polymer with different alkyl substitutions for OPVs. Chapter III is reproduced in part with permission of “A roundabout approach to control the morphological orientation and solar cell performance by modulating side chain branching position in BDT-Based Polymers” from K. C. Lee *et. al. ChemPhysChem* **2015**, 16, 1305-1314.



3.1 BDT-Based Polymers

3.1.1 Introduction

Developing polymer-based bulk-heterojunction (BHJ) solar cells that consist of electron-donating polymers and electron-accepting fullerene derivatives continues to garner research interests because of several distinct benefits in terms of compatibility with flexible and light-weight substrates, architectural tunability over multiple length scales, and high-throughput, yet with low-cost processing.¹⁻⁵ The power conversion efficiencies (PCEs) of the state-of-the-art devices have now surpassed the 8% mark.⁶⁻⁹ To achieve such high performances, one of the most critical contributions is the development of materials, along with innovations and optimizations in device structure and processing.¹⁰ Therefore, relying on universal donor-acceptor (D-A) strategies, vast numbers of new D-A copolymer donor materials have been developed in which most of the effort has been focused on the structural modification of the conjugated backbones for precisely tuning the frontier energy levels in order to harvest as much solar energy as possible, while also maintaining sufficient energetic driving force for charge separation.¹¹⁻¹⁴

Taking into account the above-mentioned prerequisites, D–A copolymers based on benzo[1,2-*b*:4,5-*b'*]dithiophene (BDT) units—relatively simple, compact, symmetric, and planar structure—have been subjected to increasing levels of interest for their use in high-performance solar cells, since their inception on BHJ solar cells in 2008. Thereafter, many D–A copolymers based on BDT with different conjugated units, such as thieno[3,4-*b*]thiophene (TT),¹⁵⁻¹⁷ 4,7-dithiophene-2-yl-2,1,3-benzothiadiazole (DTBT),¹⁸ *N*-alkylthieno[3,4-*c*]pyrrole-4,6-dione (TPD),¹⁹⁻²¹ and bithiazole,²² etc. have been successfully demonstrated with high PCE in BHJ devices. Besides manipulating their backbone structures, structural modifications can be brought about by means of alkyl side chain variations. For example, the BDT-containing 2-D polymers were synthesized by replacing alkoxy groups with alkylthienyl side chains.^{5,23-25} Recently, Beaujuge et al. reported on the synthesis of BDT-based copolymers bearing linear alkoxy side chains in the BDT motifs, instead of the branched ones. The progress of these classes of polymer materials has been impressive, with PCE as high as 9.2%,²⁶⁻²⁸ but it is also believed that superior performance is possible through implementation of the newly fine-tuned molecular structures of BDT building cores to copolymerize with suitable co-units.

Therefore, the fresh design and synthesis of BDT-containing polymers is still worthy of investigation in polymer BHJ solar cell fields, which will be made through an in-depth understanding of materials science and the associated improvement of PCEs.

Our previous studies have found that the alkyl chain branching position could play a critical role in intermolecular interactions and supramolecular self-assembly,²⁹⁻³² which correlates well with the improved charge transport properties. In addition, McCulloch et al. recently demonstrated the positive effects of this in diketopyrrolopyrrole (DPP)-based polymers on solar cell performance. As an extension of the related work on the engineering of side chains, in this context, we chose the copolymer of BDT and TPD, referred to as **PBDTPD-C_n**, and tried to shed light on the structure–property device performance relationship associated with the structural dynamics of the side chains by moving the branching position away from the BDT core (see the three **PBDTPD-C_n** polymers in **Figure 3.1**, where *n* is the number of carbon atoms between the alkoxyated oxygen and the branching point). A worth-noting point emerged from this study is that tuning a polymer’s side chains can greatly affect the preferential packing conformation in the films.

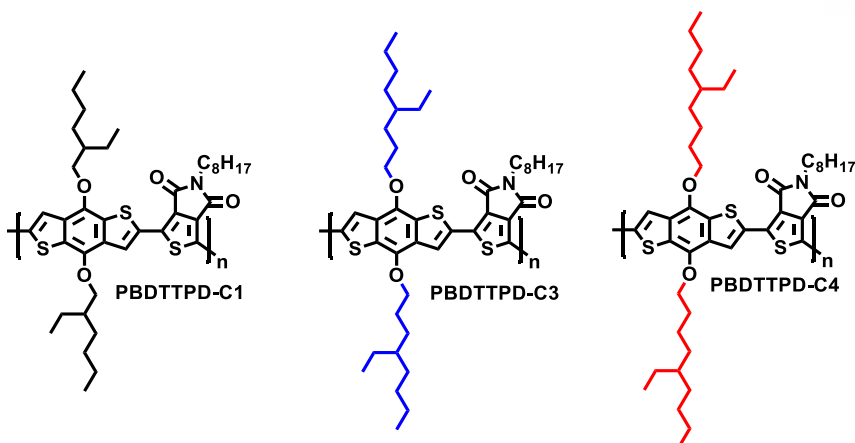
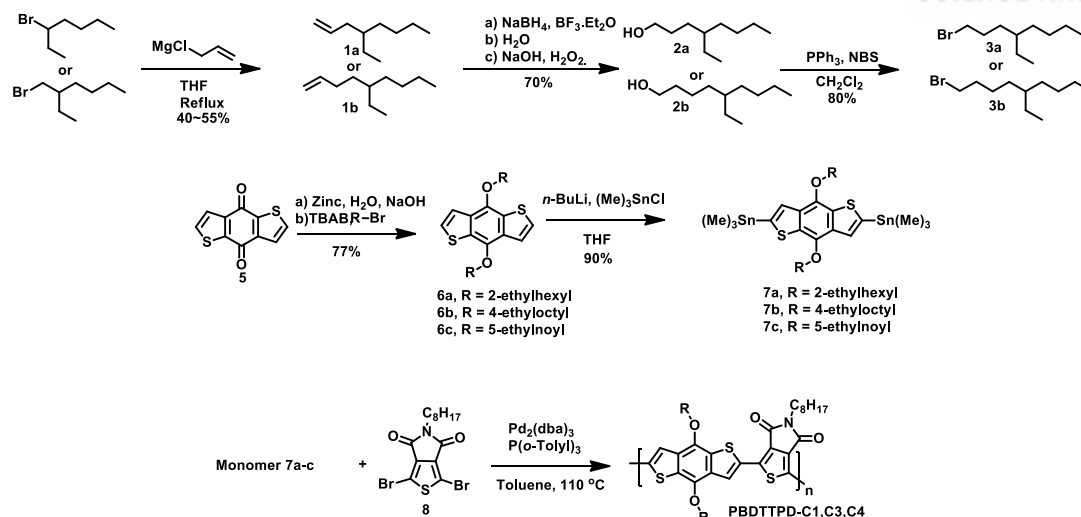


Figure 3.1. Structures of **PBDTTPD-Cn**

3.1.2 Design, Synthesis, and Characterization

The synthesis of the monomers and target polymers (**PBDTTPD-C1**, **PBDTTPD-C3**, and **PBDTTPD-C4**) are shown in **Scheme 3.1**, and the detailed synthetic procedures are provided in the experimental section. First, 1,3-dibromo-5-octylthieno-[3,4-*c*]pyrrole-4,6-dione and benzo[1,2-*b*:4,5-*b'*]dithiophene-4,8-dione were prepared by following literature procedures.^{19, 33, 34} The 4-ethyloctyl-bromide and 5-ethylnonyl-bromide used as the key branched alkyl chains were synthesized by three steps, starting with the commercially available chemicals (overall yield = 22–38%); the corresponding alkyl bromide was extended by the reaction with allylmagnesium chloride, sequentially followed by hydroboration-oxidation and bromination. Each of the branched alkyl substituents such as 2-ethylhexyl, 4-ethyloctyl, and 5-ethylnonyl were introduced into the BDT unit in the presence of Zn/NaOH, which was then transformed into the corresponding bis-stannylated monomers by lithiation and subsequent quenching with trimethyltin chloride.



Scheme 3.1. Synthetic routes to **PBDTTPD-C_n**

PBDTTPD-C1, **PBDTTPD-C3**, and **PBDTTPD-C4** were synthesized by a Pd-catalyzed Stille-coupling reaction in high yields; $\text{Pd}_2(\text{dba})_3$ was used as a catalyst, and $\text{P}(o\text{-tolyl})_3$ was used as the corresponding ligand in degassed toluene. All polymers were carefully purified by extracting with methanol, acetone, hexane, and chloroform, each for 1 d, in order to remove catalytic impurities and other small molecular parts. The number-average molecular weights (M_n) and polydispersity indexes (PDI) were obtained through gel-permeation chromatography (GPC) against polystyrene using THF as the eluent (**Table 3.1**).

Table 3.1. Photophysical and electrochemical properties of **PBDTTPD-C_n**.

Polymer	M_n (kDa)	PDI	$\lambda_{\text{max}}^{\text{sol}}$ (nm) ^a	$\lambda_{\text{max}}^{\text{film}}$ (nm)	E_g^{opt} (eV) ^b	E_{HOMO} (eV) ^c	E_{LUMO} (eV) ^c	E_g^{CV} (eV) ^d
PBDTTPD-C1	13.0	2.10	550	620	1.78	-5.44	-3.55	1.89
PBDTTPD-C3	23.0	1.92	543	622	1.81	-5.35	-3.51	1.84
PBDTTPD-C4	16.0	2.32	547	620	1.77	-5.44	-3.53	1.91

3.1.3 Optical and Electrochemical Properties

The normalized UV-visible absorption spectra of three polymers in chloroform solution and thin films are shown in **Figures 3.2a** and **b**, and the detailed values are listed in **Table 3.1**. Together with the appearance of the shoulder peaks around the absorption maxima, these polymers show very similar absorption bands in solution with major absorption peaks at 550 nm for **PBDTTPD-C1**, 543 nm for **PBDTTPD-C3**, and 547 nm for **PBDTTPD-C4**. These typical bands can be attributed to the intramolecular charge transfer (ICT) between electron-donating BDT and -accepting TPD moieties. In its solid state, the shoulders appearing near their absorption maxima

are intensified, leading to apparently broadening peaks, in which the absorptions cover 400–670 nm, with peaks centered at 600 nm. Note that the absorption band of **PBDTTPD-C4** shows a less pronounced vibronic aspect. The optical band gaps from the onset of solid film absorption were evaluated to be 1.78, 1.81, and 1.77 eV for **PBDTTPD-C1**, **PBDTTPD-C3**, and **PBDTTPD-C4**, respectively, (Table 3.1).

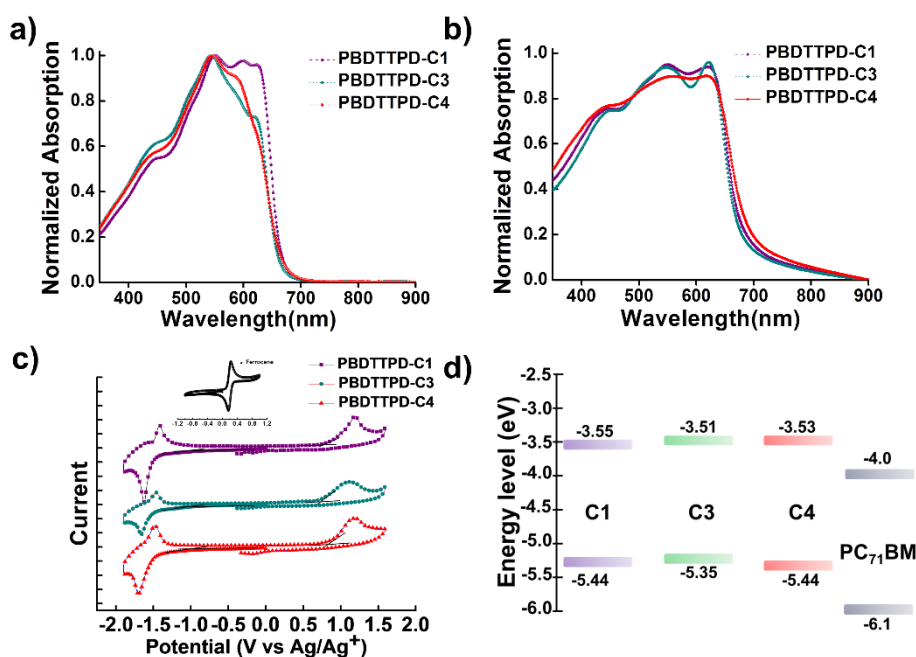


Figure 3.2. UV-vis absorption spectra of **PBDTTPD-Cn** in chloroform solution (a) and as a thin solid films spin-cast from chloroform (b) Cyclic voltammograms of **PBDTTPD-Cn** thin films (c) Energy level diagrams for **PBDTTPD-Cn** and PC₇₁BM (d).

Cyclic voltammetry (CV) was employed to investigate the frontier orbital energy levels (HOMO and LUMO) of the BDT-based polymers (Figure 3.2c). To obtain the oxidation and reduction potentials of the polymer films, the reference electrode was calibrated using ferrocene/ferrocenium (Fc/Fc⁺), which had a redox potential with an absolute energy level of -4.80 eV in a vacuum. The potential of this external standard under the same conditions was 0.20 eV versus Ag/Ag⁺. All polymers exhibited an oxidation onset between 0.75 and 0.84 eV versus Ag/Ag⁺. The HOMO levels of -5.44, -5.35, and -5.44 eV were calculated to be -0.84, -0.75, and -0.84 eV, respectively. Regarding the threshold HOMO level for air-stable conjugated polymers was estimated to be -5.2 eV.³⁵ The deep-lying HOMO levels of the BDT-based polymers, particularly for **PBDTTPD-C4**, would be beneficial, not only for their chemical stability in ambient conditions, but also for the higher open-circuit voltage (V_{oc}) value in solar cell applications. In the reduction processes, all three polymers exhibit good reversibility, with very

similar reduction onset values at ca. -1.05, -1.09, and -1.07 eV versus Ag/Ag⁺, corresponding to the estimated LUMO values of -3.55, -3.51, -3.53 eV for **PBDTTPD-Cn**. Detailed electrochemical properties are summarized in **Table 3.1**. From the CV measurement results, the distance of the branching point is obvious.

3.1.4 Computational Studies

The aim is to provide insight into one of the branched side groups that exhibit the effect of the selective fine-tuning of LUMO levels. By investigating the possible subtle change of the molecular architecture arising from moving the branching point on the BDT unit, we conducted density functional theory (DFT) calculations of the model molecules using Gaussian 09 at the B3LYP/6-31G* level. (see **Figure 3.3**) To simplify the calculations, the octyl chains on the TPD acceptor unit were replaced with methyl groups, and the backbones were simplified to a BDT-TPD-BDT structure. Interestingly, the dihedral angle of 0.6° between BDT and TPD in the optimized structure of BDT-TPD-BDT-C1 is reduced to 0.2–0.3° in BDT-TPD-BDT-C3 and -C4, implying that a strengthened coplanar conformation can be achieved by tuning the branching point further from the backbone. In addition, in all cases, the HOMOs are mostly distributed along the BDT donor unit, whereas the LUMOs are localized on the TPD acceptor moiety, implying that the distance of the branching position from BDT has a negligible effect on the electron state density distributions of the polymers.

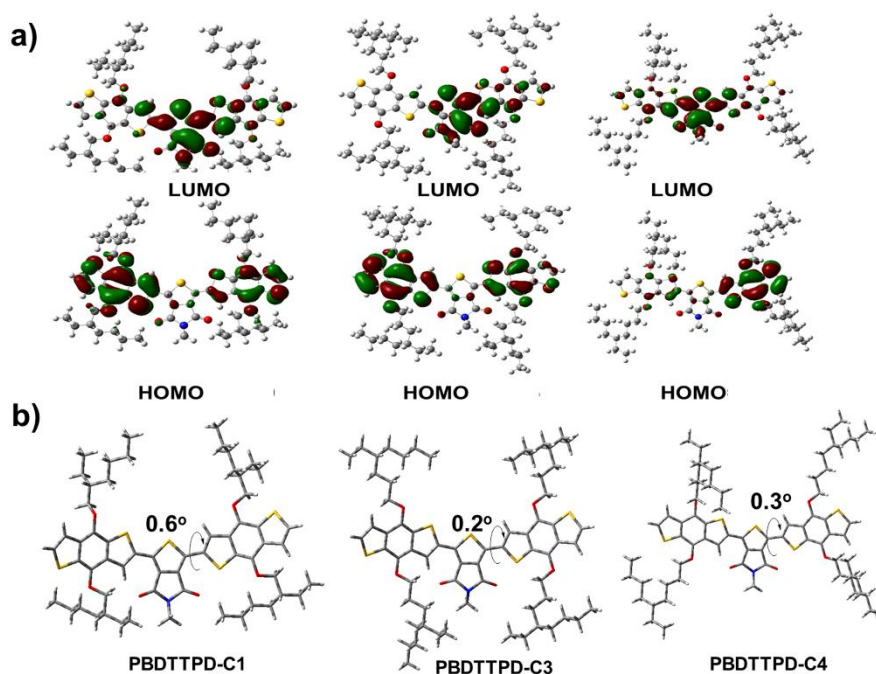


Figure 3.3. DFT-optimized geometries and charge-density isosurfaces for BDT-TPD-BDT (B3LYP/6-31G*) (a) and their dihedral angles (b).

3.1.5 Solar Cell Performance and Film Morphology

To examine the effect of the alkyl chain branching point on both performance and blend morphology in polymer-based BHJ solar cells with a PC₇₁BM acceptor, we fabricated with standard structure of indium tin oxide (ITO)/poly(3,4-ethylenedioxythiophene):poly(styrenesulfonate)(PEDOT:PSS)/BDT-based polymer:PC₇₁BM/Al, wherein the weight ratios of Polymer:PC₇₁BM were 1:1, 1:2, or 1:3 w/w, and 1,2-dichlorobenzene (*o*-DCB) was chosen as the carrier solvent for all polymers. The optimization process also included the use of a small amount of processing additives such as 1,8-diiodooctane (DIO), diphenyl ether (DPE), and 1-chloronaphthalene (CN). Each polymer device was individually optimized with processing parameters such as their polymer concentrations, blend ratios, and processing additives. The solar cells were tested under a simulated 100 mW/cm², AM 1.5G illumination. The detailed parameters of the optimized devices for each polymer are summarized in **Table 3.2**, with the corresponding current density–voltage (*J*–*V*) curves and external quantum efficiency (EQE) spectra shown in **Figures 3.4a** and **b**.

The best device performance was achieved based on **PBDTTPD-C1:PC₇₁BM** (1:2 w/w) devices processed with 3 vol% DIO, which showed a high current density (*J*_{SC}) of 11.6 mA/cm², open-circuit voltage (*V*_{OC}) of 0.84 V, a fill factor (FF) of 0.47, and an impressive PCE of 4.56%. In both **PBDTTPD-C3** and **PBDTTPD-C4**, even though FF values were comparable to that of **PBDTTPD-C1**, and even higher *V*_{OC} values were obtained without processing additives, significantly reduced JSC values led to greatly lowered PCEs. We found that after employing 3 vol% CN, the *J*_{SC} values of the devices were dramatically improved, from 1.74–2.83 to 6.55–7.09 mA/cm², and thus PCEs were increased to 2.37–2.80%, but were still lower than of that of the optimized BHJ solar cells cast from **PBDTTPD-C1:PC₇₁BM**. In **Figure 3.4b**, the EQE curves of the solar cells were fabricated under the same optimized conditions as those used for the *J*–*V* measurements. The *J*_{SC} values calculated by integrating the EQE curve with an AM1.5G reference spectrum have an average 6.1% error compared to the corresponding JSC obtained from the *J*–*V* curves. This indicates that our photovoltaic measurement is both accurate and reliable. Obviously, the EQE values for **PBDTTPD-C1** are all higher than those of **PBDTTPD-C3**- and **PBDTTPD-C4**-based cells, which are consistent with the higher *J*_{SC} values of the devices derived from **PBDTTPD-C1**.

Table 3.2. Parameters of performance for **PBDTTPD-C_n** devices with structure of ITO/PEDT:PSS/Polymer:PC₇₁BM/Al measured under AM 1.5G illumination at 100mW/cm²

	Polymer: PC ₇₁ BM (w/w)	Solvent (v/v)	J_{sc} (mA/cm ²)	V _{oc}	FF	PCE (%)
PBDTTPD-C1	1:1	CB	7.28	0.85	0.56	3.48
	1:2	CB	9.54	0.81	0.53	4.07
	1:3	CB	5.83	0.80	0.55	2.59
	1:2	99%CB+1%DIO	9.40	0.84	0.43	3.39
	1:2	97%CB+3%DIO	11.60	0.84	0.47	4.56
	1:2	95%CB+5%DIO	8.39	0.84	0.40	2.84
	1:2	97%CB+3%CN	10.50	0.84	0.45	3.98
	1:2	97%CB+3%DPE	9.92	0.83	0.47	3.90
PBDTTPD-C3	1:1	CB	1.74	0.91	0.49	0.78
	1:2	CB	1.29	0.89	0.50	0.58
	1:3	CB	1.48	0.87	0.40	0.52
	1:1	97%CB+3%DIO	5.03	0.75	0.44	1.65
	1:1	99% CB+1%CN	5.76	0.77	0.43	1.91
	1:1	97% CB+3%CN	7.09	0.76	0.52	2.80
	1:1	95% CB+5%CN	6.20	0.75	0.46	2.12
	1:1	97% CB+3%DPE	6.15	0.75	0.44	2.02
PBDTTPD-C4	1:1	CB	2.45	0.86	0.50	1.06
	1:2	CB	2.83	0.86	0.51	1.24
	1:3	CB	3.50	0.76	0.51	1.36
	1:2	97%CB+3%DIO	5.92	0.75	0.39	1.75
	1:2	99%CB+1%CN	6.63	0.66	0.51	2.24
	1:2	97%CB+3%CN	6.55	0.70	0.52	2.37
	1:2	95%CB+5%CN	5.10	0.75	0.53	2.20
	1:2	97%CB+3%DPE	6.33	0.67	0.52	2.21

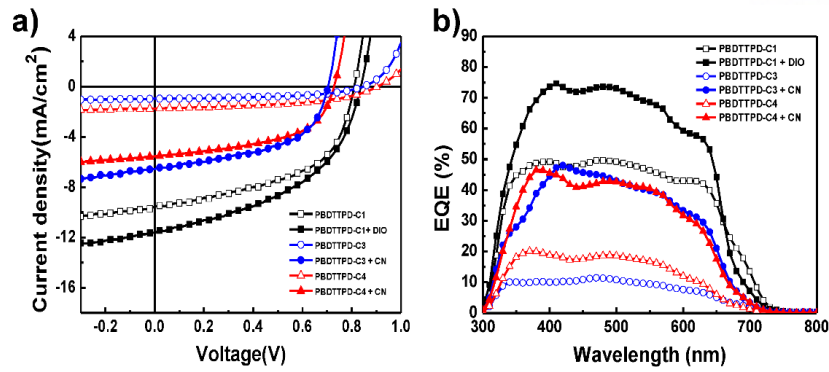


Figure 3.4. J-V Characteristics (a) and external quantum efficiency (EQE) spectra of **PBDTTPD-C1** (black), **C3** (blue) and **C4** (red) (b).

To correlate the polymer side-chain patterns effectively, the microstructural order in thin films, and device performance, we employed a grazing-incidence wide-angle X-ray scattering (GIWAXS), and examined the films of the pure polymers and optimized polymer:PC₇₁BM blends. As shown in **Figure 3.5**, all neat polymer films exhibited (*h*00) diffraction patterns along the *q_z* (out-of-plane) axis, corresponding to a lamellar structure, together with (010) peaks along the *q_{xy}* (in-plane) axis arising from the π - π stacking of polymer backbones; the detailed crystallographic parameters are presented in **Table 3.3**. Notably, the neat films of both **PBDTTPD-C3** and **PBDTTPD-C4** not only revealed more intense and sharper (100) peaks and multi-peak diffraction up to the third order, but also the (100) peaks shifted towards a slightly smaller *q* as the branching point length was increased. Thus, the lamellar d-spacing distances follow the sequence **PBDTTPD-C1** (16.98 Å) < **PBDTTPD-C3** (19.04 Å) < **PBDTTPD-C4** (19.63 Å) from GIWAXS.

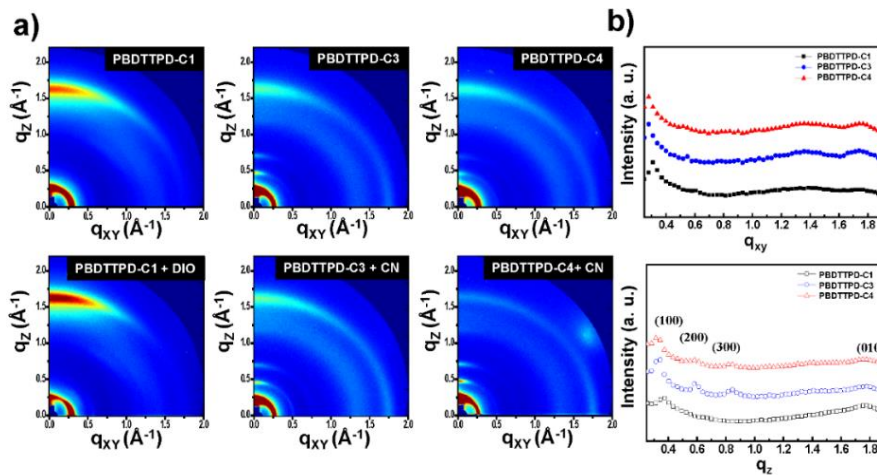


Figure 3.5. Grazing incident wide angle X-ray scattering (GIWAXS) results for neat **PBDTTPD-Cn** in-plane and out-of-plane line cuts (a) of the corresponding above patterns (b).

Table 3.3. Summary of GIWAXS analysis on **PBDTTPD-Cn** as neat and blend films.

Polymer	Direction	Angle of π - π interaction [°]	Scattering vector (q) of π - π stacking [Å^{-1}]	d-spacing [Å]	Lamella interaction (h00)	Angle of Lamella peak [°]	Scattering vector of Lamella peak [Å^{-1}]	lamella interaction distance [Å]
Neat-C1	In-plane	-	-	-	(100)	1.75	0.31	20.27
	Out-of-plane	10.06	1.77	3.55	(100)	2.09	0.37	16.98
Neat-C3	In-plane	9.94	1.75	3.59	(100)	1.58	0.28	22.44
					(200)	3.34	0.59	10.65
	Out-of-plane	10.06	1.77	3.55	(100)	1.87	0.33	19.04
					(300)	4.81	0.85	7.48
Neat-C4	In-plane	9.94	1.75	3.59	(100)	1.55	0.275	22.84
					(200)	3.34	0.59	10.65
	Out-of-plane	10.06	1.77	3.55	(100)	1.81	0.32	19.63
					(300)	4.70	0.83	7.57
Blend-C1	In-plane	9.94	1.75	3.59	(100)	1.75	0.31	20.27
	Out-of-plane	10.11	1.78	3.53	(100)	2.09	0.37	16.98
Blend-C3	In-plane	9.94	1.75	3.59	(100)	1.58	0.28	22.44
					(200)	3.39	0.60	10.47
	Out-of-plane	10.11	1.78	3.53	(100)	1.92	0.34	18.48
					(300)	4.81	0.85	7.39
Blend-C4	In-plane	9.94	1.75	3.59	(100)	1.55	0.275	22.84
					(200)	3.34	0.59	10.65
	Out-of-plane	10.11	1.78	3.53	(100)	1.87	0.33	19.04
					(300)	4.75	0.84	7.48

As seen from **Figure 3.5a**, a face-on orientation was found for all pure polymer films, with evident (010) π - π stacking reflection in the out-of-plane direction ($q_{xy} \approx 0$) and the (100) lamellar d-

spacing reflection in the in-plane direction ($q_z \approx 0$). In parallel, it should be noted that the relative intensity of the π - π spacing peak in the in-plane direction became stronger as the branching point was shifted away from the backbone, which seems to slightly encourage the edge-on character population in **PBDTTPD-C3** and **PBDTTPD-C4**. A similar effect of the position of the chain branching point on the thin-film morphology has previously been noticed in our and other groups.^{31, 32, 36}

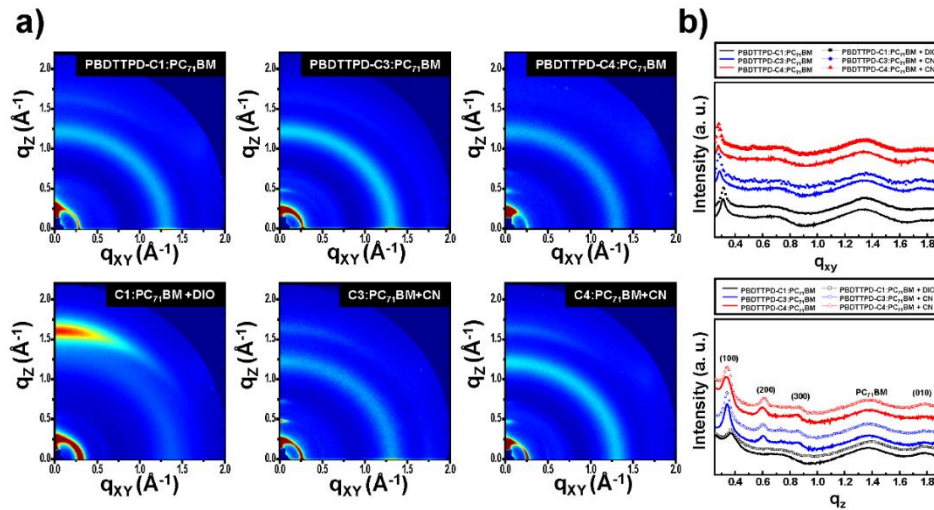


Figure 3.6. GIWAXS images for blends of **PBDTTPD-Cn:PC₇₁BM** and with additive (a). In-plane and out-of-plane line cuts of the corresponding above patterns for **PBDTTPD-Cn:PC₇₁BM** (solid line) and with additive (symbol line)films (b)

In addition to a diffraction halo centered at $1.34\text{--}1.37 \text{ \AA}^{-1}$ associated with **PC₇₁BM** (as shown in **Figure 3.6a, b**), a similar trend was observed for the polymer:**PC₇₁BM** blend films. Moving the branching point further from the backbone resulted in higher-order diffraction peaks in the out-of-plane direction, and slightly more pronounced π - π peaks in the in-plane direction. Additionally, once the processing additive was used, the intensities of the out-of-plane (010) and in-plane (100) peaks in the blending systems became more obvious and increased slightly, indicating that the crystallinity and the face-on orientation population were both enhanced.

Consequently, GIWAXS data indicated the fractions of **PBDTTPD-C1** crystallinity. In both cases, the pure polymers and blends decreased not only the lamellar ordering, but also relatively favored the face-on characteristic when compared to the analogs studied here. Therefore, we assume that the intrinsic differences in preferential polymer orientation and the overall degree of structural order correlates with the variations in material performance observed in BHJ solar cells with **PC₇₁BM**.

The surface morphologies of polymer:PC₇₁BM blends cast without and with the corresponding optimal additives were explored using tapping-mode atomic force microscopy (AFM), as shown in **Figure 3.7**. Thin films processed without additives contained a smooth and featureless texture with a RMS roughness of 2.35 nm for **PBDTTPD-C1**. In contrast, the large agglomerated clusters with RMSs of 5.22–7.68 nm were observed for **PBDTTPD-C3** and **PBDTTPD-C4**, which is consistent with the high crystallinity revealed by GIWAXS. This nonhomogeneity on the macroscopic level is most likely responsible for the inferior device performance for **PBDTTPD-C3** and **PBDTTPD-C4**. In addition, the additives were regulating the domain size of the morphology by selectively solubilizing the PC₇₁BM, facilitating the integration of the PC₇₁BM molecules into the polymer aggregates, which is in good agreement with similar reports.³⁷ According to the GIWAXS and AFM results, it can be concluded that the intrinsic differences in preferential polymer orientation and overall degree of structural order correlate with the variations in BDT-based polymer performances observed in the BHJ solar cells with PC₇₁BM.

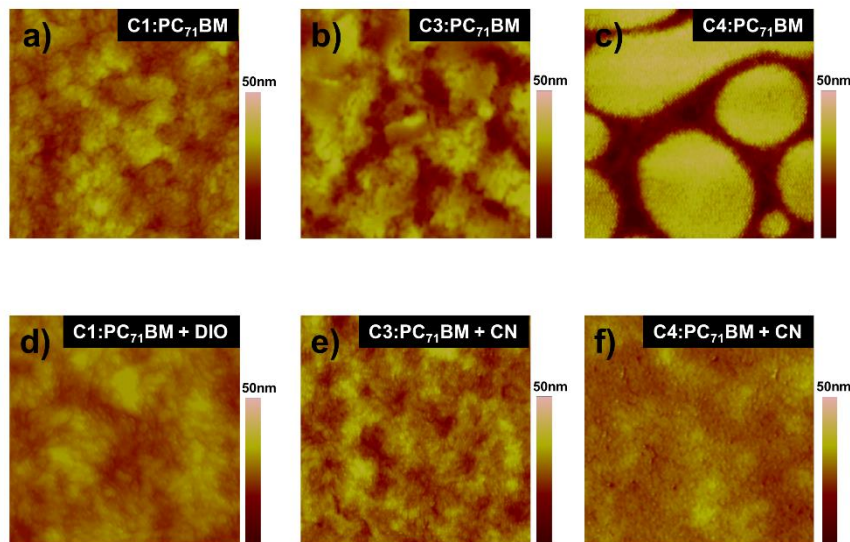


Figure 3.7. Atomic force microscopy (AFM) images ($2 \times 2 \mu\text{m}^2$) of polymer:PC₇₁BM on ITO substrate: root-mean-square (RMS) as (a) 3.32 nm (top), 2.13 nm (bottom) of **PBDTTPD-C1** (b) 5.22 nm (top), 4.02 nm of **PBDTTPD-C3** (c) 7.68 nm (top), 2.64 nm (bottom) of **PBDTTPD-C4**, respectively

To find the origin of the difference in the solar cells' performances, the charge-transport properties were investigated by examining the charge-carrier mobility of the polymer:PC₇₁BM under the each optimized condition, using the space-charge limited current (SCLC) model (hole only (ITO/PEDOT:PSS/polymer:PC₇₁BM/Au) and electron only (FTO/polymers:PC₇₁BM/Al) devices, respectively). Hole and electron mobilities are calculated by Mott-Gurney equation.

$$J_{SCLC} = \frac{9}{8} \epsilon_r \epsilon_0 \mu \left(\frac{V^2}{L^3} \right)$$

Where ϵ_r is the dielectric constant of the material, ϵ_0 is the permittivity of free space, L is the thickness of film between the cathode and anode electrodes, and V is the applied voltage (The details can be found in the Experimental Section).

The J - V characteristics are plotted in **Figure 3.8**, and the calculated hole and electron mobilities are listed in **Table 3.4** Together with the electron mobilities being nearly identical for all polymer:PC₇₁BM ($\sim 1.0 \times 10^{-4}$ cm²/V·s), small variations in their hole mobilities are also revealed in the range of 1.13×10^{-5} – 8.18×10^{-5} cm²/V·s, consequently leading to similar balanced charge transport ($\mu_{\text{electron}}/\mu_{\text{hole}}$) ratios. This would account for the quite similar FF values in the current series of BHJ solar cells.

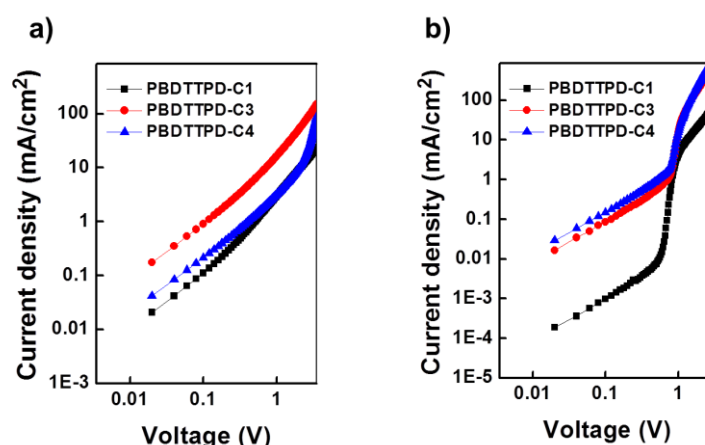


Figure 3.8. Double-logarithmic plot from dark J - V characteristics of (a) hole-only devices (ITO/PEDOT:PSS/polymer:PC₇₁BM/Au) and (b) electron only devices (FTO/polymer:PC₇₁BM/Al)

Table 3.4. Calculated electron and hole mobility of **PBDTTPD**-based polymers by space charge limited current (SCLC) devices and their thickness layers.

Polymer	Active layer (nm)	μ_{ele} (cm ² /V·s)	Active layer (nm)	μ_{hole} (cm ² /V·s)	$\mu_{\text{ele}}/\mu_{\text{hole}}$
PBDTTPD-C1	180	1.08×10^{-4}	140	2.35×10^{-5}	4.59
PBDTTPD-C3	80	1.23×10^{-4}	125	8.18×10^{-5}	1.50
PBDTTPD-C4	80	1.10×10^{-4}	110	1.13×10^{-5}	9.73

We also measured the top-contact, organic field-effect transistors (OFETs) with the architecture of Si/SiO₂/octyltrichlorosilane (OTS)/polymer/Au) as seen in **Figure 3.9** and **Table 3.5**. It is recognized that the mobilities of all polymers do not vary significantly. 2-Ethylhexyl side chains have primarily been utilized as solubilizing groups in many conjugated polymers. In this work,

not only do we introduce a 2-ethylhexyl group and two novel-designed branched alkyl chains (4-ethyloctyl and 5-ethylnonyl) into BDT-based conjugated polymers (**PBDTTPD-Cn**), but also thoroughly investigate how the branching location of alkyl chains can impact their energetics, morphologies, molecular packing, and solar cell performance. The fine modulation of the branching position on the BDT motif does not significantly affect the polymer energy levels and charge carrier mobilities, yet this strategy triggers a change of preferential polymer orientation in thin films. In other words, **PBDTTPD-C1** exhibits a pronounced face-on character, while **PBDTTPD-C3** and **PBDTTPD-C4** are slightly encouraged to form an edge-on lamellar packing in both neat polymer and blended films. Therefore, **PBDTTPD-C1** is found to reach a PCE of 4.56% in standard BHJ devices with PC₇₁BM, which represents a significant improvement over the other polymers, for which PCEs of 2.37–2.80% were achieved. Our findings exhort the value of expanding the role of a polymer’s side chains during the development of high performance polymers for organic solar cells and OFETs.

Table 3.5. Summarized the performance values of OFET device with hole mobility, threshold voltage and on-off ratio for **PBDTTPD-C1**, **C3** and **C4**.

Polymer	Thermal Annealing (°C)	Mobility (cm ² /V·s)	I _{off} (A)	I _{on} (A)	I _{on} /I _{off}	V _T (V)
PBDTTPD-C1	200	4.64E-05	2.91E-11	2.60E-08	8.90E+02	-12.73
PBDTTPD-C3	300	3.83E-05	2.76E-11	3.32E-08	1.20E+03	-15.22
PBDTTPD-C4	200	1.27E-05	9.74E-12	9.81E-09	1.01E+03	-20.81

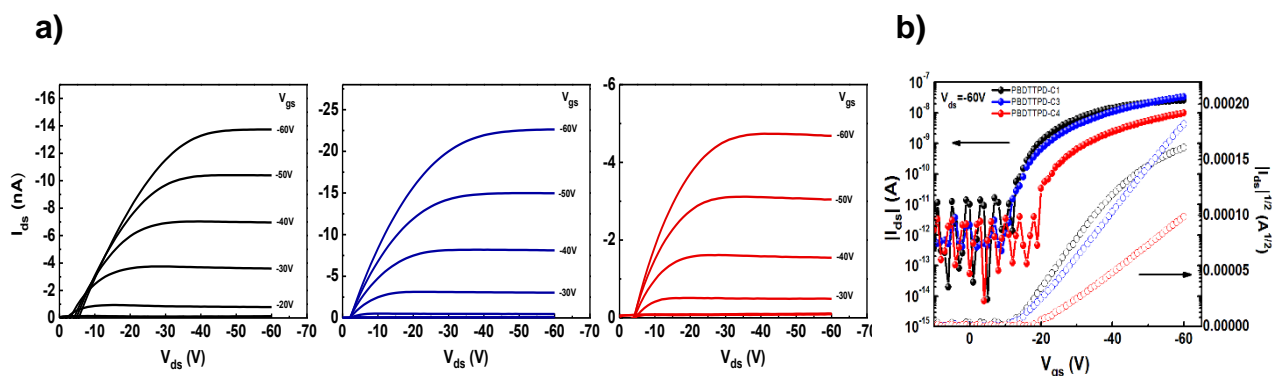


Figure 3.9. The performance of OFETs used OTS treatment as a passive layer (a) The output characteristics, (b) the transfer characteristics and plots of the square root the drain current as a function of the gate voltage for **PBDTTPD-C1**(black), **C3**(blue) and **C4**(red). (I_D: Drain current. V_G: Voltage of gate in an OFET. V_{DS}: Voltage between drain and source in an OFET)

3.1.6 Conclusions

2-Ethylhexyl side chains have primarily been utilized as solubilizing groups in many conjugated polymers. In this work, not only do we introduce a 2-ethylhexyl group and two novel-designed branched alkyl chains (4-ethyloctyl and 5-ethylnonyl) into BDT-based conjugated polymers (**PBDTTPD-Cn**), but also thoroughly investigate how the branching location of alkyl chains can impact their energetics, morphologies, molecular packing, and solar cell performance. The fine modulation of the branching position on the BDT motif does not significantly affect the polymer energy levels and charge carrier mobilities, yet this strategy triggers a change of preferential polymer orientation in thin films. In other words, **PBDTTPD-C1** exhibits a pronounced face-on character, while **PBDTTPD-C3** and **PBDTTPD-C4** are slightly encouraged to form an edge-on lamellar packing in both neat polymer and blended films. Therefore, **PBDTTPD-C1** is found to reach a PCE of 4.56% in standard BHJ devices with PC₇₁BM, which represents a significant improvement over the other polymers, for which PCEs of 2.37–2.80% were achieved. Our findings exhort the value of expanding the role of a polymer's side chains during the development of high performance polymers for organic solar cells and OFETs.

3.1.7 Experimental Section

General information: All reagents were purchased from Aldrich Co., Alfa Aesar., TCI Co. and used without purification. All solvents were used fresh solvents by distillation. Anhydrous THF and toluene were obtained by solvent purification systems. The synthesis of 1,3-dibromo-5-octylthieno-[3,4-*c*]pyrrole-4,6-dione, 4,8-bis(alkyloxy)benzo[1,2-*b*:4,5-*b'*]dithiophene (BDT), and 4,8-bis(alkyloxy)benzo[1,2-*b*:4,5-*b'*]dithiophene-2,6-bis(trimethylstannane) was prepared according to the literature methods.^{8, 19, 38} ¹H NMR and ¹³C NMR spectra were recorded on the Agilent 400 MHz spectrophotometer using CDCl₃ as solvent and tetramethylsilane (TMS) as the internal standard and UV-VIS-NIR spectra were taken on UV-1800 (SHIMADZU) spectrometer. Number-average (M_n) and weight average (M_w) molecular weights, and polydispersity index (PDI) of the polymer products were determined by gel permeation chromatography (GPC) with Perkin-Elmer Series 200 using a series of mono disperse polystyrene as standards in THF (HPLC grade) at 313 K. The electrochemical properties were measured by cyclic voltammetry (AMETEK VersaSTAT 3) with a three-electrode cell in a nitrogen bubbled 0.1 M tetra-*n*-butylammonium hexafluorophosphate (*n*-Bu₄NPF₆) solution in acetonitrile at a scan rate of 50 mV/s at room temperature. As electrode, non-aqueous Ag/Ag⁺ ion reference (0.1M of AgNO₃ in acetonitrile), Pt counter electrode, and polymer-coated platinum working electrode were employed respectively.

The Ag/Ag⁺ reference electrode was calibrated using a ferrocene/ferrocenium redox couple as an external standard, whose oxidation potential is set at -4.8 eV with respect to zero vacuum level.

4-Ethyl-oct-1-ene (1a): The mixture of allylmagnesium chloride (2.0 M in THF, 1 eq.) and 3-heptylbromide (1.0 eq.) in THF (100 mL) was refluxed for overnight. After cooling to room temperature, the reaction mixture was poured into water and quenched with 10% H₂SO₄ (10~50 mL), extracted with ethyl ether. The crude product was purified by chromatography of silica using hexane to afford compound (40 ~ 55 %) as colorless oil. ¹H NMR (CDCl₃, 400MHz) δ ppm = 5.83-5.73 (m, 1H), 5.03-4.97 (m, 2H), 2.05-2.02 (m, 2H), 1.88-1.81 (m, 1H), 1.37-1.23 (m, 8H), 0.95-0.85 (m, 6H).

5-Ethyl-non-1-ene (1b): The same procedure as described for compound **1a** but with 2-ethylhexylbromide ¹H NMR (CDCl₃, 400MHz) δ ppm = 5.83-5.72 (m, 1H), 5.02-4.96 (m, 2H), 2.05-2.01 (m, 2H), 1.44-1.23 (m, 9H), 0.94-0.85 (m, 6H).

4-Ethyl-oct-1-ol (2a): To a mixture of 4-ethyl-oct-1-ene (1 eq.) and NaBH₄ (1 eq.) in dry diglyme (10~20 mL) was added BF₃.OEt₂ (0.7 eq.) dropwise for 1 h and stirred at room temperature for 2 h under an argon atmosphere. Water (5 mL) and 3 M NaOH (20 mL) were added slowly in order and stirred more 2 h at 40 °C. The solution was treated with H₂O₂ (20 mL) slowly and stirred 1 h at room temperature. After extraction with diethyl ether, chromatography on silica gel with ethyl acetate/hexane (1:8) as eluent to afford compound (70 %) as a colorless oil. ¹H NMR (CDCl₃, 400MHz) δ ppm = 3.59-3.48 (m, 2H), 3.31 (s, 1H), 1.48-1.44 (m, 1H), 1.23-1.10 (m, 10H), 0.83-0.75 (m, 6H).

5-Ethyl-nonan-1-ol (2b): The same procedure as described for compound **2a** but with 5-ethyl-non-1-ene ¹H NMR (CDCl₃, 400MHz) δ ppm = 3.66-3.62 (m, 2H), 3.57-3.55 (m, 2H), 3.38 (s, 1H), 1.58-1.43 (m, 2H), 1.43-1.18 (m, 11H), 0.90-0.82 (m, 6H).

4-Ethyl-octylbromide (3a): To mixture of 4-ethyl-oct-1-ol (1 eq.) and triphenylphosphine (1.8 eq.) in dichloromethane (30~50 mL) was cooled to 0 °C and NBS (1.5 eq.) was added to the reaction mixture, and that of mixture was stirred for overnight at room temperature. After extraction with DCM, water, chromatography on silica gel with hexane as eluent to afford compound (80 %) as light yellow oil. ¹H NMR (CDCl₃, 400MHz) δ ppm = 3.38 (m, 2H), 1.82-1.80 (m, 2H), 1.71-1.20 (m, 11H), 0.90-0.82 (m, 6H).

5-Ethyl-nononylbromide (3b): The same procedure as described for compound **3a** but with 5-ethyl-nonan-1-ol ¹H NMR (CDCl₃, 400MHz) δ ppm = 3.41 (m, 2H), 1.87-1.82 (m, 2H), 1.43-1.38 (m, 2H), 1.41-1.22 (m, 11H), 0.91-0.82 (m, 6H).

4,8-Bis((4-ethyl-octyl)oxy)benzo[1,2,-b:4-5-b']dithiophene (6b): ¹H NMR (CDCl₃, 400MHz) δ ppm = 7.51 (d, *J* = 5.6 Hz, 2H), 7.37 (d, *J* = 5.6 Hz, 2H), 4.29 (t, *J* = 6.4 Hz, 4H), 1.92-1.84 (m, 4H), 1.58-1.50 (m, 4H), 1.39-1.30 (m, 18H), 0.95-0.89 (m, 12H). ¹³C NMR (CDCl₃, 100MHz) δ

ppm = 144.57, 131.57, 130.08, 125.94, 120.34, 74.38, 38.71, 32.82, 29.50, 29.99, 27.87, 25.88, 23.17, 14.18, 10.90.

4,8-Bis((5-ethylnoyl)oxy)benzo[1,2,-b:4-5-b']dithiophene (6c): ^1H NMR (CDCl_3 , 400MHz) δ ppm = 7.50 (d, $J = 5.6$ Hz, 2H), 7.37 (d, $J = 5.6$ Hz, 2H), 4.31 (t, $J = 6.8$ Hz, 4H), 1.90-1.85 (m, 4H), 1.60-1.53 (m, 4H), 1.37-1.29 (m, 22H), 0.94-0.86 (m, 12H). ^{13}C NMR (CDCl_3 , 100MHz) δ ppm = 144.55, 131.52, 130.17, 125.96, 120.33, 73.95, 38.89, 33.07, 32.88, 31.04, 29.03, 25.91, 23.30, 23.19, 14.21, 10.92.

4,8-Bis((4-ethyloctyl)oxy)benzo[1,2-b:4,5-b']dithiophene-2,6-diyl)bistrimethylstannane (7b): ^1H NMR (CDCl_3 , 400MHz) δ ppm = 7.52 (s, 2H), 4.29 (t, $J = 6.4$ Hz, 4H), 1.54-1.49 (m, 2H), 1.37-1.49 (m, 20H), 1.90-1.83(m, 4H), 0.93-0.86 (m, 12H), 0.59-0.28 (s, 18H). ^{13}C NMR (CDCl_3 , 100MHz) δ ppm = 143.98, 143.13, 140.65, 140.48, 134.04, 133.37, 132.98, 131.21, 128.16, 128.02, 127.87, 125.81, 120.41, 73.89, 73.70, 73.65, 38.95, 38.91, 33.13, 33.09, 32.90, 31.04, 290.4, 25.91, 23.39, 23.31, 23.19, 14.21, 10.95, -6.48, -6.56, -8.33, -10.09-10.17.

4,8-Bis((5-ethylnoyl)oxy)benzo[1,2-b:4,5-b']dithiophene-2,6-diyl)bistrimethylstannane (7c): ^1H NMR (CDCl_3 , 400MHz) δ ppm = 7.53 (s, 2H), 4.32-4.28 (t, $J = 6.4$ Hz, 4H), 1.89-1.83 (m, 4H), 1.58-1.52 (m, 3H), 1.35-1.24 (m, 23H), 0.91-0.84 (m, 12H), , 0.52-0.37 (s, 18H). ^{13}C NMR (CDCl_3 , 100MHz) δ ppm = 143.13, 140.48, 134.04, 132.97, 128.02, 127.87, 125.81, 120.41, 73.89, 73.70, 73.65, 38.95, 38.91, 33.13, 33.09, 32.30, 31.04, 29.04, 25.91, 23.40, 23.31, 23.19, 14.21, 10.95, -6.48, -6.56, -8.33, -10.09, -10.17.

General procedure for Stille polymerization and polymer purification: Monomer **7a-c** (0.216 mmol) and monomer **8** (0.216 mmol) were taken in a Schlenk tube under argon atmosphere with 5 mL of anhydrous toluene. After degassing for 20 min, the mixture of $\text{Pd}_2(\text{dba})_3$ (3 mol%) and $\text{P}(o\text{-tolyl})_3$ (7 mol%) were added and heated at 110 °C for 24 h. After cooling to room temperature, it was poured into methanol and the resulting precipitate was filtered. The polymer was purified by Soxhlet extraction using methanol, acetone and hexane, and finally extracted with chloroform. The chloroform solution was then concentrated by evaporation and re-precipitated in methanol. The resulting deep purple colored solids were collected and dried overnight under vacuum. The polymers were characterized by ^1H NMR, GPC.

PBDTPD-C1: Isolated yield = 55%. $M_n = 13.0$ kDa, $M_w = 27.0$ kDa, PDI = 2.10 (against PS standard), ^1H NMR (CDCl_3 , 400MHz) δ ppm = 8.33 (br, 2H), 4.37-3.75 (br, 6H), 2.32- 0.87 (br, 45H).

PBDTPD-C3: Isolated yield = 55%. $M_n = 23.0$ kDa, $M_w = 44.0$ kDa, PDI = 1.92 (against PS standard), ^1H NMR (CDCl_3 , 400MHz) δ ppm = 8.33 (br, 2H), 4.37-3.76 (br, 6H), 2.17- 0.95 (br, 51H).

PBDTTPD-C4: Isolated yield = 65%. M_n = 16.0 kDa, M_w = 37.0 kDa, PDI = 2.32 (against PS standard), $^1\text{H NMR}$ (CDCl_3 , 400MHz) δ ppm = 8.32 (br, 2H), 4.25-3.76 (br, 6H), 2.17- 0.95 (br, 53H).

Fabrication and characterization of organic solar cells

Organic solar cells (OSCs) were fabricated with a configuration of ITO/PEDOT:PSS/**PBDTTPD-Cn**:PC₇₁BM/Al. The patterned indium tin oxide (ITO) on glass was pre-cleaned with detergent, and ultrasonic bath of distilled water, acetone and isopropanol. And substrates are treated in an ultraviolet-ozone chamber for 20 min after dried in an oven overnight at 100 °C. Poly(3,4-ethylenedioxythiophene):poly(styrene sulfonate) (PEDOT:PSS, Baytron P clevios™ AI 4083, Germany) was spin-coated onto the ITO glass as 45nm thin layer and dried at 140 °C for 10 min, transferred into a nitrogen filled glove box. Solutions containing mixture of **PBDTTPD-Cn**:PC₇₁BM in *o*-dichlorobenzene (*o*-DCB) solvent with concentration of 2wt% for **PBDTTPD-C1** and **PBDTTPD-C3**, 1wt% for **PBDTTPD-C4** were spin-cast on the PEDOT:PSS layer. The mixed solutions of **PBDTTPD-Cn**:PC₇₁BM were with and without additive. Then, Al cathode (100 nm) was deposited on the active layer by thermal evaporation in pumped down in vacuum ($<10^{-6}$ Torr) condition. The thickness of the photoactive layer was measured using a surface profiler (KLA_tencor (USA)). The active area of the device was 13 mm². *J-V* characteristics were measured by a computer-controlled Keithley 2635A Source Measurement under an AM 1.5G illumination at 100 mW/cm² coupled with a xenon lamp. EQE (PV measurements Inc.) spectra were obtained by applied monochromatic light from a xenon lamp. The J_{SC} value of monochromatic power was calibrated using a silicon photodiode for ambient conditions.

Fabrication of the organic field-effect transistors (OFETs)

All OFETs were fabricated on heavily n-type doped silicon wafer coated thick SiO₂ layer as gate electrode and gate dielectric. The device structure was top contact bottom gate architecture. The semiconducting **PBDTTPD-Cn** were spin-cast from solution at 1700 rpm after cleaned wafers were pretreated with a solution of 1.0 mM octyltrichlorosilane (OTS) in toluene under N₂ filled condition to refine apolar and smooth surface. Source and drain electrodes were deposited by thermal evaporation. The thickness of top electrode (source and drain) was 80 nm. The channel's width to length ratio (W/L) of the devices was 59/1. Electrical characterization was tested using a keithley semiconductor parametric equipment (keithley 4200) under N₂ atmosphere.

Fabrication of the space charge limited current device (SCLC)

Hole only devices for measuring hole mobility were fabricated as diode configuration of ITO/PEDOT:PSS/polymer:PC₇₁BM/Au. While electron only devices were fabricated with diode

configuration of FTO/polymer:PC₇₁BM/Al. The blend solutions were each optimized condition of **PBDTTPD-Cn**, which equate to polymer solar cells. The solutions were spin coated on ITO and FTO substrates at each optimal spin-rate. The thickness of devices was measured by using surface profiler (KLA_tencor (USA)) as shown in **Table 3.4**. The gold and aluminium were deposited by thermal evaporation as electrode (thickness \approx 100 nm) under high vacuum condition. The devices were measured under dark condition taking in the range of \sim 3 V.

Reference

- (1) Yu, G.; Gao, J.; Hummelen, J. Wudl, F.; Heeger, A. J. *Science* **1995**, *270*, 1789.
- (2) Wienk, M. M.; Kroon, J. M.; Verhees, W.J ; Knol, J. Hummelen, J. C. ; van Hal, P. A; Janssen, R.A. *Angew. Chem., Int. Ed.* **2003**, *115*, 3493.
- (3) Li,G.; Zhu, R.; Yang, Y. *Nat. Photonics* **2012**, *6*, 153..
- (4) Günes,S.; Neugebauer, H.; Sariciftci, N. S. *Chem. Rev.* **2007**, *107*, 1324.
- (5) Huo, L; Zhang, S; Guo, X.; Xu, F.; Li,Y; Hou, J. *Angew. Chem., Int. Ed.* **2011**, *123*, 9871.
- (6) Dou, L.; Chen, C. -C.; Yoshimura, K.; Ohya, K.; Chang, W.-H.; Gao, J.; Liu, Y.; Richard, E.; Yang, Y. *Macromolecules* **2013**, *46*, 3384.
- (7) Guo, X. ; Zhang, M. ; Ma, W. ; Ye, L.; Zhang, S. ; Liu, S. ;Ade, H. Huang, F. ;Hou, J. *Adv. Mater.* **2014**, DOI: 10.1002/adma.201400411.
- (8) Cabanetos, C. m. ; El Labban, A.; Bartelt, J. A.; Douglas, J. D.; Mateker, W. R.; Fréchet, J. M.;McGehee, M. D.; Beaujuge, P. M. *J. Am. Chem. Soc.* **2013**, *135*, 4656..
- (9) He, Z.; Zhong, C.; Huang, X. ; Wong, W. Y.; Wu, H.; Chen, L.; Su, S.; Cao, Y. *Adv. Mater.* **2011**, *23*, 4636.
- (10) Takimiya, K.; Osaka, I.;Nakano, M. *Chem. Mater.* **2014**, *26*, 587.
- (11) Huang, Y. ; Liu, F.; Guo, X.; Zhang, W.; Gu, Y.; Zhang, J.; Han, C. C.; Russell, T. P.; Hou, J. *Adv. Energy Mater.* **2013**, *3*, 930.
- (12) Dutta, G. K.; Kim, T.; Choi, H.; Lee, J.; Kim, D. S.; Kim, J. Y.; Yang, C. *Polym. Chem.* **2014**, *5*, 2540.
- (13) Kim, B.; Yeom, H. R.; Yun, M. H.; Kim, J. Y.; Yang, C. *Macromolecules* **2012**, *45*, 8658.
- (14) Uy, R. L. ; Yan, L.; Li, W.; You, W. *Macromolecules* **2014**, *47*, 2289.
- (15) Chen, H.-Y.; Hou, J.; Zhang, S.; Liang, Y.; Yang, G.; Yang, Y.; Yu, L. ; Wu, Y.; Li, G. *Nat. Photonics* **2009**, *3*, 649.
- (16) Hou, J.; Chen, H.-Y.; Zhang, S. ; Chen, R. I.; Yang, Y.; Wu, Y.; Li, G. ; *J. Am. Chem. Soc.* **2009**, *131*, 15586.
- (17) Liang, Y.; Feng, D.; Wu, Y.; Tsai, S.-T.; Li, G.; Ray, C.; Yu, L. *J. Am. Chem. Soc.* **2009**, *131*, 7792.
- (18) Price, S. C.; Stuart, A. C.; Yang, L.; Zhou, H.; You, W. *J. Am. Chem. Soc.* **2011**, *133*, 4625.
- (19) Zou, Y.; Najari, A.; Berrouard, P. ; Beaupré, S.; Réda Aïch, B.; Tao, Y.; Leclerc, M. *J. Am. Chem. Soc.* **2010**, *132*, 5330.

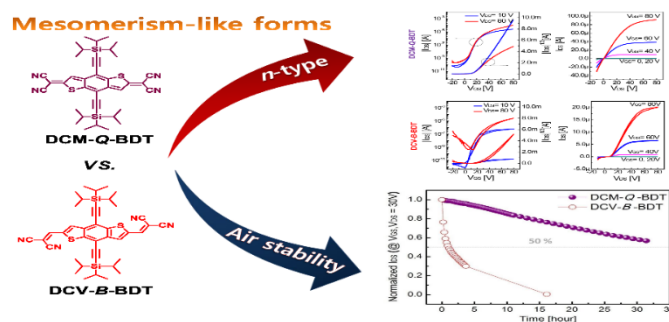
- (20) Zhang, Y.; Hau, S. K.; Yip, H.-L.; Sun, Y.; Acton, O.; Jen, A. K.-Y. *Chem. Mater.* **2010**, *22*, 2696.
- (21) Zhang, G.; Fu, Y.; Zhang, Q.; Xie, Z. *Chem. Commun.* **2010**, *46*, 4997.
- (22) Zhang, M.; Fan, H.; Guo, X.; He, Y.; Zhang, Z.-G.; Min, J.; Zhang, J.; Zhao, G.; Zhan, X.; Li, Y. *Macromolecules* **2010**, *43*, 8714.
- (23) Hou, J.; Huo, L.; He, C.; Yang, C.; Li, Y. *Macromolecules* **2006**, *39*, 594.
- (24) Hou, J.; Tan, Z. a.; Yan, Y.; He, Y.; Yang, C.; Li, Y. *J. Am. Chem. Soc.* **2006**, *128*, 4911.
- (25) Wang, M.; Hu, X.; Liu, P.; Li, W.; Gong, X.; Huang, F.; Cao, Y. *J. Am. Chem. Soc.* **2011**, *133*, 9638.
- (26) He, Z.; Zhong, C.; Su, S.; Xu, M.; Wu, H.; Cao, Y. *Nat. Photonics* **2012**, *6*, 591.
- (27) Cheng, Y.-J.; Yang, S.-H.; Hsu, C.-S. *Chem. Rev.* **2009**, *109*, 5868.
- (28) Zhou, H.; Yang, L.; You, W. *Macromolecules* **2012**, *45*, 607.
- (29) Saito, S.; Nakakura, K.; Yamaguchi, S. *Angew. Chem., Int. Ed.* **2012**, *124*, 738.
- (30) Ding, L.; Li, H.-B.; Lei, T.; Ying, H.-Z.; Wang, R.-B.; Zhou, Y.; Su, Z.-M.; Pei, J. *Chem. Mater.* **2012**, *24*, 1944.
- (31) Lee, J.; Han, A.-R.; Yu, H.; Shin, T. J.; Yang, C.; Oh, J. H. *J. Am. Chem. Soc.* **2013**, *135*, 9540.
- (32) Lee, J.; Han, A.-R.; Kim, J.; Kim, Y.; Oh, J. H.; Yang, C. *J. Am. Chem. Soc.* **2012**, *134*, 20713.
- (33) Xia, Y.; Cho, J. H.; Lee, J.; Ruden, P. P.; Frisbie, C. D. *Adv. Mater.* **2009**, *21*, 2174.
- (34) Veres, J.; Ogier, S. D.; Leeming, S. W.; Cupertino, D. C.; Mohialdin Khaffaf, S. *Adv. Funct. Mater.* **2003**, *13*, 199.
- (35) Thompson, B. C.; Kim, Y.-G.; Reynolds, J. R. *Macromolecules* **2005**, *38*, 5359.
- (36) Meager, I.; Ashraf, R. S.; Mollinger, S. Schroeder, B. C.; Bronstein, H.; Beatrup, D.; Vezie, M. S.; Kirchartz, T.; Salleo, A.; Nelson, J. *J. Am. Chem. Soc.* **2013**, *135*, 11537.
- (37) Lou, S. J.; Szarko, J. M.; Xu, T.; Yu, L.; Marks, T. J.; Chen, L. X. *J. Am. Chem. Soc.* **2011**, *133*, 20661.
- (38) Lee, Y. H.; Ohta, A.; Yamamoto, Y.; Komatsu, Y.; Kato, K.; Shimizu, T.; Shinoda, H.; Hayami, S. *Polyhedron* **2011**, *30*, 3001.

* Chapter III is reproduced in part with permission of “*ChemPhysChem* **2015**, *16*, 1305-1314”.
Copyright 2015 Wiley.

Chapter IV

Solution Processable TIPS-Benzodithiophene Based Small Molecules for *n*-Channel OFETs

In chapter IV, we presented synthesis and characterization of quinoid and benzenoid type small molecules based on benzodithiophene (BDT) with triisopropylsilylethynyl group for *n*-channel OFETs. Chapter IV is reproduced in part with permission of “Dicyanomethylene-quinoid vs. dicyanovinyl-Benzenoid organic semiconductors: understanding structure-property correlations in mesomerism-like Forms” from K. C. Lee *et. al. Organic Electronics* 37, **2016**, 402-410.



4.1 BDT-Based Small Molecules

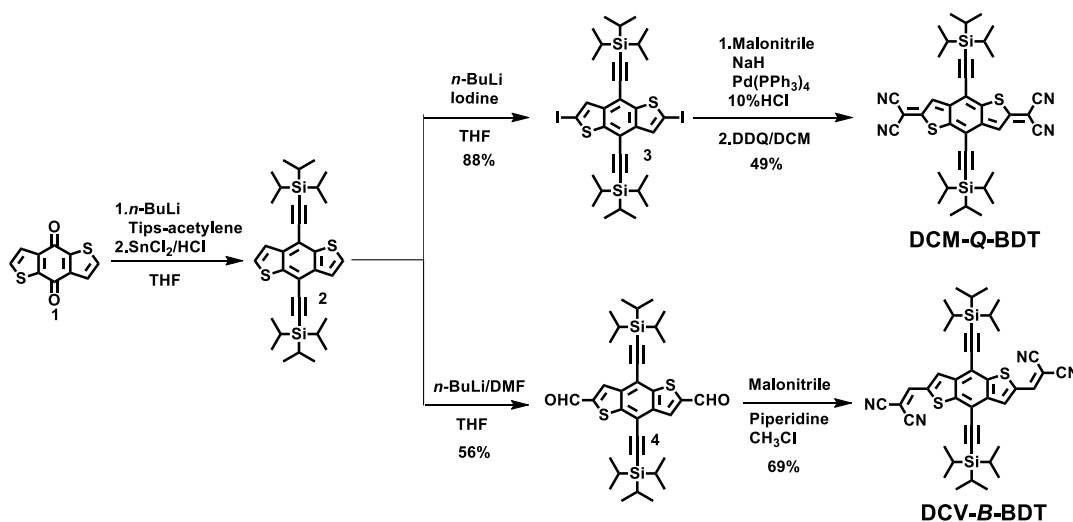
4.1.1 Introduction

Solution-processable organic semiconductors (OSCs) have been extensively researched due to their unique optoelectronic properties and excellent mechanical flexibility for wearable electronics. For the realization of organic complementary circuits,¹⁻⁴ which enable a lower standby power (ideally 0) and a higher operational speed, both *p*- and *n*-channel organic field-effect transistors (OFETs) are required. Even though there are some successful examples of *n*-type organic semiconductors (OSCs), such as fullerene and arylenediimide derivatives,⁵⁻⁷ progress in the area of *n*-type OSCs has generally lagged behind the development of *p*-type OSCs due to the relative difficulty of obtaining *n*-type OSCs with good processability, air stability, and high electrical performance.

In order to attain such ideal *n*-type OSCs, a high electron affinity (*i.e.*, the low-lying lowest unoccupied molecular orbital [LUMO]) as well as a large intermolecular orbital overlapping via strong π - π stacking are critically necessary for facilitating charge injection and transport with a strong robustness in air.⁸ Incorporation of electron-withdrawing substituents into the π -conjugated cores enables the lowering of LUMO energy levels so that the electron charge carriers are less susceptible to H₂O and O₂,^{9,10} which has proven to be a facile and effective approach for air-stable *n*-type OSCs.⁶ Dicyanomethylene and dicyanovinyl units are among the strongest electron-

withdrawing and the most frequently used functionalities. Therefore, many *n*-channel OFETs based on dicyanomethylene- or dicyanovinyl-capped OSCs have been reported, and some of them have displayed excellent device performance.^{8,13-17,45} To date, however, there have been no systematic investigations of the different properties in a comparison between the two termini within the same π -conjugated platform.^{18-24, 47-48}

Linearly fused benzo [1,2-*b*:4,5-*b'*] dithiophene (BDT) with a centrosymmetric structure is well-known to have a strong tendency to π -stack in the solid state.²⁵ Although this rather unique property has recently been exploited for the demonstration of a number of high-performance OSCs in community solar cells,^{26,27} its applications as OFET OSCs have rarely been studied. Together with the aim of obtaining a quantitative understanding of OSCs' nature employing each type of terminus afore mentioned, our ongoing interest in the chemistry of BDT and the development of high-performing *n*-type OSCs has prompted us to investigate the synthesis and properties of BDTs end-capped with the dicyanomethylene and dicyanovinyl groups, respectively (DCM-*Q*-BDT and DCV-*B*-BDT, **Scheme 4.1**), where bulky triisopropylsilylacetylene (TIPS) side chains are introduced on the central phenyl ring of the BDT unit in order to simultaneously improve the solubility, oxidative stability, and π -orbital overlapping of the OSCs. In a comparative study, we present detailed structure–function relationships and explain how the dicyanomethylene-quinoid versus dicyanovinyl-benzenoid structures change the optical properties, energetics, morphology, molecular packing, and carrier transport of the OSCs. The solution-processed top-gate/bottom-contact (TG/BC) OFETs of DCM-*Q*-BDT without post-thermal treatment show high electron mobility up to 0.23 cm²/V·s. Furthermore, the OFETs using DCM-*Q*-BDT have excellent long-term air-stable *n*-channel properties; DCM-*Q*-BDT has longer half-life times of 35 hrs than that of DCV-*B*-BDT by one order of magnitude.



Scheme 4.1. Synthetic routes for DCM-*Q*-BDT and DCV-*B*-BDT.

4.1.2 Synthesis and Characterization

The synthetic routes of DCM-*Q*-BDT and DCV-*B*-BDT are shown in **Scheme 4.1**. First, the TIPS-functionalized BDT (**2**) was prepared by the reaction of the 4,8-dihydrobenzo [1,2-*b*:4,5-*b'*]dithiophen-4,8-dione (**1**) with trialkylsilyl ethynyllithium followed by deoxygenation/aromatization with stannous chloride, as described in the literature.^[20] After the lithiation of **2** with *n*-butyllithium, the subsequent addition of either excess iodine or DMF gave the key precursors **3** and **4**, respectively. Finally, the target OSC DCM-*Q*-BDT was synthesized from **3** through a typical palladium-catalyzed Takahashi coupling reaction, followed by oxidation with 2,3-dichloro-5,6-dicyano-1,4-benzoquinone (DDQ). On the other hand, Knoevenagel condensation between malononitrile and **4** in piperidine yielded the desired DCV-*B*-BDT. The final molecules were further purified by crystallization from THF after column chromatography, and their chemical structures were characterized by NMR, MS, and elementary analysis. The 5% weight-loss temperatures (T_d) of DCM-*Q*-BDT and DCV-*B*-BDT were 225 and 325 °C, respectively as seen in **Figure 4.1**, indicating that the benzenoid form is more beneficial for thermal stabilizing material than the quinoid analogue.⁴⁶ However, the results revealed that both the compounds are thermally stable below 220 °C, allowing research on film morphology and device fabrication over a broad temperature range from RT up to 200 °C.

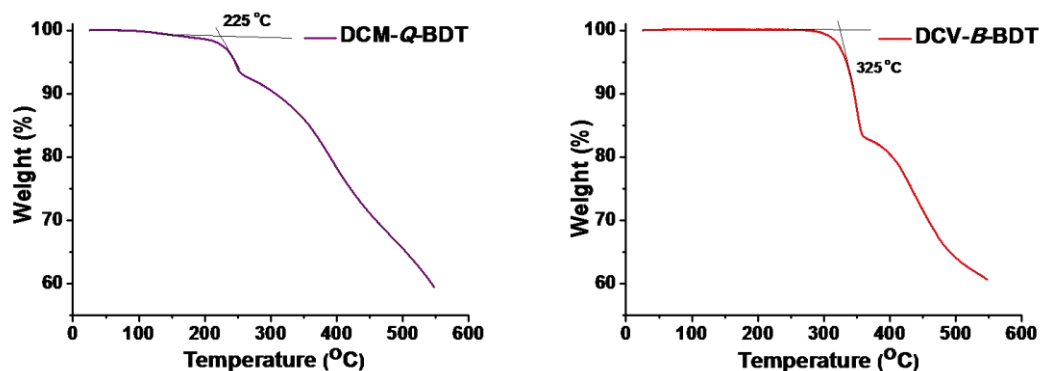


Figure 4.1. Thermogravimetric analysis (TGA) for DCM-*Q*-BDT and DCV-*B*-BDT

4.1.3 Optical and Electrochemical Properties and DFT Calculation

The optoelectronic properties of DCM-*Q*-BDT and DCV-*B*-BDT were characterized using UV-Vis absorption. **Figure 4.2a** and **b** show the absorption spectra of the molecules in chloroform solutions and in thin films, and the corresponding data are summarized in **Table 4.1**. The solution spectrum of DCM-*Q*-BDT showed two distinct absorption bands, including a weak band in the shorter wavelength region (300–330 nm) and a strong band with a typical vibronic structure in the longer wavelength region (470–590 nm). On the other hand, DCV-*B*-BDT in the solution

exhibited three primary absorption bands centered at 345, 436, and 539 nm, respectively. Both DCM-*Q*-BDT and DCV-*B*-BDT displayed red-shifted and broadened absorptions in the films compared with those in the solutions. In particular, the longer wavelength bands in DCM-*Q*-BDT film were significantly spanned. This indicates that both OSCs have strong intermolecular interactions in the solid state. It is interesting to note that despite the extended π -conjugation length of the dicyanovinyl unit over dicyanomethylene, the optical bandgap estimated from the absorption onset of the DCM-*Q*-BDT film was found to be 1.67 eV, which is 0.38 eV smaller than that of DCV-*B*-BDT ($E_g^{\text{opt}} = 2.05$ eV), as a reflection of the quinoid character along the core of DCM-*Q*-BDT.^{28, 29}

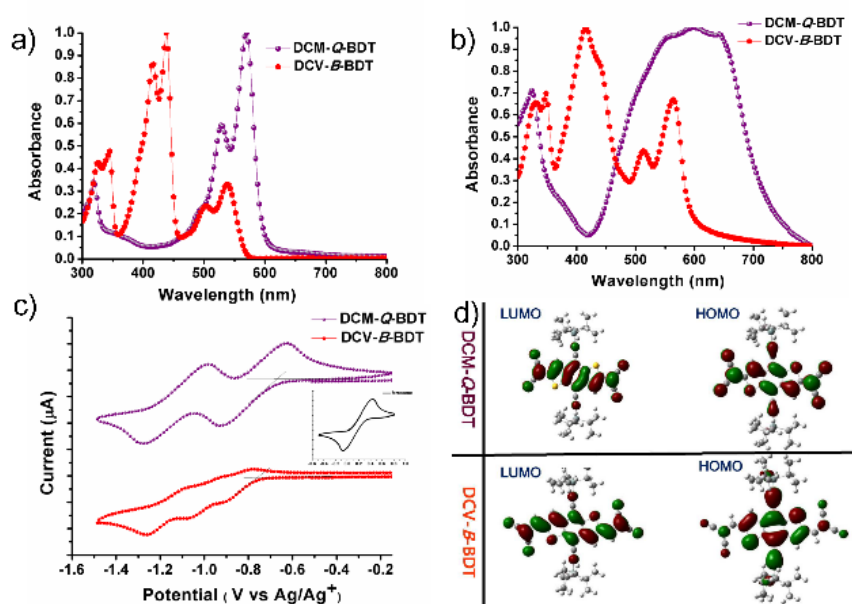


Figure 4.2. UV-Vis absorption spectra of DCM-*Q*-BDT and DCV-*B*-BDT in chloroform solution (a) and as a thin solid films spin-cast from chloroform (b) Cyclic voltammograms of DCM-*Q*-BDT and DCV-*B*-BDT in dichloromethane solution (c) DFT calculation for DCM-*Q*-BDT and DCV-*B*-BDT (d).

Table 4.1. Optical and electrochemical properties of DCM-*Q*-BDT and DCV-*B*-BDT.

	$\lambda_{\text{max}}^{\text{sol}}$ (nm) ^a	$\lambda_{\text{max}}^{\text{film}}$ (nm)	E_g^{opt} (eV) ^b	E_{HOMO} (eV) ^c	E_{LUMO} (eV) ^d
DCM- <i>Q</i> -BDT	539,318	600,325	1.67	-5.79	-4.12
DCV- <i>B</i> -BDT	569,436,345	564,416,347	2.05	-6.06	-4.01

^aChloroform solution; ^bDetermined from the onset of the electronic absorption spectra; ^cDetermined by subtracting the optical bandgap from reduction potential; ^dCyclic voltammetry determined with Fc/Fc+ ($E_{\text{HOMO}} = -4.80$ eV) as the external reference.

Cyclic voltammetry of DCM-*Q*-BDT and DCV-*B*-BDT was conducted under N₂ in *n*-

Bu₄NPF₆/CH₂Cl₂ solution by using ferrocene as the external standard. As shown in **Figure 4.2c**, DCM-*Q*-BDT gave two reversible reduction waves, whereas DCV-*B*-BDT displayed three quasi-reversible reduction waves; the first onset potential was 0.64 V for DCM-*Q*-BDT and 0.75 V for DCV-*B*-BDT, but no oxidation waves were available in the potential range. The LUMO energies of DCM-*Q*-BDT and DCV-*B*-BDT estimated through the equation $E_{\text{LUMO}} = -(E_{(\text{red})}^{\text{onset}} - E_{(\text{ferrocene})}^{\text{onset}} + 4.8)$ eV were 4.12 and 4.01 eV, respectively, both of which were 4.0 eV below the vacuum level, well within the requirement for operable *n*-type OFET OSCs.^{30, 31} Note that the relative lower-lying LUMO level of DCM-*Q*-BDT clearly indicates that the quinoid structure contributes to an increase in the electron-deficient nature compared with the benzenoid system. The molecular geometry and frontier orbital distributions were calculated by using density functional theory (DFT) at the B3LYP/6-31G* level. As shown in **Figure 4.2d**, in both cases, the HOMOs and LUMOs are spread over the entire π -frameworks. Interestingly, the HOMO of DCM-*Q*-BDT and LUMO of DCM-*B*-BDT show similar orbital distribution, vice versa.

4.1.4 Evaluation of OFET Device Properties

To evaluate the charge transport properties of DCM-*Q*-BDT and DCV-*B*-BDT, TG/BC OFETs were fabricated by spin-coating a chloroform solution onto a glass substrate (for details of the device fabrication process, see the experimental section). **Figure 4.3** shows the transfer and output characteristics of DCM-*Q*-BDT and DCV-*B*-BDT OFETs, and all the transistor parameters are summarized in **Table 4.2**. Even though two mesomerism-like OSCs possessed low-lying LUMO energy levels (< 4.0 eV) originating from strong electron-withdrawing cyano groups, there were somewhat different electrical behaviors; DCM-*Q*-BDT showed typical *n*-channel transistor characteristics, whereas DCV-*B*-BDT OFETs showed ambipolar-like transporting with weak hole mobility. Interestingly, in both cases, the best device performance was achieved by post-annealing free devices. DCM-*Q*-BDT showed a slightly better field-effect mobility (μ_{FET}) (0.099 ± 0.091 cm²/V·s [max. 0.23 cm²/V·s]) than that of DCV-*B*-BDT OFETs (0.084 ± 0.010 cm²/V·s [max. 0.10 cm²/V·s]). Even the average μ_{FET} of both OFETs showed a small difference; however, the maximum μ_{FET} of DCM-*Q*-BDT OFETs was more than two times larger than that of DCV-*B*-BDT ones. The performance of DCM-*Q*-BDT and DCV-*B*-BDT OFETs was decreased highly rapidly by the post-annealing process.

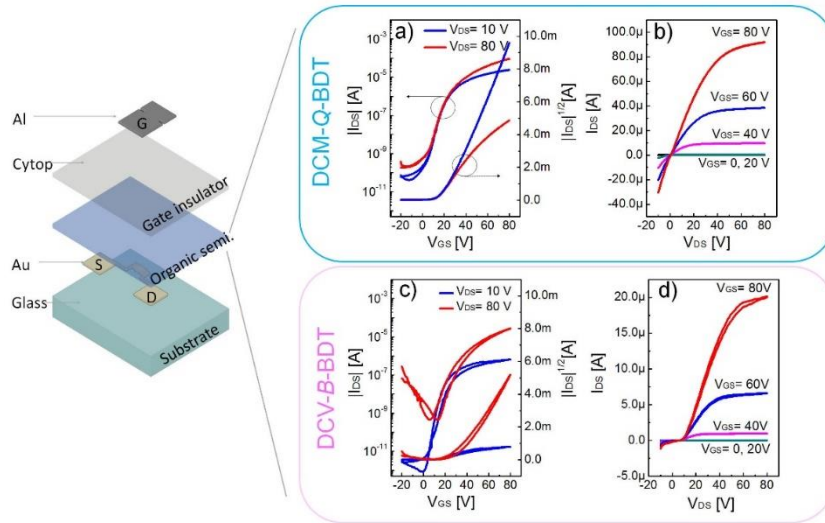


Figure 4.3. Top-gate/bottom-contact structure of OFETs and transfer and output curves of DCM-*Q*-BDT (a), (b) and DCV-*B*-BDT OFETs(c), (d) without post-annealing treatments.

Table 4.2. Electrical characteristics of DCM-*Q*-BDT and DCV-*B*-BDT OFETs depending on the post-annealing temperature.

OSC(5mg/ml in CF)	Post-annealing temp.[°C]	Mobility [cm ² /V·s]		V _{Th} [V]	I _{on} /I _{off} [-]	R _c [Ω·cm]
		Average ^a	Max.			
DCM- <i>Q</i> -BDT	W/O	0.0989±0.0906	0.231	24.78 ± 7.14	~10 ⁵	1.18 x 10 ³
	100	0.0381 ± 0.0396	0.091	5.02±18.68	~10 ⁴	1.87 x 10 ⁴
	150	0.0002 ± 0.0003	0.0007	5.32±4.80	~10 ⁴	1.82 x 10 ⁸
	200	0.00008± 0.0008	0.0002	-	~10 ²	1.53 x 10 ⁹
DCV- <i>B</i> -BDT	w/o	0.0837 ± 0.0099	0.101	34.9 ±1.44	~10 ⁴	2.53 x 10 ⁶
	100	0.0533 ± 0.0061	0.062	40.05 ±2.22	~10 ⁵	2.88 x 10 ⁷
	150	0.0457 ± 0.0137	0.065	42.32 ±2.86	~10 ⁴	1.32 x 10 ⁷
	200	0.0076 ± 0.0046	0.016	45.14 ±2.21	~10 ⁴	5.69 x 10 ⁷

^a Reported values are an average of at least 25 devices.

This is opposite to the results from normal OFETs, since the crystallinity of OSC film is commonly improved by the thermal post-annealing process.^{2,3,8} This degradation is presumably due to the formation of cracking in the crystal domains.^{32,33} An efficient charge injection (i.e., a low contact resistance [R_c]) is another important parameter for achieving high μ_{FET} in OFETs. At the transistor output curves (**Figure 4.3**), DCM-*Q*-BDT OFETs showed a fairly good contact property with the Au electrode, whereas DCV-*B*-BDT OFETs exhibited a large sub-linearity of the output characteristics at low V_{DS} corresponding to high R_c based on the Schottky barrier.¹³⁴ We extracted more accurate R_c by using the well-known Y-function method (YFM),³⁵⁻³⁷ and the values are summarized in **Table 4.2**. DCV-*B*-BDT OFETs (2.53 MΩ·cm) showed ~1,000 times larger R_c than DCM-*Q*-BDT ones (1.18 KΩ·cm). The large difference in R_c for electron injection is mainly due to the difference of the LUMO energy level of two OSCs. The measured LUMO energy level of DCM-*Q*-BDT (-4.12 eV) is quite different to that of DCV-*B*-BDT (-4.01 eV). The large mismatch between the LUMO energy level and work function of the Au electrode (4.6 ~ 5

eV) leads to strong R_c in DCV-*B*-BDT OFETs. The air stability of post-annealing free DCM-*Q*-BDT and DCV-*B*-BDT OFETs was tested by measuring devices in air (60% humidity and 25 °C). As shown in **Figure 4.5**, DCM-*Q*-BDT OFETs exhibited fairly good and much better air stability than DCV-*B*-BDT ones. The half-life times of the drain current were approximately 35 hr for the DCM-*Q*-BDT OFETs and 1 hr for DCV-*B*-BDT ones.

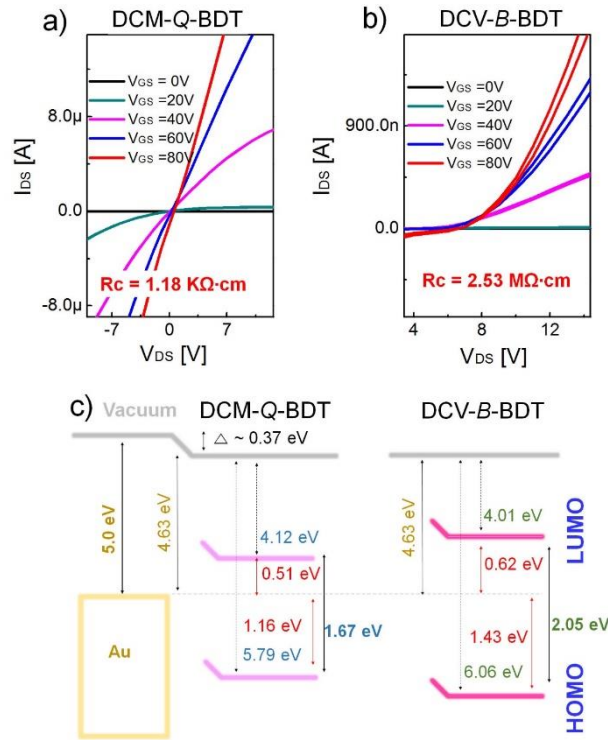


Figure 4.4. Output curves at low V_{DS} of OFETs with extracted contact resistance by YFM with DCM-*Q*-BDT (a) and DCV-*B*-BDT (b), Schematic energy diagram between OFETs electrode and organic semiconductors for carrier injection DCM-*Q*-BDT and DCV-*B*-BDT(c).

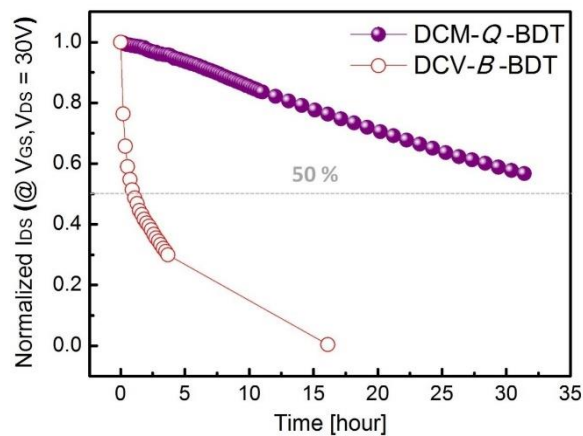


Figure 4.5. Normalized I_{ds} change of DCM-*Q*-BDT and DCV-*B*-BDT OFETs according to the time in the air for ambient (60% humidity and 25 °C) stability.

To achieve high air stability for *n*-type OFETs, there are two major factors in the *n*-type OSCs –

energetic factor and kinetic factor. The air and operational stability of OFETs are an important issue for commercialization. The stability of *n*-type OFETs is known to be relatively worse than their *p*-type counterpart, since many trap sites are generated at around -3.8 eV by exposure in air (humid oxygen).^{9,38,39} Energetically, the LUMO energy levels of *n*-type OSCs have to be designed below -4.0 eV for air stability. In addition, the molecular packing and the thin-film morphology of *n*-type OSC films play important roles in the air stability of *n*-type OFETs. Kinetically, the dense molecular packing, good film morphology with high crystallinity, and low density of grain boundaries with large grain sizes are positive kinetic factors for realizing air-stable *n*-type OFETs.^{40,41} The high air and operational stability of DCM-*Q*-BDT is based on not only the relatively lower-lying LUMO energy level (-4.12 eV) compared with DCV-*B*-BDT (-4.01 eV), but also the better film morphology and crystallinity of DCM-*Q*-BDT than DCV-*B*-BDT ones (discussed below).

4.1.5 Thin-film Microstructure and Morphology

The post-annealing free thin films that showed the best OFET performances were characterized by atomic force microscopy (AFM) and X-ray diffraction (XRD) to elucidate the relationships between molecular structure, film morphology/crystallinity, and device performance. The samples were prepared following the same procedures as those for OFET devices without gold electrodes. As shown in Normalized I_{ds} change of DCM-*Q*-BDT and DCV-*B*-BDT OFETs according to the time in the air for ambient (60% humidity and 25 °C) stability. **Figure 4.6**, both films exhibited randomly orientated rod-like grains with certain terrace structures; DCM-*Q*-BDT films generated higher surface roughness (RMS) (~33 nm) than DCV-*B*-BDT (~10 nm). This observation implies that the quinoid structure appears to favour the formation of large crystalline domains, which are beneficial for charge transport property. The XRD measurements of the corresponding films exhibited regular-interval peaks up to the third or fourth order (**Figure 4.7**), suggesting a well-defined lamellar structure and a highly dense packed molecular conformation in the solid state.

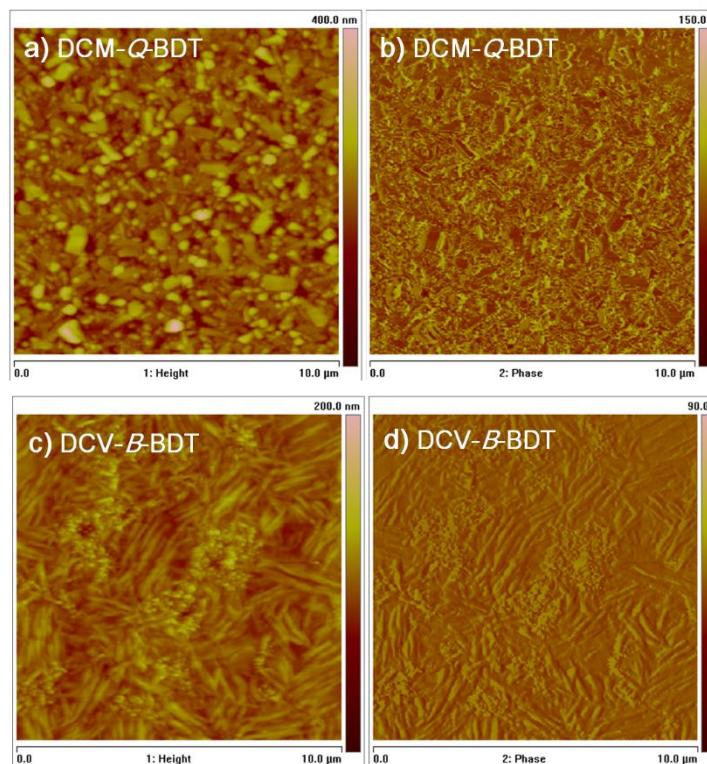


Figure 4.6. Atomic force microscopy (AFM) images of DCM-*Q*-BDT and DCV-*B*-BDT on glass substrate at room temperature: height (a); phase (b) for DCM-*Q*-BDT and height (c); phase (d) for DCV-*B*-BDT, respectively.

The first diffraction peaks of DCM-*Q*-BDT were observed at 5.12° , corresponding to a d -spacing of 17.26 \AA , while the DCV-*B*-BDT showed the d -spacing of 13.04 \AA ($2\theta = 6.78^\circ$), which was notably smaller than that of TIPS-pentacene (16.83 \AA),⁴² most often referred to as solution-processable high-performance OSCs. This demonstrates that the benzenoid structure had a relatively denser lamellar packing compared with the quinoid analogue, though higher mobilities were observed in DCM-*Q*-BDT film (*vide supra*). Since attempts to grow single crystals of both molecules by using various methods were unsuccessful, grazing-incidence wide-angle X-ray diffraction (GIWAXD) measurements, which provide information on both the out-of-plane (q_z) and in-plane (q_{xy}) directions, were performed to further study the orientation and crystallinity of the thin films. As shown in **Figure 4.8a**, number of the diffraction spots showed up for the given samples, indicating highly oriented polycrystalline films; both the films exhibited a series of well-defined multiple diffractions along q_z , consistent with the peaks observed in the specular lab-based XRD above (see **Table 4.3**). Unlike the diffraction patterns of common OSCs, however, there were scarcely any (*010*) diffraction peaks in both the q_z and q_{xy} directions for all of the thin films. DCV-*B*-BDT films had arcs for the q_z direction, suggesting oriented film with broad orientation distribution, while for DCM-*Q*-BDT, well-pronounced ellipses were produced, which is evidence of well-aligned crystallite with a single crystalline-like feature. Moreover, according

to Scherrer analysis, the crystalline coherence length of the (100) Bragg reflection is larger for DCM-*Q*-BDT (581.5 Å) relative to DCV-*B*-BDT (181.1 Å). The coherence length is related to both the total number of scattering lattice plains in a given crystallite and the degree of crystalline disorder.^{43,44} Combined with these findings determined from AFM and GIWAXD results, we can surmise that the outgrowth via a more anisotropic orientation and a higher degree of crystallinity for the quinoid molecule are solutions for superior mobility.

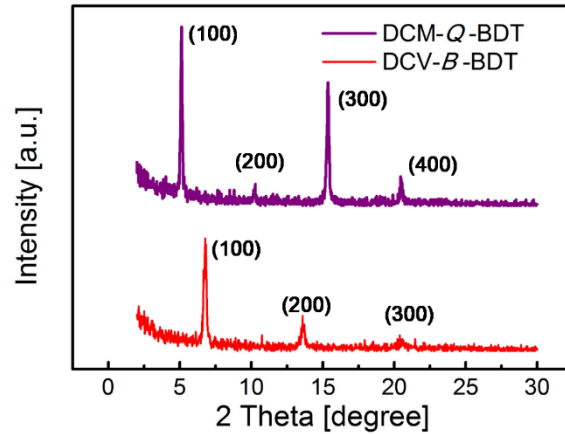


Figure 4.7. XRD results of DCM-*Q*-BDT and DCV-*B*-BDT thin films at room temperature.

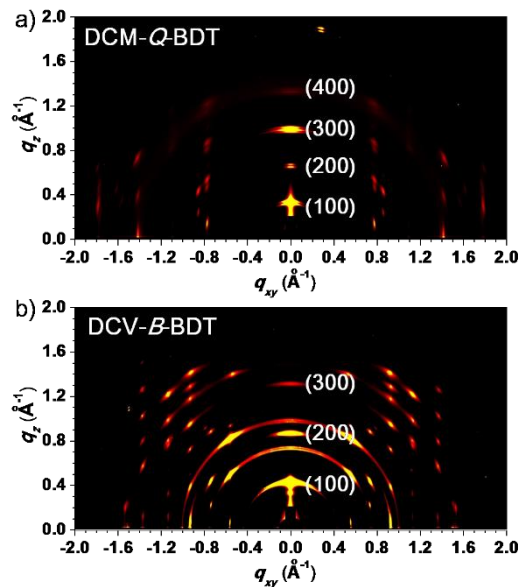


Figure 4.8. GIWAXD images of DCM-*Q*-BDT (a) and DCV-*B*-BDT (b) at room temperature.

Table 4.3. Crystallographic parameters calculated from GIWAXD profiles of DCM-*Q*-BDT and DCV-*B*-BDT.

Crystallographic parameters		DCM- <i>Q</i> -BDT	DCV- <i>B</i> -BDT
<i>q_z</i> profile	<i>q</i> (Å ⁻¹)	0.369	0.494
	<i>d</i> -spacing (Å)	17.0	12.7
	FWHM (Å ⁻¹)	0.010	0.030
	Coherence length (Å)	581.5	187.1

4.1.6 Conclusion

In conclusion, we have synthesized and characterized two mesomerism-like structures, dicyanomethylene-quinoid and dicyanovinyl-benzenoid OSCs, based on BDT (DCM-*Q*-BDT and DCV-*B*-BDT). A comparative investigation of their photophysical properties, energy levels, film microstructures, and OFET device performances can enable the determination of the relevant structure–property relationship in this class of molecules, which is summarized as follows: (i) DCM-*Q*-BDT has a lower-lying LUMO energy level with a lower bandgap compared with DCV-*B*-BDT, which is attributed to the inherent electron-deficient property of the quinoid structure. (ii) DCM-*Q*-BDT is found to display excellent potential for use in *n*-type solution-processed OFET applications; DCM-*Q*-BDT has twice as high electron mobility and 35-fold better air stability than DCV-*B*-BDT. (iii) We have successfully demonstrated that the obvious difference in OFETs is considered to originate from changes of packing orientation, degree of crystallinity, and LUMO energy level in the quinoid over benzenoid molecule films. This study advances our fundamental understanding of how quinoid versus benzenoid molecules influence their intrinsic properties and reveals the potential of the quinoid-type structure for *n*-type OSCs.

4.1.7 Experimental Section

General: The reagents and all starting materials were purchased from Aldrich Co., Alfa Aesar, and TCI Co. used without further purification. All solvents are ACS grade unless otherwise noted. Anhydrous THF was obtained by solvent purification system. ¹H NMR and ¹³C NMR spectra were recorded on an Agilent 400 MHz spectrophotometer using CDCl₃ as solvent and tetramethylsilane (TMS) as the internal standard and EI-MS spectra were obtained from 450-GC & 320-MS (Bruker, Germany). UV-Vis-NIR spectra were taken on UV-1800 (SHIMADZU) spectrometer. DFT calculations were performed using the Gaussian 09 package with the nonlocal hybrid Becke three-parameter Lee-Yang-Parr (B3LYP) function and the 6-31G* basis set to

elucidate the HOMO and LUMO levels after optimizing the geometry of DCM-*Q*-BDT and DCV-*B*-BDT using the same method. Cyclic voltammetry (CV) measurements were performed on an AMETEK VersaSTAT 3 with a three-electrode cell system in a nitrogen bubbled 0.1 M tetra-*n*-butylammonium hexafluorophosphate (*n*-Bu₄NPF₆) solution in dichloromethane at a scan rate of 100 mVs⁻¹ at room temperature. An Ag/Ag⁺ electrode, platinum wire, and platinum were used as the reference electrode, counter electrode, and working electrode, respectively. The Ag/Ag⁺ reference electrode was calibrated using a ferrocene/ferrocenium redox couple as an external standard, whose oxidation potential is set at -4.8 eV with respect to zero vacuum level. The HOMO energy levels were obtained from the equation HOMO (eV)= optical bandgap - LUMO (no obvious oxidation peak was observed). The LUMO levels of polymers were obtained from the equation LUMO (eV)= - ($E_{(\text{red})}^{\text{onset}} - E_{(\text{ferrocene})}^{\text{onset}} + 4.8$). Thermogravimetric analysis (TGA) was performed by Simultaneous DSC/TGA instrument (TA Instruments, USA) at the heating rate of 10 °C min⁻¹.

*2,6-Diiodo-4,8-bis(triisopropylsilylethynyl)-benzo[1,2-*b*:4,5-*b'*]dithiophene (3)*: TIPS-BDT (800 mg, 1.45 mmol) was dissolved in dry THF (190 mL) and cooled to -78 °C under argon condition. Afterwards, 2.5 M *n*-butyllithium in hexane (1.8 mL, 3.19 mmol) was added dropwise and the solution was kept for 2 h at -78 °C. After that iodine (1.27 g, 5.0 mmol) was added and the solution mixture was kept stirring for 30 min at that temperature. Then, the solution was allowed to warm to room temperature and stirred for overnight. After complete reaction, quenched with saturated sodium sulfite and extracted with water and diethylether. The organic layer was dried with magnesium sulfate, filtered, and concentrated to which was added to an excess of methanol. The solid was collected and recrystallization from THF gave compound **3** as yellow solid (1.06 g, yield 91%). ¹H NMR (400 MHz, CDCl₃, TMS), δ (ppm): 7.72 (s, 2H), 1.20-1.22 (m, 42H); ¹³C NMR (100 MHz, CDCl₃), δ (ppm): 145.03, 138.89, 133.01, 132.96, 128.77, 128.25, 123.12, 123.04, 102.88, 101.56, 81.05, 18.75, 11.30.

DCM-Q-BDT: NaH (60%) (204 mg, 5.11 mmol)/THF (20 mL) suspension was cooled to 0 °C and malononitrile (141 mg, 2.13 mmol) was added. The resulting solution was stirred at 0 °C for 20 min, then compound **2** (342 mg, 0.43 mmol) and Pd(PPh₃)₄ (98.5 mg, 85.2 μmol) were added under the protection of N₂ and the solution turned to red color in a few minutes. After addition, the reaction mixture was heated at reflux for 5 h. After cooling to room temperature, a small amount of 10% HCl solution was added to neutralize the solution. Then the THF solvent was evaporated, 10% HCl solution (5 mL) and water (20 mL) were added. The resulting solid was collected by filtration and washed with water and then with ethanol and dried under vacuum. The solid was suspended in CH₂Cl₂ and DDQ (145 mg, 0.639 mmol) was added. The reaction mixture was stirred at room temperature for 30 min. Solvent was removed and the crude product was

purified through chromatograph on silica gel (hexane: CH₂Cl₂ = 1:1) to afford solid compound. The solid was collected and recrystallization from THF gave final product as purple needles (140 mg, yield 49%). ¹H NMR (400 MHz, CDCl₃, TMS), δ (ppm): 7.58 (s, 2H), 1.20-1.22 (m, 42H); ¹³C NMR (100 MHz, CDCl₃), δ (ppm): 167.86, 147.07, 146.16, 130.72, 114.34, 112.79, 111.94, 111.84, 97.81, 18.63, 11.08; EI-MS: 677.4 [M]⁺; Anal. Calcd. For C₃₈H₄₄N₄S₂Si₂ (%): C, 67.41; H, 6.55; N, 8.27; Found: C, 67.33; H, 6.59, N, 8.15.

4,8-bis(triisopropylsilylethynyl)-benzo[1,2-b:4,5-b']dithiophene-2,6-dicarbaldehyde (4): The solution of TIPS-BDT (337 mg, 0.68 mmol) in dry THF (15 mL) was cooled at -78 °C. After that 2.5 M *n*-butyllithium in hexane (1.28 mL, 2.05 mmol) was injected into the solution slowly. The solution was stirred for 30 min at -78 °C and for 30 min at -10 °C. After that, the solution was cooled at -78 °C and excess DMF (10 mL) was injected into the solution slowly. The solution was stirring at -78 °C for 30 min and then warmed to room temperature. After that the reactant was quenched with water, extracted with ethyl acetate and dried with MgSO₄. The crude product was purified by column chromatography (hexane: CH₂Cl₂ = 10:1) to afford the product as yellow solid (230 mg, yield 56%). ¹H NMR (400 MHz, CDCl₃, TMS), δ (ppm): 10.18 (s, 2H), 8.25 (s, 2H), 1.21-1.26 (m, 42H); ¹³C NMR (100 MHz, CDCl₃), δ (ppm): 184.55, 145.72, 143.26, 139.58, 132.78, 115.68, 105.87, 100.62, 18.76, 11.24.

DCV-B-BDT: The compound **4** (500 mg, 0.82 mmol) was dissolved in chloroform (30 mL). After that malononitrile (544 mg, 8.24 mmol) was added and stirred for 20 min at room temperature. Then, piperidine (100 μL) was slowly added to the solution and refluxed for overnight. After finishing the reaction, the crude product was extracted with water and CH₂Cl₂. Then, the reaction mixture was dried with MgSO₄. Afterward, the crude product was purified by column chromatography (hexane: CH₂Cl₂ = 1:1) to afford the product as red solid. The solid was collected and recrystallization from THF gave final product as red needles (400 mg, yield 69%). ¹H NMR (400 MHz, CDCl₃, TMS), δ (ppm): 8.17 (s, 2H), 8.01 (s, 2H), 1.20-1.27 (m, 42H); ¹³C NMR (100 MHz, CDCl₃), δ (ppm): 150.74, 139.13, 138.70, 138.11, 134.71, 114.81, 111.99, 107.78, 100.08, 83.34, 18.72, 11.18; EI-MS: 703.5 [M]⁺; Anal. Calcd for C₄₀H₄₆N₄S₂Si₂ (%): C, 68.33; H, 6.59; N, 7.97; Found: C, 68.21; H, 6.51; N, 7.77.

Field-Effect Transistor Fabrication: The top-gate/bottom-contact (TG/BC) structure OFETs were fabricated on a glass (Corning Eagle 2000) substrate. To form the S/D electrodes, a ~3 nm-thick Ni adhesion layer and ~13 nm-thick pure Au (99.999%) electrodes were deposited by a vacuum thermal evaporation process after the conventional photolithography process for defining the S/D patterns, followed by lift-off of the photoresistant layer. The source and drain (S/D) electrodes of fabricated OFETs were of various channel lengths (*L*) of 10, 20, 30, or 50 μm, with a 1-mm channel width (*W*). The substrates with S/D electrodes were cleaned sequentially in an ultrasonic

bath with acetone, *iso*-propanol and de-ionised water for 10 min each. The substrates with patterned S/D electrode were then baked in a 110 °C oven for 30 min. An *n*-type OSC, self-developed DCM-*Q*-BDT and DCV-*B*-BDT were dissolved in anhydrous chloroform (Sigma-Aldrich) to obtain 5 mg/mL solutions. The organic semiconductors were coated by spin-coating (~30nm thickness), respectively. The solution was fully dropped on the substrate because the solvent is easily evaporated. The spin coated *n*-type OSC films were thermally annealed at the room temperature (RT), 100 °C, 150 °C, and 200 °C, respectively, for 30 min in the N₂ filled glove box. The fluoropolymer poly-(perfluorobutenylvinylether) (CYTOP™, CTL-809M) and a perfluorocarbon-containing solvent (CT-Solv. 180) supplied by Asahi Glass were blended (2:1 ratio) to use as the gate dielectric. A Cytop thin-film was formed on the coated organic semiconductor layer by application of a spin-coating method, followed by thermal annealing at 80 °C for ~30 min in the same N₂-filled glove box used to remove the residual solvents. The thickness of the CYTOP polymer layers was 380 nm ($C_i = 4.89 \text{ nF cm}^{-2}$). The OFET device fabrication was completed by depositing the aluminium (Al) top-gate electrodes (~50 nm thick) via vacuum thermal evaporation using a metal shadow mask.

The electrical characteristics of fabricated OFETs were measured using a Keithley 4200 semiconductor characterization system with optional instrumentation (Keithley 4200-PA remote preamp) in an N₂-filled glove box. The conventional μ_{FET} and corresponding V_{Th} were extracted at the saturation region using gradual channel approximation equations for a standard metal oxide semiconductor FET (MOSFET). The source drain electrode contact resistance (R_c) of the individual transistors is calculated at the liner region (at $V_d = 10\text{V}$, $V_g = \sim 80\text{V}$) by the Y-function method and also the extracted R_c were normalized using channel width ($R_c \cdot W$).

GIWAXD Characterization: Grazing-incidence wide-angle X-ray diffraction (GIWAXD) measurements were conducted at PLS-II 9A U-SAXS beamline of the Pohang Accelerator Laboratory in Korea. X-rays coming from the in-vacuum undulator (IVU) were monochromated (wavelength $\lambda = 1.10994 \text{ \AA}$) using a double crystal monochromator and focused both horizontally and vertically (450 (H) × 60 (V) μm^2 in FWHM @sample position) using K-B type mirrors. The GIWAXD sample stage was equipped with a 7-axis motorized stage for the fine alignment of sample, and the incidence angle of X-ray beam was set to be 0.13° to 0.135° for DCM-*Q*-BDT and DCV-*B*-BDT films. GIWAXD patterns were recorded with a 2D CCD detector (Rayonix SX165) and X-ray irradiation time was 6-9 s, dependent on the saturation level of the detector. Diffraction angles were calibrated using a sucrose standard (Monoclinic, P21, $a = 10.8631 \text{ \AA}$, $b = 8.7044 \text{ \AA}$, $c = 7.7624 \text{ \AA}$, $\beta = 102.938^\circ$) and the sample-to-detector distance was ~231 mm.

References

- (1) Usta, H.; Facchetti, A.; Marks T. J. *Acc. Chem. Res.*, **2011**, *44*, 501.
- (2) Facchetti, A.; Yoon, M.H. ; Stern, C.L.; Katz, H.E.; Marks, T. J. *Angew. Chem. Int. Ed.*, **2003**, *42*, 3900.
- (3) Murphy, A. R.; Fréchet, J. M. *Chem. Rev.*, **2007**, *107*, 1066.
- (4) Mas-Torrent, M.; Rovira, C. *Chem. Soc. Rev.*, **2008**, *37*, 827.
- (5) Jones, B.A.; Facchetti, A.; Wasielewski, M.R.; Marks, T. J. *J. Am. Chem. Soc.*, **2007**, *129*, 15259.
- (6) Yan, H.; Zheng, Y.; Blache, R.; Newman, C.; Lu,S.; Woerle, J.; Facchetti, A. *Adv. Mater.*, **2008**, *20*, 3393
- (7) Meng, Q.; Hu, W. *PCCP*, **2012**, *14* 14152.
- (8) Qiao, Y.; Guo, Y.; Yu, C.; Zhang, F.; Xu, W.; Liu, Y.; Zhu, D. *J. Am. Chem. Soc.*, **2012**, *134*, 4084.
- (9) Anthopoulos, T. D.; Anyfantis, G.; Papavassiliou, G. C. de Leeuw, D. M. *Appl. Phys. Lett.*, **2007**, *90*, 122105.
- (10) Lucas, B.; Trigaud, T.; Videlot-Ackermann, C. *Polym. Int.*, **2012**, *61*, 374.
- (11) Jones, B. A.; Ahrens, M. J.; Yoon, M. H.; Facchetti, A.; Marks, T. J.; Wasielewski, M. R. *Angew. Chem.*, **2004**, *116*, 6523.
- (12) Usta, H.; Facchetti, A.; Marks, T. J. *J. Am. Chem. Soc.*, **2008**, *130*, 8580.
- (13) Mori, T.; Yanai, N.; Osaka, I.; Takimiya, K. *Org. Lett.*, **2014**, *16*, 1334.
- (14) Guo, X.; Watson, M. D. *Org. Lett.*, **2008**, *10*, 5333.
- (15) Guo, X.; Kim, F. S.; Jenekhe, S. A.; Watson, M. D. *J. Am. Chem. Soc.*, **2009**, *131*, 7206.
- (16) Zhang, C.; Zang, Y.; Gann, E.; McNeill, C. R.; Zhu, X.; Di, C.-a.; Zhu, D. *J. Am. Chem. Soc.*, **2014**, *136*, 16176.
- (17) Zhang, F.; Hu, Y.; Schuettfort, T.; Di, C.-a.; Gao, X.; McNeill, C. R.; Thomsen, L. Mannsfeld, S. C.; Yuan, W.; Siringhaus, H. *J. Am. Chem. Soc.*, **2013**, *135*, 2338.
- (18) Handa, S.; Miyazaki, E.; Takimiya, K.; Kunugi, Y. *J. Am. Chem. Soc.*, **2007**, *129*, 11684.
- (19) Zhong, H.; Smith, J.; Rossbauer, S.; White, A. J.; Anthopoulos, T. D.; Heeney, M. *Adv. Mater.*, **2012**, *24* 3205.
- (20) Wang, S.; Wang, M.; Zhang, X.; Yang, X.; Huang, Q.; Qiao, X.; Zhang, H.; Wu, Q.; Xiong, Y.; Gao, J. *Chem. Commun.*, **2014**, *50* 985.
- (21) Kashiki, T.; Miyazaki, E.; Takimiya, K. *Chem. Lett.*, **2009**, *38*, 568.

- (22) Guo, X.; Kim, F.S.; Seger, M.J.; Jenekhe, S.A.; Watson, M.D. *Chem. Mater.*, **2012**, *24*, 1434.
- (23) Guo, X.; Facchetti, A.; Marks, T. J. *Chem. Rev.*, **2014**, *114*, 8943.
- (24) Yoon, W. S.; Park, S. K.; Cho, I.; Oh, J. A.; Kim, J. H.; Park, S. Y. *Adv. Funct. Mater.*, **2013**, *23*, 3519.
- (25) Wang, S.; Ren, S.; Xiong, Y.; Wang, M.; Gao, X.; Li, H. *ACS Appl. Mater. Interfaces*, **2013**, *5*, 663.
- (26) Hou, J.; Chen, H.-Y.; Zhang, S.; Chen, R.I.; Yang, Y.; Wu, Y.; Li, G. *J. Am. Chem. Soc.*, **2009**, *131*, 15586.
- (27) Ye, L.; Zhang, S.; Huo, L.; Zhang, M.; Hou, J. *Acc. Chem. Res.*, **2014**, *47*, 1595.
- (28) Kishi, R.; Dennis, M.; Fukuda, K.; Murata, Y.; Morita, K.; Uenaka, H.; Nakano, M. *J. Phys. Chem. C*, **2013**, *117*, 21498.
- (29) Wang, G.; Kan, Y.; Geng, Y.; Duan, Y.; Wang, L.; Wu, H.; Dong, X.; Su, Z. *Theor. Chem. Acc.*, **2014**, *133*, 1.
- (30) Babel, A.; Jenekhe, S. A., *J. Am. Chem. Soc.*, **2003**, *125*, 13656.
- (31) Chen, Z.; Zheng, Y.; Yan, H. Facchetti, A. *J. Am. Chem. Soc.*, **2008**, *131*, 8.
- (32) Bae, J.-H.; Kim, H.; Horowitz, G.; Lee, S.-D. *Solid-State Electron.*, **2011**, *63*, 163.
- (33) Chen, J.; Tee, C. K.; Yang, J.; Shaw, C.; Shtein, M.; Anthony, J.; Martin, D. C. *J. Polym. Sci., Part B: Polym. Phys.*, **2006**, *44*, 3631.
- (34) Baeg, K.-J.; Bae, G.-T.; Noh, Y.-Y. *ACS Appl. Mater. Interfaces*, **2013**, *5*, 5804.
- (35) Ghibaudo, G., *Electron. Lett.*, **1988**, *24*, 543.
- (36) Yoo, D.; Nketia-Yawson, B.; Kang, S.J.; Ahn, H.; Shin, T.J.; Noh, Y.-Y.; Yang, C. *Adv. Funct. Mater.*, **2015**, *25*, 586.
- (37) Xu, Y.; Minari, T.; Tsukagoshi, K.; Chroboczek, J.; Ghibaudo, G. *J. Appl. Phys.*, **2010**, *107*, 114507.
- (38) Yoon, M.-H.; Kim, C.; Facchetti, A.; Marks, T. J. *J. Am. Chem. Soc.*, **2006**, *128*, 12851.
- (39) Usta, H.; Risko, C.; Wang, Z.; Huang, H.; Deliomeroğlu, M. K.; Zhukhovitskiy, A.; Facchetti, A.; Marks, T. J. *J. Am. Chem. Soc.*, **2009**, *131*, 5586.
- (40) Gao, X.; Hu, Y. *J. Mater. Chem. C*, **2014**, *2*, 3099.
- (41) Oh, J. H.; Sun, Y.-S.; Schmidt, R. d.; Toney, M. F.; Nordlund, D. ; Könemann, M.; Würthner, F.; Bao, Z. *Chem. Mater.*, **2009**, *21*, 5508.

- (42) Anthony, J. E.; Brooks, J. S.; Eaton, D. L.; Parkin, S. R. *J. Am. Chem. Soc.*, **2001**, *123*, 9482.
- (43) Mei, J.; Kim, D. H.; Ayzner, A. L.; Toney, M. F.; Bao, Z. *J. Am. Chem. Soc.*, **2009**, *131*, 20130.
- (44) Diao, Y.; Tee, B. C.; Giri, G.; Xu, J.; Kim, D. H.; Becerril, H. A.; Stoltenberg, R. M.; Lee, T. H.; Xue, G.; Mannsfeld, S. C. *Nat. Mater.*, **2013**, *12*, 665.
- (45) Liu, L.; Ren, Z.; Xiao, C.; Dong, H.; Yan, S.; Hu, W.; Wang, Z. *Org. Electron.*, **2016**, *35*, 186.
- (46) Shu, C.-F.; Shu, Y.-C.; Gong, Z.-H.; Peng, S.-M.; Lee, G.-H.; Jen, A. K. *Chem. Mater.*, **1998**, *10*, 3284.
- (47) Liu, L.; Ren, Z.; Xiao, C.; He, B.; Dong, H.; Yan, S.; Hu, W.; Wang, Z. *Chem. Commun.*, **2016**, *52*, 4902.
- (48) Mi, C.; Tan, R.; Sun, D.; Ren, Z.; Sun, X.; Yan, S. *J. Mater. Chem. C*, **2015**, *3*, 10249.

* Chapter IV is reproduced in part with permission of "Organic Electronics 37, 2016, 402-410".
Copyright 2016 Elsevier.

Chapter V

Acknowledgments (Eng. ver.)

Firstly, I am extremely grateful to *Prof. Changduk Yang* as my advisor, for his constant support and fruitful discussion during Ph.D. course. With guiding my research, he not only provided various research opportunities such as overseas study and international conference to improve synthetic skill but gave helpful advice for school life whenever I am having a hard time.

As doctoral defense committees, I would like to thank Prof, *Jin Young Kim*, *Prof. Sung you Hong*, *Prof. Haesung Park*, and *Prof. Sung Heum Park* for advising and boosting me about research presentation, despite of their tight schedule.

I am much grateful to all of coworkers, *Prof. Jin Young Kim* and their research members (*Seyeong*, *Taehyo*, *Na Gyeong*), *Prof. Yong-Young Noh* and their research members (*Won Tae Park*, *Dr. Gi-Seong Ryu*) for cooperation and help. Furthermore, I really want to thank ATOMS alumni and current members. *Boram* as the first graduate as well as alumna from our group, *Dr. Jonggi Kim*, who first received a Ph.D. from our group, *Dr. Yi Ho Kim* who showed excellent research results in spite of office worker. *Dr. Gitish* and *Dr. Salini* who worked our group as postdoc from India. *Dr. Tao* as postdoc from China. *Dohyuk*, *Hyojin* and *Mijin* who showed good attitudes and work results as master's degree student, *Kwang Hyun* as who did a lots of works as researcher, *Dr. Junghoon Lee* and *Dr. Gyoungsik Kim*, who have discussed with me about research, *Chen* who is schoolmate as well as soulmate from China, *Sang Myeon* who is captain from our group, *Jungho* as a diligent worker, *Tanya* as excellent device maker from India, *Yujin*, *Hyejin*, and *So-Huei* who is pretty and cute younger sisters as well as juniors, *Daehee* as soft person, *Byoungkyu* who is curious, *Minkyu* who has silent but strong mind, *Yong Joon* who is mood maker.

I acknowledge HCAM members, including *Dr. Heejoo Kim*, *Dr. Byoung Hoon Lee*, *Dr. Geunjin Kim*, *Dr. Jaemin Kong*, *Prof. Jongjin*, *Prof. Seoung Ho Lee*, *Prof. Kwanghee Lee* and *Prof. Yoon Kyung Jung* for giving strong motivation and helpful advices during Ph.D. degree.

I also express my gratitude to *Prof. Reynolds* accepting me in his research group at Georgia Tech for nearly a year during which I have learned diverse experience and to his group members for helping me to utilize my facilities. I also deeply thanks to *Prof. Hyo Won Lee* and *Dr. Ihl Young Choi* as the master's course advisor and co-advisor, who guided me the basis of organic synthesis. Furthermore, I want to thank my study members at Chungbuk University and high school friends for their inspiration to elevate my moral courage. Finally, I owe my heartfelt gratitude to my loving *parents*, whose love, affection and prayers enabled me to achieve Ph.D degree. I wish to acknowledge the encouragement and moral support of my family members; especially my sweet younger sister, *Eun Mi*, her reliable husbands, *Usik*, my lovely niece, *Jeong hyeon*.

감사의 글 (Kor. ver.)

2012년 겨울이 들어설 무렵 입학하여 어느덧 세월이 지나 졸업을 앞둔 2017년이 다가왔습니다. 결코 쉽지 않은 박사진학 결정부터 마무리 하는 이 시점까지 짧지 않은 시간이지만 짧지 않은 기억으로 다가오는 건 아마도 배움에 대한 아쉬움과 부족한 노력에 대한 푸념일 지도 모르겠습니다. 가장 먼저 저에게 인생의 지표 및 연구자로서의 교육을 해주시고 지원을 아낌없이 해주신 양창덕 지도 교수님께 깊은 감사 드립니다. 교수님의 지도와 지원이 없었다면 결코 해낼 수 없었을 것입니다. 아직은 부족하지만 학위 과정 동안 교수님께 배운 다양한 경험과 연구를 바탕으로 앞으로 연구자로서 더욱더 노력하겠습니다. 또한 박사학위 논문 및 발표를 검토해주시고 지도편달해주신 유니스트 김진영교수님, 홍성유교수님, 박혜성 교수님, 깊은 감사 드리며 특히 학위 심사자 이자 오랜 기간 저의 멘토로서 아낌없는 조언과 격려를 해주신 박성흠교수님 감사 드립니다. 그리고 태양전지 제작 및 분석을 통하여 저의 연구에 많은 도움 주신 유니스트 김진영 교수님 그리고 연구실 사람들, 세영이, 태효, 나경, 유기트랜지스터 제작 및 분석을 통한 공동연구를 수행한 동국대 노용영 교수님과 연구실 분들, 원태씨, 류기성 박사님, 그 외 연구를 도와주신 많은 분들께 깊은 감사를 드립니다. 이분들의 공동연구로 인해 저의 실험이 더욱 더 빛날 수 있었습니다. 그리고 학위과정 동안 좋은 일 이든 나쁜 일 이던 동거동락해온 ATOMS 이전 그리고 현재 동료들, 첫번째 석사졸업자 보람이, 우리연구실 첫번째 박사학위자 이자 친형 같은 김종기 박사님, 제가 인생선배로서 연구실 선배로서 존경하는 김이호 박사님, 랩장 시절 많이 고생하고 수고했던 도혁, 효진, 미진, 인도 포닥 으로 지금은 교수가 된 Gitish 박사, 낙천적인 삶을 살던 Salini 박사, 중국으로 돌아가서 연구생활 하는 Tao 박사, 그리고 동갑내기이자 뛰어난 연구를 보여준 광현 앞으로도 연구자로서 잘하리라 생각합니다. 또한 지금은 박사로서 연구에 매진하고 있고 학위기간 동안 많은 이야기를 나누었던 이정훈 박사, 김경식 박사, 나의 동기이자 앞으로 뛰어난 연구자가 될 소울메이트 첸, 인도에서 온 새침한 타냐, 현재 랩장 이자 계획표작성 달인 상면이 성실하고 꾸준한 멘탈 정호, 우리랩의 이쁜(?) 여자 후배이자 과묵한 동생들인 유진, 소희, 혜진이, 부드러운 해병대 출신 대희, 형을 좋아라 하는 병규, 조용히 잘생긴(?) 민규, 미래가 촉망되는 용준까지... 나의 동료들은 때로는 지치고 힘든 학위과정에서 연구뿐만 아니라 잠시 쉬어갈 수 있었던 휴식 같은 고마운 분들입니다. 이 자리를 빌어 진심으로 감사 드리며 좋은 모습으로 다시 만나길 기원합니다. 또한 비록 미국에 있는 바람에 연구실에서 같이 있지는 못하였지만 오랜 기간 동안 연구자 선배로서 때론 누나처럼 조언을 아껴주시지 않던 정윤경 교수님께도 감사 드립니다.

그리고 학위 시작 하기 전 오랫동안 일하면서 저의 진학에 결정적인 역할을 한 광주 히거터에서의 생활은 결코 잊지 못할 것 같습니다. 특히 히거센터에서 같이 일해온 이광희 교수님 학생 및 박사님들, 친한 형이자 고민을 들어주던 김희주 박사님, 지금은 다 박사학위를

취득하고 열심히 연구에 매진하는 김근진 박사, 예일대 있는 공재민 박사, 교수 임용된 이병훈 박사, 앞으로도 모두 좋은 결과 있길 기원하겠습니다. 또한 연구원시절 많은 조언을 주신 경상대 이종진 교수님, 협소한 저의 화학적 분야에 많은 조언해주신 대구대 이성호 교수님께도 감사 드리며 앞으로 좋은 모습 보여드릴 수 있도록 노력하겠습니다.

뿐만 아니라 저의 유기화학적 배경 및 실험의 기초를 가르쳐주신 석사지도교수이신 이효원 교수님과 최일영박사님께 이 자리를 빌어 감사 드리고 싶습니다. 그리고 충북대 석사시절 연구실 동료들, 동기들에게도 감사한 마음을 전하며 특히, 충북대 정독실 회원이자 현재도 끈끈한 연을 이어가는 재기, 형상이, 영두, 재혁, 소한, 영호, 항상 멀리서 응원해줘서 고맙고 감사 하게 생각합니다. 모두들 하는 일 잘되고 계속 연을 이어갔으면 좋겠습니다. 그리고 고등학교 동기이자 나의 고향친구들 동수, 인호, 대용에게도 고마움을 전하며 때로는 위로를 해주고 격려를 해주들 이들이 있었기에 무사히 학위과정을 마칠 수 있었습니다.

마지막으로 저의 가장 강력한 응원군이자 영원한 나의 편인 가족들, 특히 늦은 나이 학위를 한다고 했을 때 무엇보다도 격려해주시고 물심양면으로 도와주신 아버지, 어머니 진심으로 감사하고 사랑합니다. 기대하신 만큼 보답할 수 있는 아들이 되도록 노력할 때니 지켜봐 주십시오. 또한 나의 하나뿐인 동생이자 이젠 나보다 어른스러운 은미 지금은 사랑스런 나의 조카 정현이의 엄마가 되었지만 늘 곁에서 응원해줘서 고맙고 또한 듬직하고 착한 매제 우식이도 이자리를 빌어 진심으로 고맙고 지금처럼 행복하게 잘사는 모습 보여줬으면 좋겠습니다. 이렇듯 많은 분들의 관심과 격려덕분에 제가 무사히 학위를 마칠 수 있었던 것 같습니다. 다시 한번 감사 드리며 앞으로도 학문적으로나 인성적으로 성장하는 과학자로서 끊임 없이 노력하는 사람이 되도록 하겠습니다. 감사합니다.

2017년 1월2일 월요일

이규철 올림

Curriculum Vitae

Kyu Cheol Lee

Ulsan National Institute of Science and Technology (UNIST)
Energy Engineering Department
50, UNIST-gil, Eonyang-eup, Ulju-gun, Ulsan, Republic of Korea
Phone: +82-10-6552-5808 /E-Mail: Leekc80@gmail.com

Education

Ulsan National Institute Science and Technology (UNIST), Ulsan, Korea 02/2017.
Ph.D. in Department of Energy Engineering
Advisor: Prof. Changduk Yang
Thesis: Design, Synthesis, and Characterization of Polymer and Small-Molecule Organic Semiconductors based on Tricyclic Heterocycles for Opto-Electronic Devices

Chungbuk National University, Cheongju, Korea 02/2009.
M.S. in Department of Chemistry
Advisor: Prof. Hyo Won Lee
Co-advisor: Dr. Ihl Young Choi (KRICT)
Thesis: Michael Addition Reaction to Indoles and Synthetic Study on Flustramine B

Chungbuk National University, Cheongju, Korea 02/2007.
(Military service 2000/09 ~2002/11)
B.S. in Department of Chemistry

Experiences

Georgia Institute of Technology (Georgia Tech.): 11/2015 ~11/2016
: School of Chemistry & Biochemistry
-Position: Student intern
Research activities
✓ Development of active layer materials for thermal stable organic solar cell.
✓ Solar cell device fabrication

Research for Institute Solar and Sustainable Energies (RISE) 03/2012 ~09/2012
: Synthesis research team
- Position: Researcher.
Research activities
✓ Development of active layer materials for organic solar cell.
✓ .Synthesis of conjugated & conducting Polymers

Korea Institute of Footwear & Leather Technology (KIFLT): 01/2012 ~02/2012.
: Organic material and research department.
-Position: Head research worker
Research activities
✓ Synthesis of adhesive & cohesive materials, and property valuation research.

Heeger Center for Advanced Materials (HCAM): 04/2009 ~ 08/2011.
: Synthesis Research team
- Position: Researcher.

Research activities

- ✓ Development of active layer materials for organic solar cell.
- ✓ Synthesis of conjugated & conducting polymers

Korea Research Institute of Chemical Technology (KRICT): 12/2007 ~ 03/2009.

: Bio & drug discovery division, center for medicinal chemistry.

-Position: Research student.

Research activities

- ✓ Development of medicine for Alzheimer's disease
- ✓ Synthesis of organic compounds for drug design & discovery.

Publications (first authored)

1. **Kyu Cheol Lee**, Gi-Seong Ryu, Shanshan Chen, Gyoungsik Kim, Yong-Young Noh* and Changduk Yang*, "Dicyanomethylene-Quinoid vs. Dicyanovinyl-Benzenoid Organic Semiconductors: Understanding Structure-Property Correlations in Mesomerism-like Forms", *Organic Electronics*, **2016**, 37 402-410.
2. **Kyu Cheol Lee**, Taehyo Kim, Seyeong Song, Yiho Kim, Gitish. K. Dutta, Dong Suk Kim*, Jin Young Kim*, Changduk Yang*, "Medium bandgap copolymers based on carbazole and quinoxaline exceeding 1.0 V open-circuit voltages", *RSC Advances*, **2016**, 6, 17624-17631.
3. **Kyu Cheol Lee**, Seyeong Song, Junghoon Lee, Dong Suk Kim*, Jin Young Kim*, and Changduk Yang*, "A Roundabout Approach to Control The Morphological Orientation and Solar Cell Performance by Modulating Side Chain Branching Position in BDT-Based Polymers", *ChemPhysChem*, **2015**, 16(6), 1305-1314.
4. **Kyu Cheol Lee**, Won-Tae Park, Yong-Young Noh*, and Changduk Yang*, "Benzodipyrrolidone(BDP)-Based Polymer Semiconductors Containing a Series of Chalcogen Atoms: Comprehensive Investigation of the Effect of Heteroaromatic Blocks on Intrinsic Semiconducting Properties", *ACS Applied Materials & Interfaces*. **2014**, 6 (7), 4872-4882.
5. Heejoo Kim*, Byoung Hoon Lee, **Kyu Cheol Lee**, Geunjin Kim, Jin Young Yu, Nara Kim, Seoung Ho Lee and Kwanghee Lee*, "Role of the Side Chain in the Phase Segregation of Polymer:Fullerene Bulk Heterojunction Composites", *Advanced Energy Materials*, **2013**, 3(12), 1575-1580. **(Equally contributed)**
6. Gyoungsik Kim, **Kyu Cheol Lee**, Jonggi Kim, Jungho Lee, Sang Myeon Lee, Jeong Chul Lee, Jung Hwa Seo, Won-Youl Choi, and Changduk Yang*, "An unprecedented [5,6]-Open Adduct via a Direct Benzyne-C60 Cycloaddition" *Tetrahedron*, **2013**, 69(35), 7354-7359. **(Equally contributed)**

Publications (co-authored)

1. Tao Cheng, Shanshan Chen, **Kyu Cheol Lee**, Sang Myeon Lee and Changduk Yang* "A dithienodisilacyclohexadiene (DTDS)-based conjugated model semiconductor: understanding unique features and monitoring structural transition" *RSC Advances*, **2016**, 6, 11933-11936
2. Shanshan Chen, **Kyu Cheol Lee**, Zhi-Guo Zhang, Dong Suk Kim, Yongfang Li*, and Changduk Yang* "An Indacenodithiophene-Quinoxaline Polymer Prepared by Direct Arylation Polymerization for Organic Photovoltaics", *Macromolecules*, **2016**, 49 (2), 527-536
3. Jungho Lee, Tomasz Marszalek, **Kyu Cheol Lee**, Jonggi Kim, Wojciech Pisula* and Changduk Yang*, "Improvement in solubility and molecular assembly of cyclopentadithiophene-benzothiadiazole polymer", *Macromolecular Chemistry and Physics*, **2015**, 21, (216) 1244-1250.
4. Ihl Young Choi*, **Kyu Cheol Lee**, Hyo Won Lee*, "CeCl₃·7H₂O-NaI-SiO₂ Catalyzed Aza-Michael Addition of N-Heterocyclesto Enones under Solvent Free Conditions" *Bull. Korean Chem. Soc.* **2012**, 33,(11) 3535-3536.
5. Hongkyu Kang, Geunjin Kim, In-Wook Hwang, Yonghee Kim, **Kyu Cheol Lee**, Sung Heum

Park, Kwanghee Lee* “High-performance polymer tandem devices combining solar cell and light-emitting diode”, *Solar Energy Materials & Solar Cells*, **2012**, 107 148–153.

Patent

KR 10-2008-0015671 “Cycloalkylpyrrole and Piperazine Derivatives and Salts, and Their s Pharmaceutical Compositions Containing The same.”

Conference presentation (International)

1. “Pechmann Dye- Based Organic Semiconducting Polymers for Applications in Organic Field-Effect Transistors (OFETs)”, International Conference on Advanced Electromaterials (ICAE) in ICC Jeju, Korea November 17-20, 2015.
2. “Pechmann Dye- Based Organic Semiconducting Polymers for Applications in Organic Field-Effect Transistors”, International Union of Pure and Applied Chemistry (IUPAC) in Busan, Korea August 6-13, 2015.
3. “Synthesis of Conjugated Polymers Based on Benzodipyrrolinone with Chalcogen (S, Se, O) Elements for Organic Thin Film Transistors”, Gordon Research Conference, in Lucca (Barga) Italy May 4-9, 2014.

References

Prof. Sung Heum Park

Department of physics,
Pukyong National University
Busan 608-737, Republic of Korea
Tel: +82-51-629-5574
E-mail: spark@pknu.ac.kr

Prof. Yong-Young Noh

Department of Energy and
Materials Engineering, Dongguk
University (DGU),
30, Pildong-ro, 1-gil, Jung-gu,
Seoul, Republic of Korea,
Tel: +82-02-2260-4974
E-mail: yynoh@dongguk.edu

Prof. Changduk Yang

Department of energy engineering,
Ulsan National Institute of Science
and Technology (UNIST),
50, UNIST-gil, Eonyang-eup,
Ulju-gun, Republic of Korea
Tel: +82-52-217-2920
E-mail: yang@unist.ac.kr

Appendix

Permission from all cited journal in this dissertation

Chapter II. *ACS Appl. Mater. Interfaces* 2014, 6, 4872–4882.

2016. 11. 18.

Rightslink® by Copyright Clearance Center



RightsLink®

Home

Account Info

Help



ACS Publications
 Most Trusted. Most Cited. Most Read.

Title: Benzodipyrrolidone (BDP)-Based
 Polymer Semiconductors
 Containing a Series of Chalcogen
 Atoms: Comprehensive
 Investigation of the Effect of
 Heteroaromatic Blocks on
 Intrinsic Semiconducting
 Properties

Logged in as:
 Kyu Cheol Lee

LOGOUT

Author: Kyu Cheol Lee, Won-Tae Park,
 Yong-Young Noh, et al

Publication: Applied Materials

Publisher: American Chemical Society

Date: Apr 1, 2014

Copyright © 2014, American Chemical Society

PERMISSION/LICENSE IS GRANTED FOR YOUR ORDER AT NO CHARGE

This type of permission/license, instead of the standard Terms & Conditions, is sent to you because no fee is being charged for your order. Please note the following:

- Permission is granted for your request in both print and electronic formats, and translations.
- If figures and/or tables were requested, they may be adapted or used in part.
- Please print this page for your records and send a copy of it to your publisher/graduate school.
- Appropriate credit for the requested material should be given as follows: "Reprinted (adapted) with permission from (COMPLETE REFERENCE CITATION). Copyright (YEAR) American Chemical Society." Insert appropriate information in place of the capitalized words.
- One-time permission is granted only for the use specified in your request. No additional uses are granted (such as derivative works or other editions). For any other uses, please submit a new request.

BACK

CLOSE WINDOW

Copyright © 2016 Copyright Clearance Center, Inc. All Rights Reserved. [Privacy statement](#). [Terms and Conditions](#).
 Comments? We would like to hear from you. E-mail us at customercare@copyright.com

Chapter III. *ChemPhysChem* 2015, 16, 1305-1314.

2016. 11. 18.

Rightslink® by Copyright Clearance Center

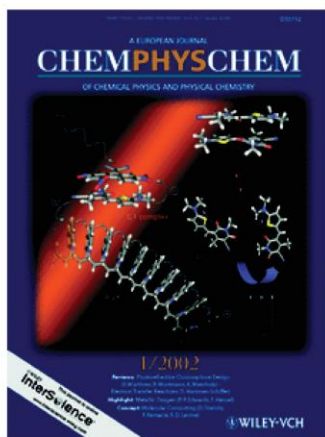


RightsLink®

Home

Account
Info

Help



Title: A Roundabout Approach to Control Morphological Orientation and Solar-Cell Performance by Modulating Side-Chain Branching Position in Benzodithiophene-Based Polymers

Author: Kyu Cheol Lee, Seyeong Song, Junghoon Lee, Dong Suk Kim, Jin Young Kim, Changduk Yang

Publication: ChemPhysChem

Publisher: John Wiley and Sons

Date: Oct 21, 2014

© 2015 WILEY-VCH Verlag GmbH & Co. KGaA, Weinheim

Logged in as:
Kyu Cheol Lee

LOGOUT

Order Completed

Thank you for your order.

This Agreement between Kyu Cheol Lee ("You") and John Wiley and Sons ("John Wiley and Sons") consists of your license details and the terms and conditions provided by John Wiley and Sons and Copyright Clearance Center.

Your confirmation email will contain your order number for future reference.

Printable details.

License Number	3991800000610
License date	Nov 18, 2016
Licensed Content Publisher	John Wiley and Sons
Licensed Content Publication	ChemPhysChem
Licensed Content Title	A Roundabout Approach to Control Morphological Orientation and Solar-Cell Performance by Modulating Side-Chain Branching Position in Benzodithiophene-Based Polymers
Licensed Content Author	Kyu Cheol Lee, Seyeong Song, Junghoon Lee, Dong Suk Kim, Jin Young Kim, Changduk Yang
Licensed Content Date	Oct 21, 2014
Licensed Content Pages	10
Type of use	Dissertation/Thesis
Requestor type	Author of this Wiley article
Format	Electronic
Portion	Full article
Will you be translating?	No
Title of your thesis / dissertation	Synthesis and Characterization of Conjugated Polymer and Small Molecules for Optoelectronic Devices
Expected completion date	Feb 2017
Expected size (number of pages)	1
Requestor Location	Kyu Cheol Lee Dal-dong Nam-gu ulsan, 670380 Korea, Republic Of Attn: Kyu Cheol Lee
Publisher Tax ID	EU826007151
Billing Type	Invoice

<https://s100.copyright.com/AppDispatchServlet>

1/2

Chapter IV *Organic Electronics* 37, 2016, 402-410.

2016. 11. 18.

Rightslink® by Copyright Clearance Center



RightsLink®

Home

Account
Info

Help



Title: Dicyanomethylene-quinoid vs. dicyanovinyl-benzenoid organic semiconductors: Understanding structure-property correlations in mesomerism-like forms

Author: Kyu Cheol Lee, Gi-Seong Ryu, Shanshan Chen, Gyoungsik Kim, Yong-Young Noh, Changduk Yang

Publication: Organic Electronics

Publisher: Elsevier

Date: October 2016

© 2016 Elsevier B.V. All rights reserved.

Logged in as:
Kyu Cheol Lee

LOGOUT

Order Completed

Thank you for your order.

This Agreement between Kyu Cheol Lee ("You") and Elsevier ("Elsevier") consists of your license details and the terms and conditions provided by Elsevier and Copyright Clearance Center.

Your confirmation email will contain your order number for future reference.

[Printable details.](#)

License Number	3991790922978
License date	Nov 18, 2016
Licensed Content Publisher	Elsevier
Licensed Content Publication	Organic Electronics
Licensed Content Title	Dicyanomethylene-quinoid vs. dicyanovinyl-benzenoid organic semiconductors: Understanding structure-property correlations in mesomerism-like forms
Licensed Content Author	Kyu Cheol Lee, Gi-Seong Ryu, Shanshan Chen, Gyoungsik Kim, Yong-Young Noh, Changduk Yang
Licensed Content Date	October 2016
Licensed Content Volume	37
Licensed Content Issue	n/a
Licensed Content Pages	9
Type of Use	reuse in a thesis/dissertation
Portion	full article
Format	electronic
Are you the author of this Elsevier article?	Yes
Will you be translating?	No
Order reference number	
Title of your thesis/dissertation	Synthesis and Characterization of Conjugated Polymer and Small Molecules for Optoelectronic Devices
Expected completion date	Feb 2017
Estimated size (number of pages)	1
Elsevier VAT number	GB 494 6272 12
Requestor Location	Kyu Cheol Lee Dal-dong Nam-gu ulsan, 670380 Korea, Republic Of Attn: Kyu Cheol Lee
Total	0.00 USD

[ORDER MORE](#)

[CLOSE WINDOW](#)

<https://s100.copyright.com/AppDispatchServlet>

1/2